Severe plastic deformation of metallic materials by equal channel angular swaging: Theory, experiment and numerical simulation

Vom Fachbereich Maschinenbau

an der Technischen Universität Darmstadt

zur

Erlangung des Grades eines Doktor-Ingenieurs (Dr.-Ing.)

genehmigte

Dissertation

vorgelegt von

M.Sc. Mehmet Okan Görtan

aus Kocaeli, Türkei

Berichterstatter:	Prof. Dr.-Ing. Dipl.-Wirtsch.-Ing. P. Groche
Mitberichterstatter:	Prof. Dr.-Ing. C. Müller
Tag der Einreichung:	03.06.2014
Tag der mündlichen Prüfung:	21.07.2014

Darmstadt 2014

D17

Acknowledgements

This work is created during the time I spent as a research assistant (Wissenschaftlicher Mitarbeiter) in the Institute for Production Engineering and Forming Machines (PtU) of Technische Universität Darmstadt, under supervision of Prof. Dr.-Ing. Dipl.-Wirtsch.-Ing. Peter Groche.

Completion of this work would not have been possible without the guidance of my “Doktorvater”, Prof. Dr.-Ing. Dipl.-Wirtsch.-Ing. Peter Groche. I would like to express my special thanks to him for his support, tolerance, patience and understanding.

I would also like to extend my thanks to Prof. Dr.-Ing. Clemens Müller for co-supervising my work and his support during the longstanding project work with him.

Hereby, I would like to state my gratitude to Dr.-Ing. Enrico Bruder for his cooperation during the project “Production of UFG materials by rotary swaging” upon which my thesis bases.

I would like to acknowledge all of my coworkers at PtU, the research assistants, our secretaries and our workshop staff who welcomed me to the institute and to Germany from the first day on and supported me during the extended “Adaption to Germany” process.

I would like to thank all my friends who helped me carry this burden through the joy of their companionship. Among them, Pinar Topal and Ibrahim Topal deserve my special gratitude for their hospitality in the last phases of my thesis work.

Moreover, I wish to express my gratitude to my family for their encouragement and support during my doctoral studies.

Finally, I would like to thank my wife, Dr. Fatma Arzu Görtan, with all my heart for her patience and continuous support. Without her, the completion of this thesis wouldn’t be possible.

Mehmet Okan Görtan Darmstadt, May 2014

Contents

Symbols and Abbreviations

Symbols, Latin Letters

Symbol	Unit	Explanation
A	mm^2	Cross-section area
B	MPa	Strain hardening effect
C	-	Strain rate sensitivity
c	J/kg K	Specific heat
D	mm	Diameter
E	GPa	Young's modulus
F	mm^2	Area of the stationary tool walls
F	N	Force
F_{axial}	N	Axial force
F_{low}	N	Force acting on the lower tool
F_{radial}	N	Radial force
$F_{resulting}$	N	Resulting force
F_{up}	N	Force acting on the upper tool
$F_{yielding}$	N	Yielding force
h	W/m^2 K	Heat transfer coefficient
k	MPa	Shear yield strength
k	W/m K	Thermal conductivity
L_0	mm	Length of the entry channel
L_1	mm	Length of the middle channel
L_2	mm	Length of the exit channel
m	-	Thermal softening exponent
n	-	Number of severe plastic deformation cycles
n	-	Strain hardening exponent
P	MPa	Pressure, punch pressure
P_0	MPa	Back pressure
P_1	MPa	Punch pressure
r	mm	Radius
r_i	mm	Inner corner radius

r_o	mm	Outer corner radius
r_t	-	Total reduction
r_t	mm	Tool radius
r_{wp}	mm	Workpiece radius
s	-	Osculation
t	mm	Thickness
t	s	Time
T	°C or °K	Temperature
t_0	mm	Initial thickness
T_0	°C	Initial temperature
T_{melt}	°C	Melting temperature
T_{room}	°C	Room temperature
V	mm/s	Speed
w	mm	Width
w_{eq}	mm	Equivalent width
X, Y, Z	-	Major directions

Symbols, Greek Letters

Symbol	Unit	Explanation
μ	-	Friction coefficient
γ	-	Shear strain
δ	-	Second parameter to define the position inside the plastic deformation zone
ε	-	Strain
ε'	1/s	Strain rate
ε_0	-	Reference strain
ε'_0	1/s	Reference strain rate
ε_{vM}	-	Von Mises strain
ζ_d	-	Deformation heat dissipation factor
ζ_f	-	Friction heat dissipation factor
η	°	Angle between slip lines
λ	°	Angle of friction
ν	-	Poisson's ratio
ρ	kg/m^3	Density
σ	MPa	Tensile stress
σ_y	MPa	Yield strength
τ	MPa	Friction stress
ϕ	°	Half channel angle
φ	°	Half arc of curvature
χ	-	First paramter to define the position inside the plastic deformation zone
ψ	-	Shearing fan

Abbreviations

2D	Two dimensional
3D	Three dimensional
ALE	Arbitrary Lagrangian-Eulerian
ARB	Accumulative roll bonding
C2S2	Continuous confined strip shearing
DMZ	Dead metal zone
EBSD	Electro backscatter diffraction
ECA	Equal channel angular
ECAD	Equal channel angular drawing
ECAP	Equal channel angular pressing
ECAS	Equal channel angular swaging
FEA	Finite element analysis
FEM	Finite element method
FS	Full split
GHG	Greenhouse gasses
HAGB	High angled grain boundaries
HMP	Heinrich Müller Pforzheim
HPT	High pressure torsion
IEA	International Energy Agency
I-ECAP	Incremental ECAP
PDZ	Plastic deformation zone
PS	Partial split
PtU	Institute for Production Engineering and Forming Machines
RD-ECAP	Rotary die ECAP
RSE	Repetitive side extrusion
SCT	Sliding compression test
SEM	Scanning electron microscope
SF	Shearing fan
SLF	Slip-line field
SP	Single plane
SPD	Severe plastic deformation
TEPS	Total equivalent plastic strain
UFG	Ultrafine grained
VDI	Verein Deutscher Ingenieure
VP	Visio-plasticity

1 Introduction

Research about metal forming was driven majorly by the scientific curiosity before the 18th century. After industrial revolution, this research was additionally boosted by the industrial needs to understand the behavior of forming processes in order to increase the efficiency and reliability of the transition from handcraft to automated mass production [OSA08]. After completion of this transformation, the focus of the recent research shifted away from mass production towards lower volume manufacturing methods, such as high-speed forming or micro-forming [ALL11]. However, current research activities are motivated by a more critical issue which threatens human life over a long term, namely climate change. Climate change in form of global warming is caused by the increase of greenhouse gasses (GHG) emerging after burning fossil fuels. The production of two major industrial metals, steel and aluminum, account for approximately 10% of the overall GHG emissions and it is therefore a significant driver of climate change [IEA08]. In order to assure the sustainability of the industry, it is highly advised to reduce the GHG emissions related to the material production by 50% in the next 40 years and that, despite the increase in demand for these industrial materials [CCC08]. The first thing that comes to mind to cope with that problem is to increase the efficiency of the material production stages. However, raw material production processes are extremely efficient and according to International Energy Agency (IEA), even with the universal implementation of best practice applications in the industry, emissions can only be reduced by approximately 13% [IEA09]. Such an improvement alone is clearly insufficient to reach the 50% GHG emission reduction target and it is obvious that a broader strategy which incorporates all aspects of the product cycle should be integrated to achieve the intended goals. A significant enhancement in the energy consumption within this cycle can be achieved by using less material for the production applications. It is possible with the successful implementation of lightweight design approaches and lightweight materials [CAR11].

Current lightweight material technologies utilize high-strength steels, non-ferrous metals such as aluminum-, magnesium- and titanium-alloys or secondary heat

treatment processes to improve the specific strength of materials. Nevertheless, the recent climate change scenario requires further improvement of the specific strength of these. Production of enhanced lightweight metals without adding costly alloying elements to current materials or applying energy consuming heat treatments still represent a major challenge for the material production industry.

The above mentioned requirements can be met with fine-grained materials produced by severe plastic deformation (SPD). SPD-processes refine the grain size of the conventional engineering materials down to the nano level by inducing high plastic strain and simultaneously generating new grains in the processed samples. The resulting fine grained materials are characterized by a combination of an extraordinary high strength and considerable ductility which result from grain refinement [VAL02]. Although many different SPD processes have been developed in the last three decades which are capable of improving the mechanical properties of engineering materials, the industrial utilization is still in an early stage and limited to a few applications [AZU08]. The reason for that lies in the high effort to realize these processes. The conventional SPD techniques are mostly discontinuous and the sample geometries do not meet the requirements of the production industry.

The new SPD process “Equal Channel Angular Swaging” (ECAS) is developed to produce bulk high-strength/high-ductility materials by combining the conventional SPD technique of equal channel angular pressing (ECAP) with the incremental bulk forming method of rotary swaging. The developed process minimizes the forming forces in the feeding direction of the material by optimizing the friction and has therefore a high potential for a continuous and economical production of bulk fine grained metals.

The aims of the current work are the fundamental investigations on the design strategies of ECAS forming tools and processes as well as the demonstration of the general feasibility to process metallic materials by ECAS. In order to cover a wide area for materials, two different metals, commercially pure (CP) copper and a low carbon cold forge steel (C4C), will be used in the investigations.

The analyses will be conducted using analytical and numerical methods as well as experiments. The results of these analyses serve as design guidelines for future applications of the ECAS process.

2 State of the Art

In general, the average grain size plays a significant and dominant role in the physical and especially mechanical properties of polycrystalline metals. According to the Hall-Petch relationship, the yield stress of metals increases with the decrease of the grain size [HAL51]. Therefore, metals with small grains are distinguished by a higher strength compared to their coarse grained counterparts. Accordingly, fine grained materials have awakened an increasing interest in the manufacturing industry.

The grain size of commercial polycrystalline metals are modified with the application of thermomechnical treatments to the specific alloy during production. However, there is an impassable limit of the order of few micrometers concerning the grain size for the current thermomechnical processes. Therefore, the attention has been shifted towards the development of new methods to produce ultrafine grained (UFG) metals in the last decade. UFG materials are defined as polycrystalline metals with average grain sizes under ~ 1µm and a homogeneous microstructure with a majority of grain boundaries having high angle misorientations [VAL06].

So far, two different approaches, “bottom-up” and “top-down”, have been followed to fabricate UFG materials [ZHU04]. In the “bottom-up” approaches, solid metals are produced by the assembly of individual atoms through the deposition from the gas phase or by compacting of nanocyristalline particles [GLE89]. Nevertheless, samples produced with these techniques are fairly small in size and contain a high level of porosity. Moreover, the fabrication techniques allow introduction of impurities into the produced samples. Hence, “bottom-up” methods are not suitable for large-scale industrial applications and are not the subject of this study.

In “top-down” methods, relatively coarse grained commercial bulk solid materials are subjected to high straining to refine the grain structure of the processed materials. As a result, larger samples can be produced. Moreover, the introduction of impurities can be completely omitted. However, in order to reach an UFG microstructure, it is necessary to deform the materials excessively. Such a deformation with conventional

metal forming methods, such as rolling or extrusion, would result in very small product cross-sections in the deformed samples [VAL06]. To overcome this crucial problem, different severe plastic deformation (SPD) processes have been developed in the last three decades. In general, SPD can be described as metal forming processes where a very large strain is introduced into bulk solids without changing the geometry of the solid [AZU08]. The severe straining of the material enables a grain refinement down to nano-level. UFG materials produced by SPD methods are distinguished by an extraordinary combination of high strength and considerable ductility or improved fatigue behavior and are therefore suitable for lightweight applications.

In the following subchapters, the characteristics, advantages and drawbacks of major SPD processes and their derivatives will be reviewed together with the design methods for these techniques as well as methods to improve these current SPD techniques.

2.1 Severe Plastic Deformation of Metals

Development of SPD processes is inspired by the early work of Bridgman in the 1940s where he discovered that steels can withstand extensive plastic strains without fracture if an excessive pressure is applied on them [BRI46]. However, successful implementation of this discovery came about five decades later in the early 90s [VAL90, VAL91]. Since then, many SPD processes have been proposed and developed.

2.1.1 Major Severe Plastic Deformation Processes

Among many different SPD processes, high pressure torsion (HPT), accumulative roll bonding (ARB) and equal channel angular pressing (ECAP) are the major and most investigated ones (Fig. 2-1).

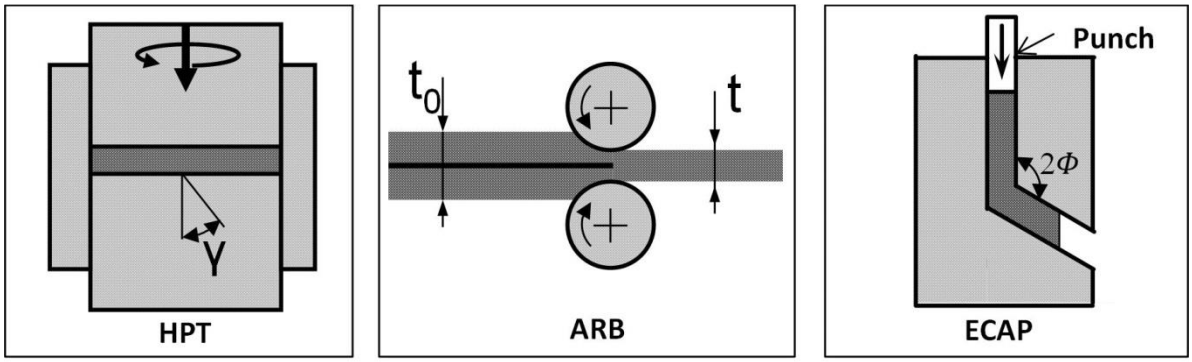

Figure 2-1 Major SPD processes

High Pressure Torsion (HPT)

The most similar SPD process to the “Bridgman Anvil” application is HPT. During HPT, flat disc shaped samples are placed between two anvils and subjected to a high compression while they are twisted by rotation of one anvil (Figure 2-1.left) [ZHI08]. Due to the hydrostatic stress state, the severe plastic straining of metallic materials is possible by rotating the anvil many times without the occurrence of cracks in the processed samples. The shear strain (γ) and equivalent von Mises strain (ε_{vM}) is given with following equations:

$$\gamma = \frac{2\pi n}{t} r \qquad \textit{Equation 2-1}$$

$$\varepsilon_{vM} = \frac{2\pi n}{t\sqrt{3}} r \qquad \textit{Equation 2-2}$$

where the values n, r and t are number of rotations, the distance from the center of the axis of rotation and the thickness of the sample, respectively [VOR04, WET04].

Although it is acknowledged by many researchers that finer microstructures can be achieved with HPT compared to the other SPD processes, the efficiency of HPT is limited to coin-shaped samples with fairly small geometries [EST13]. Even though the theoretical deformation in the middle axes of the samples is equal to zero, a homogeneous microstructure and hardness distribution can be achieved by thin discs with a thickness of 1 mm [XU07]. Studies with slightly larger samples with a diameter of 10 mm and a height of 8.5 mm illustrate that the homogeneity of the refinement in the microstructure cannot be ensured by bulk materials [SAK05]. Moreover, since the samples should be confined by the anvils, this process is suitable for batch type

production. Due to these restrictions about the size of the produced samples and the production characteristics, the development of HPT to a continuous and cost efficient process is highly unlikely. Therefore, SPD samples fabricated by HPT are predominantly used for laboratory studies.

Accumulative Roll Bonding (ARB)

The continuous and hence more economical major SPD process of accumulative roll bonding (ARB) was proposed in the late 90s [SAI98]. ARB is primarily used for the straining of sheet metals. Before this process, two metal sheets are degreased and their surface is wire brushed. The brushed sheets are stacked together and heated up to a temperature below recrystallization temperature to enable a successful bonding between different layers and to increase the ductility of the processed materials. Heated sheets are then rolled mostly with a conventional rolling facility to their half thickness. In order to generate an ultrafine structure, the formed metal sheets are cut to half and previous steps are repeated so that a high strain is accumulated in the material.

The thickness reduction by ARB process is mostly selected as 50% so that sheet material has the initial thickness after every forming cycle. The thickness of the initial strip (t), total reduction (r_t) and equivalent von Mises strain (ε_{vM}) after n cycles can be calculated with the following equations:

$$t = \frac{t_0}{2^n} \qquad \textit{Equation 2-3}$$

$$r_t = \frac{t_0 - t}{t_0} = 1 - \frac{t}{t_0} = 1 - \frac{1}{2^n} \qquad \textit{Equation 2-4}$$

$$\varepsilon_{vM} = \left\{\frac{2}{\sqrt{3}} \ln\left(\frac{1}{2}\right)\right\} \times n = 0.80 \times n \qquad \textit{Equation 2-5}$$

where t_0 is the initial thickness of the strip [SAI98].

A major advantage of ARB over other SPD processes is the continuous and fast fabrication. Rolling speeds up to approximately 55 m/min with laboratory type rolling mills are already reported [LU09]. With the utilization of more efficient industry type mills, this speed can be increased.

Another major advantage of ARB process is that it makes use of commercially available rolling facilities. An additional investment is not necessary for laboratories and production facilities which dispose of such a mill. Moreover, it can be applied in the fabrication of a wide variety of materials such as commercially pure Al and Al-alloys [LEE02, TOR13], Cu [SHA08], commercially pure Ti and Ti-alloys [TER07, KEN11], Mg-alloys [PER04, VAL05], different steel types [KRA04, LI06, BON13, TSU99] and multilayered composites [YAN10] as well as matrix composites [JAM10, JAM11].

Beside these advantages over other SPD processes, ARB has many significant drawbacks. Therefore, there has been no industrial application of sheet materials processed by this technique. First of all, the shear strain, which is crucial for the grain refinement is confined in the vicinity of the contact surface of the sheet metal with the forming rolls during ARB [LEE02, INO13]. A homogeneous grain refinement can just be achieved by stacking the contact surfaces of the processed material. Moreover, samples processed with ARB are solely sheet materials which are majorly subjected to bending stresses during their product life-cycle. However, an increase in the bending strength can only be achieved after repetitive forming of the same material [KRA04]. Therefore, many rolling steps are required which necessitates the repetition of the time-consuming and expensive preparation procedures before ARB. Furthermore, in order to assure an effective bonding between the layers of the sheet metal, ARB process has to be conducted mostly at elevated temperatures and is therefore energy inefficient.

Equal Channel Angular Pressing (ECAP)

Due to its scalability properties, ECAP is the most investigated and developed SPD process. During ECAP, a rod shaped material is pressed through a die which has two or more channels mostly with the same cross-section intersecting at a certain angle. A simple shear strain is introduced to the processed material while it passes through the intersections between the die-channels. Since the cross-section of the channels is the same, the processed rods have theoretically the initial geometry after forming, which enables a repetitive pressing of the same material, leading to accumulation of very high strains.

The sequential forming of the same material enables the rotation of the sample around its axis between the successive SPD steps. Segal (1995) was the first one to

notice the potential of rotation of the billets between consequent ECAP steps [SEG95]. He reports that deformation with different routes results in dissimilar microstructures and strength by nickel and Armco iron. According to the rotation of the billet, four basic processing routes are defined (Figure 2-2). In route A, the samples are processed without any rotation, while in route C they are rotated 180° between consecutive forming steps. In route B_A, processed materials are rotated 90° in alternating directions. The only difference between route B_A and B_C is that the samples are rotated always in the same direction in B_C. A newly proposed processing route E combines the Route C with Route B_C. In that route, the samples will be rotated 90° around their axes after every second forming step with route C [PUR09]. Since the processing route has a significant effect on the mechanical properties and microstructure of ECAP processed materials, it is of high importance.

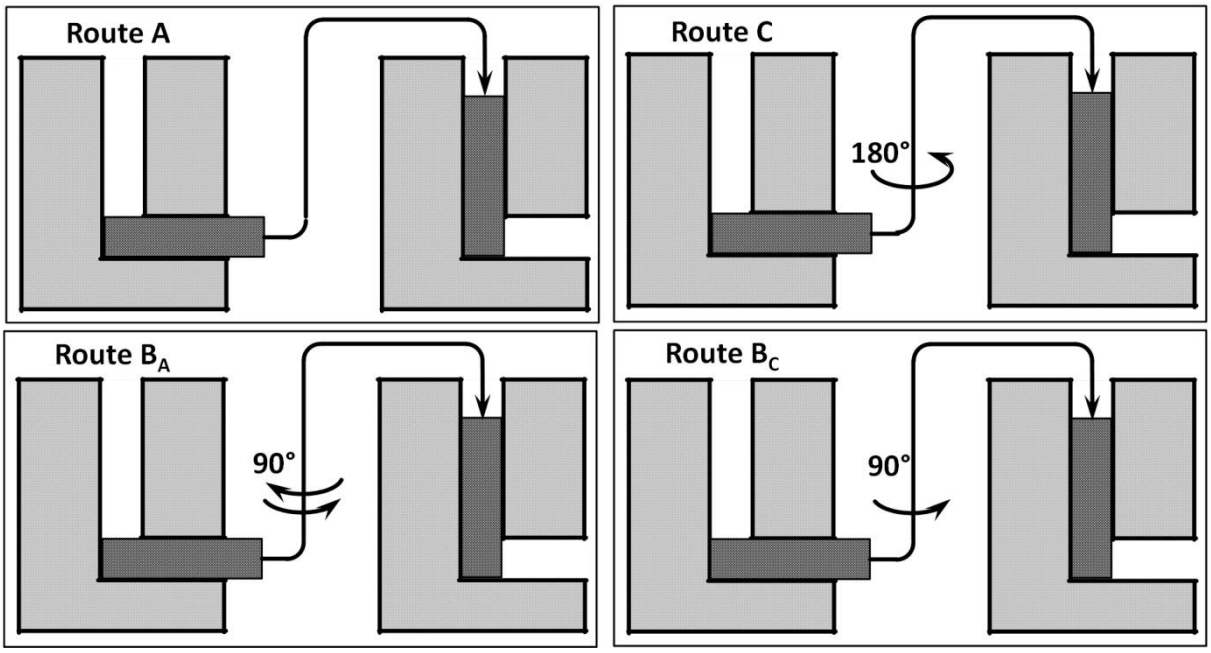

Figure 2-2 Major processing routes for ECAP

As by the other major SPD processes, the processing of different metallic materials is possible with ECAP, such as titanium, copper, aluminum, magnesium and steel as well as their alloys [STO01, SAS00, XU10, ZHI06, SHI05].

The most significant advantage of ECAP over other SPD processes is the scalability in size and geometry of the samples. The fabrication of square, rectangular and round samples as well as sheet materials is possible with this method [AZU02,

FER08, ALE04, LAP08]. Moreover, the cross-section of the produced samples varies from couple of square millimeters up to 10,000 square millimeters [HOR01, SRI06].

Owing to the advantages over other SPD methods, ECAP has been drawing the attention of researchers all around the world. The macromechanics of ECAP has been the subject of many studies. The deformation by this forming method can neither be characterized as a simple shear along a single shear line nor homogeneous. Therefore, usually simplified methods have been used to describe the material yielding [BEY04].

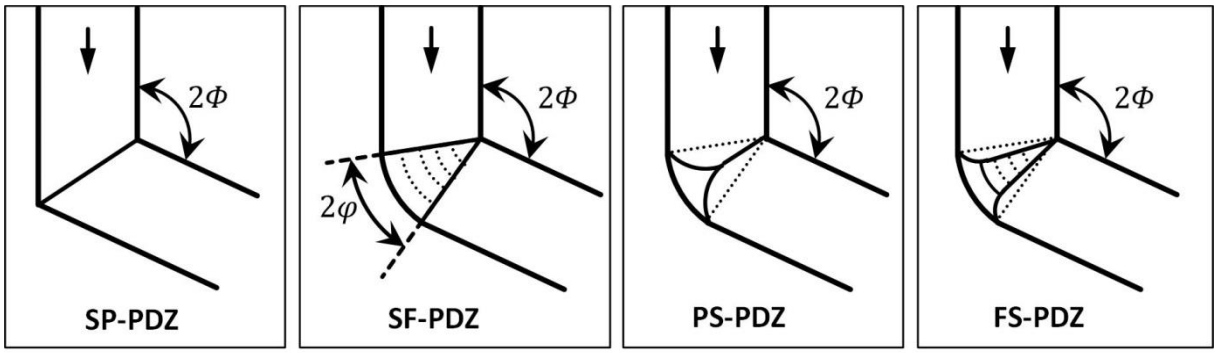

Figure 2-3 Four different models for the plastic deformation zone shape

Overall, four different models have been proposed to describe the plastic deformation zone (PDZ) by ECAP (Fig. 2-3). First study assumes the deformation zone as a single plane (SP) consisting of a simple shear line. Accordingly, the shear strain (γ) and equivalent von Mises strain (ε_{vM}) in the forming section of the ECAP die after n cycles is calculated with following equations [SEG95]:

$$\gamma = 2 \times \mathrm{n} \times \cot\phi \qquad \textit{Equation 2-6}$$

$$\varepsilon_{vM} = \frac{2 \times n}{\sqrt{3}} \cot\phi \qquad \textit{Equation 2-7}$$

where Φ is the half channel angle. This approach is later enhanced by considering the effect of the arc of curvature on the outer side (2φ) of the forming channel [IWA96]. In this case, the PDZ is considered as a shearing fan (SF) rather than a simple shearing plane.

$$\gamma = n\,[2\cot(\phi+\varphi) + \varphi\csc(\phi+\varphi)] \qquad \textit{Equation 2-8}$$

$$\varepsilon_{vM} = n\left[\frac{2\cot(\phi+\varphi) + \varphi\csc(\phi+\varphi)}{\sqrt{3}}\right] \qquad \textit{Equation 2-9}$$

However, these formulas are only valid when the arc of curvature (2φ) is smaller than ($\pi - 2\phi$). Otherwise, the cross-sectional area of the sample is reduced as it passes through the ECAP-die [IWA96].

In a later study, an alternative relationship has been proposed to model the plastic strain for the case of round corners on the samples [GOF00]:

$$\gamma = n\left[2\cot(\phi+\varphi) + \frac{2\varphi}{sin^2(\phi+\varphi)}\right] \qquad \textit{Equation 2-10}$$

$$\varepsilon_{vM} = n\left[\frac{2\cot(\phi+\varphi) + 2\varphi}{\sqrt{3}}\right] \qquad \textit{Equation 2-11}$$

For both cases, setting the arc of curvature (2φ) to zero reduces the proposed formulas to Equation 2-6 of Segal [SEG95]. The deviation between these two approaches reaches for an ECAP tool with a channel angle (2ϕ) of 90° and arc of curvature (2φ) of 28.7° approximately 4.8% and reduces significantly for higher channel angles. Therefore, it is reasonable to assume that both equations are equally capable of estimating the strain imposed in the ECAP process [AID01]

The third model partially splits (PS) the PDZ into two sections: a zone near the outer corner of the forming die where the material forms a free round surface and a second zone where the shearing takes place along a single line [STO01]. Such an approach predicts the strain non-uniformity in the PDZ and allows modeling the different modes of deformation by ECAP processing:

$$\gamma = n\,[2\cot(\phi+\chi) + \tan(\chi-\delta)] \qquad \textit{Equation 2-12}$$

$$\varepsilon_{vM} = n\left[\frac{2\cot(\phi+\chi) + \tan(\chi-\delta)}{\sqrt{3}}\right] \qquad \textit{Equation 2-13}$$

where χ and δ are parameters which define the position of the investigated point in the PDZ [STO07].

The last approach combines the angular shearing fan starting from the inner corner of the ECAP die of SF-PDZ model with the rotation zone of the PS-PDZ model and predicts a fully splitted (FS) yielding during ECAP processing [SEG03]. Accordingly, the shear strain for material travelling in the rotation zone on the outer side of the die is calculated with Equation 2-12 and the one in the shearing fan with Equation 2-10. A major disadvantage of this approach is that it predicts an abrupt decrease of the shear strain along the boundary between split fan and free rotation zone. Although there are many approaches to model the shear deformation during ECAP processing, the difference between the predicted strain values are fairly small, especially for a die system with a larger channel angle than 90° and a small arc of curvature [STO05].

Besides strain development during ECAP processing, the force requirement to deform materials was also in the focus of former analytical studies. The slip-line field (SLF) theory is utilized in these investigations. By the SLF theory, it is assumed that the material yields along planes of maximum shear stress (in PDZ) which are oriented at 45° to the axes of principal stresses [HOS07]. Outside PDZ, it is considered as perfectly rigid. Moreover, plain-strain deformation prevails in the PDZ. Therefore, this theory is mostly used to describe 2D processes such as rolling and is not suitable for forming operations where cylindrical samples are deformed in radial direction. However, since the main deformation mode by ECAP is plane shear, SLF theory is suitable also for cylindrical ECAP samples.

Furthermore, SLF theory is incapable of demonstrating the effects of temperature generation or strain rate. Nevertheless, implementing the temperature and strain rate dependent yield strengths in the model enables an accurate prediction of deformation forces for a particular process.

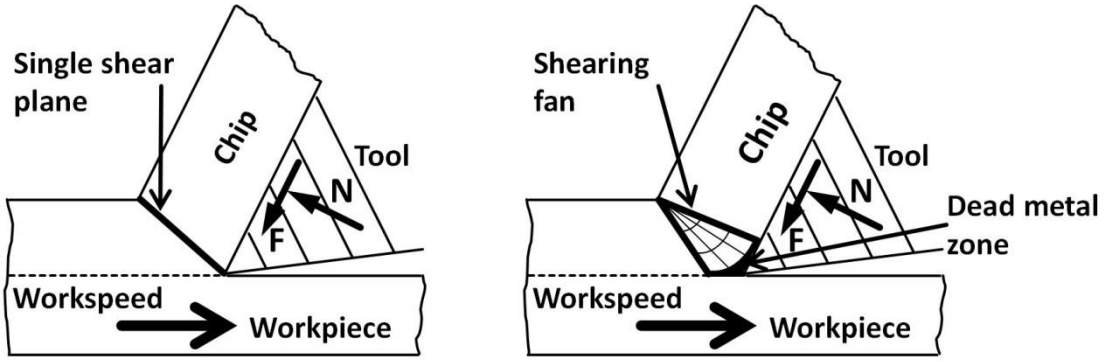

Figure 2-4 Single shear plane and shearing fan deformation system by orthogonal cutting [ERN41]

Due to the resemblance of the mechanics of ECAP to orthogonal cutting (Figure 2-4), the same SLF approach has been used to predict the process forces by ECAP [ERN41]. As by orthogonal cutting process, two different deformation systems have been investigated (Figure 2-5). For both cases, it is assumed that the material moves progressively inside the entry and exit channels with a constant speed, V.

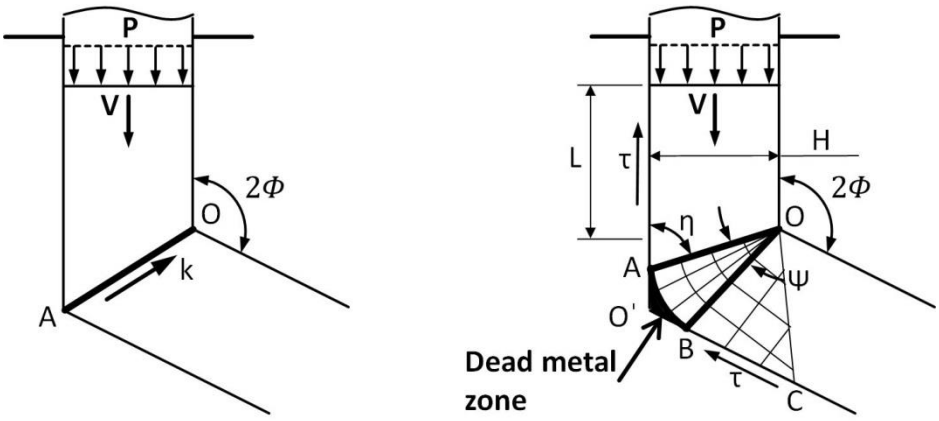

Figure 2-5 Single shear plane and shearing fan deformation system by ECAP [SEG99]

The first solution assumes the plastic deformation zone as a single plane between the inner and outer corners of the tool system and no force is applied on the sample at the exit channel of the tool. In that case, the tool-workpiece interfaces are considered as frictionless. Consequently, the pressure, P, required to push the sample through the single plane PDZ is calculated with the following formula [SEG99]:

$$P = 2k \cot \phi$$ *Equation 2-14*

where *k* is the shear yield strength of the investigated material.

The second solution considers additionally the effect of friction stresses,τ, along tool channel walls on the geometry of the PDZ. In that case, the PDZ includes a central fan AOB, a dead metal zone (DMZ) AO'B where the material is stationary and only yields at the boundary AB of that section and a uniform stress zone BOC. It is assumed that the shearing fan, Ψ, is caused by the friction stress on the tool walls and is defined similar to the orthogonal cutting theory as:

$$\psi = 2(\eta - \phi)$$ *Equation 2-15*

where η is the angle between slip lines (AO and BO) and the tool walls. Accordingly, it is defined as $\eta = \frac{[\pi - Arc\ \cos(\tau/k)]}{2}$. This relationship is only valid when $\psi > 0$. Therefore, the punch pressure is represented as follows:

$$P = 2k \cot \eta + 4k(\eta - \phi) + \frac{\tau}{(\sin \eta (\sin \eta + \cos \eta))}$$ *Equation 2-16*

Moreover, it is suggested that the DMZ is only present when the friction stress on the die walls is equal or exceeds the value of $k \cdot cos\phi$. Otherwise, Equation 2-16 reduces to the frictionless state defined with Equation 2-14. Hence, the formation of DMZ is highly unlikely for channel angles (2ϕ) greater than 90°.

For the case where an additional back pressure P_0 is applied on the sample, punch pressure, P, is calculated simply by adding the P_0 to the Equation 2-16 [SEG03]. However, the effect of that additional pressure, P_0, on the pressure state in the entry channel of the tool system and accordingly on the friction state is neglected in these previous studies. Moreover, due to the small clearance between the sample and the ECAP tool walls, it is assumed that the contact in the entry channel is only present when the punch pressure, P, exceeds the yield strength of the material [SEG04]. Nevertheless, since metals are deformed elastically under loads lower than their yield strength, this assumption is physically invalid. Nonetheless, the effect of friction in the entry channel is demonstrated with the following formula [SEG04]:

$$P = P_1 + \frac{\mu F k}{A} \qquad \textit{Equation 2-17}$$

where P_1 is the punch pressure calculated either with Equation 2-14 or Equation 2-16, μ is the friction coefficient, F is the area of the stationary die walls in the entry channel and A is the cross-section area of the sample.

The developed analytical approaches enable a quick estimation of punch forces for a single turn ECAP process. The estimations also agree well with the numerical investigations assuming frictionless contact [ZUY99, XU08]. However, these formulations have some drawbacks for cases where the friction is not neglected. First of all, for the commercially more interesting case without the formation of DMZ, Equation 2-17 considers only friction forces in the entry channel. Such a simplification yields in underestimated results. Moreover, the reaction forces acting, for instance on the right wall of the entry channel in Figure 2-5 and their related friction forces are completely neglected in these approaches. These reaction forces are of high importance especially when a channel angle (2ϕ) other than 90° is used. Furthermore, the effect of the back pressure on friction forces is omitted in the previous studies about the analytical representation of punch forces. Additional press forces after material reaches the second deformation zone by a 2-turn ECAP are also considered as back pressure.

Beside the crucial advantages, ECAP technique has some limitations in its basic form. First of all, the length of the ECAP processed workpiece is limited, on one hand, by the ratio of the sample length to diameter to prevent buckling of the press punch, on the other hand; by the limited travel distance of the conventional press rams, with which the basic ECAP is majorly conducted [FER08]. Due to the limitation of the sample length and batch type process characteristics, ECAP is regarded as a discontinuous forming method with low efficiency and high costs. Secondly, ECAP is characterized with a strain inhomogeneity at the end section of the samples and in the vicinity of the contact areas with the tools. This disadvantage reveals itself as non-uniform microstructure and mechanical properties on the cross section as well as macro-cracks at the end of the processed samples. The parts of processed material with the inhomogeneities or macro-cracks has to be mostly removed and thrown away thus wasting a significant portion of the material and further increases the production costs. Although the inhomogeneity problem on the contact areas can be solved by applying a back pressure on to the samples during forming, this back

pressure increases the contact normal stresses on the tool surfaces and hence the friction losses and increases therefore the risk of punch buckling [McK10a, McK10b, FRI11].

Although ECAP is the most investigated and developed SPD project, the process related drawbacks increase the production costs of UFG materials with this technique. Therefore, the industrial applications of ECAP processed samples are limited to a few applications where the material costs do not play a major role in the buying decision.

2.1.2 Secondary Equal Channel Angular Pressing Processes

In order to overcome the process related problems, which hinders a wide commercialization of UFG materials, many secondary SPD processes have been developed over the last two decades. The following subchapters give an overview of enhanced and optimized ECAP processes. The improved secondary ECAP processes mostly address the continuity or efficiency problem.

Derivative Processes

Repetitive side extrusion (RSE) process, rotary-die ECAP (RD-ECAP) and friction optimized ECAP are the three major derivative processes similar to the conventional ECAP [AOK03, AOK07, AZU02a, AZU02b, AZU07, NIS01, KIM03] (Figure 2-6). RSE is distinguished with a high back pressure which is applied on the samples during forming to enable a homogeneous shear deformation and to prevent defects in the processed material. The homogeneous shear deformation results in a more homogeneous distribution of microstructure and mechanical properties along the cross-section of the processed material while the prevention of the defects increases the efficiency of the overall process by improving the material utilization. However, in this process, the application of a back pressure necessitates an active control of the mostly hydraulic driven back pressure punch. Moreover, contact normal stresses on the tool surfaces and the corresponding friction losses increase as a result of the back pressure in RSE process.

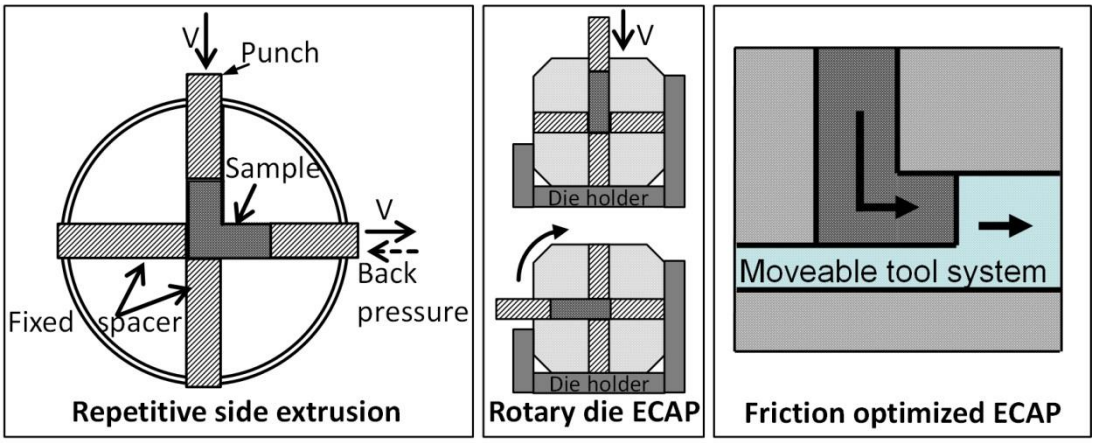

Figure 2-6 Schematic representation of repetitive side extrusion (left) [AZU02a], rotary die ECAP (center) [NIS01] and friction optimized ECAP (right) [AZU07] processes

Rotary-die ECAP (RD-ECAP) aims at the improvement of the process by optimizing the sample removal and re-insertion work between two consecutive passes. A RD-ECAP die consists of four forming channels with the same cross-section intersecting in the middle of the tool system with a 90° angle. A high strain can be accumulated in the materials by pressing the sample through the first channel, than rotating the tool system around its center axis and repeating the press procedure (Figure 2-6.center).

RD-ECAP process permits the successive forming of the same sample without removing it from the tool system and thus enables a significant amount of time saving. Nevertheless, after finishing the multi-pass forming of one sample, an additional extraction mechanism is required to remove the deformed sample from the die. Moreover, only the processing route C is possible with the RD-ECAP method. Furthermore, the workpiece can just be lubricated before the first forming pass. The lack of lubrication after the first pass causes an increase in the friction forces during the process and results in an inhomogeneity in the microstructure and mechanical properties [MA05]. Therefore, more forming passes are required to generate a homogeneous microstructure by the RD-ECAP process compared to the conventional ECAP.

Another derivative process which directly addresses the friction problem is the friction-optimized ECAP (Figure 2-6.right). By this technique, the entry or the exit channel of the ECAP tool system surrounding the specimen moves together with the sample during forming. Thus, the friction losses on the side walls of entry or exit

channel can be omitted [MAT06]. Such a tool arrangement enables the forming of long parts with an extremely large cross-sectional area [FRI11]. Moreover, friction-optimized ECAP is also used by the one of the very few commercial applications of UFG materials [FER08].

However, as by the basic ECAP, front and end sections of the processed materials have microstructural inhomogeneities.

Integrated Processes

Integrated extrusion-ECAP and parallel channel ECAP are the two significant examples for integrated processes [LIU98, NAK00, ORL11, ROS02]. Integrated extrusion-ECAP enables the accumulation of very high plastic strains in the deformed material in only one processing step. Moreover, the subsequent severe plastic forming after extrusion suppresses the dynamic recrystallization. However, this process has to be conducted at elevated temperatures. Hence the energy efficiency is highly reduced. Furthermore, due to the necessity to work at elevated temperatures, the material spectrum formable with that process is limited to copper, aluminum, magnesium and their alloys. Because of the temperature limit of the tool materials, the deformation of higher strength materials such as steels is not possible with that processing route.

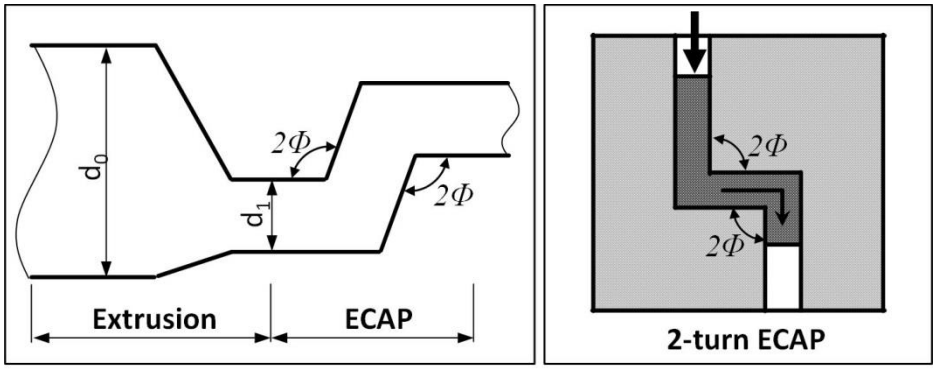

Figure 2-7 Schematic representation of integrated extrusion-ECAP (left) [ORL11] and 2-turn ECAP (right) [ROS02]

Parallel channel ECAP (also known as 2-turn ECAP) facilities enable multiple forming of the same sample in one tool system. Unlike conventional ECAP, these tool systems consist of three or more channels which intersect at an obtuse angle [LIU98, NAK00, ROS02]. Such a multiple forming permits the accumulation of the strains to

higher levels after less number of forming passes (Figure 2-7.right). Thus, an UFG microstructure can be reached more quickly. Moreover, since the forming sections after the first yielding line act as an artificial back pressure punch, the processed samples are more homogeneous in terms of microstructure and mechanical properties.

However, the second shearing of the material in case of 2-turn ECAP more than doubles the press forces required to form the sample. The underlying reasons are on the one hand the increase in the strength of the material after the first forming section and on the other hand the increase in the friction losses related to the rise of the contact normal stresses after the second forming section [KIM02]. Therefore, the sample length is more strictly limited in 2-turn ECAP compared to the conventional ECAP. Moreover, the ejection of the processed samples after a multi-pass forming poses a major challenge. Combined with the increased press forces and contact normal stresses, sticking of the samples in the tool system is more likely than in conventional ECAP.

The previously explained secondary ECAP processes are capable of improving the efficiency of conventional ECAP or the homogeneity in the ECAP processed samples. However, every derivative has also its disadvantages. Due to their low productivity, these processes are only used in laboratory studies. For mass production, continuous processes should be developed. Following subchapters give an inside into the continuous or automated ECAP processes developed in the last two decades.

Continuous Processes

The first continuous ECAP derivative is the equal channel angular drawing (ECAD) which bases on the concept of pulling the material through the SPD-die rather than pushing it [CHA98]. By this means, the buckling risk of an ECAP punch is completely eliminated (Figure 2-8). Thus, theoretically, samples with infinite length can be severely plastic deformed. Moreover, ECAD process can be used as an intermediate state in industrial processes to increase the strength of materials [PER03]. Furthermore, ECAD can be also applied to sheet metals [ZIS06].

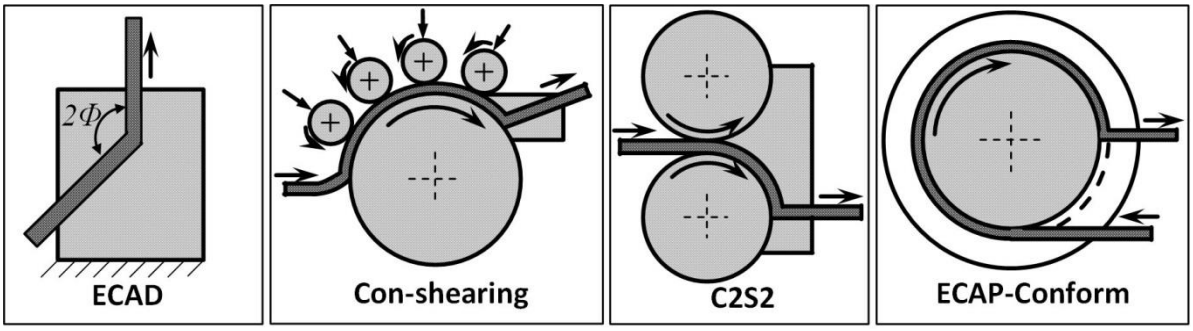

Figure 2-8 Schematic representation of ECAD [CHA99], Con-shearing [SAI99], continuous confined strip shearing [LEE01] and ECAP-Conform [RAA04]

However, this first continuous SPD process has many drawbacks. First of all, in order to prevent the fracture of the processed materials under high tensile loads, a high channel angle has to be selected, which, in turn, decreases the induced plastic strain in one pass. Moreover, the tensile loads result in a thinning in the samples. Thus, deformed materials have smaller cross-sections. As a result of the thinning, the tool channels cannot be filled in the second pass which leads to a strain heterogeneity. Therefore, ECAD is not suitable for a continuous production [ALK02].

Another continuous ECAP derivative, Con-shearing is proposed in the late 90s [SAI99]. In Con-shearing, the shear deformation is continuously introduced to sheet metal strips. During the process, samples are fed into an ECAP die by means of one central roll with a rough surface and many satellite rolls with smooth surfaces (Figure 2-8). A pressure below the yield strength of the processed material is applied onto the satellite rolls in order to generate the friction force on the surface of the center roll required to feed the metal strips into the ECAP die. In order to prevent buckling of the sample metal, guide shoes are placed between the satellite rolls. From process point of view, it is advantageous to have a high friction factor on the driven central roll and a low friction factor on the ECAP die.

The Con-shearing process is successfully applied on aluminum alloys [SAI00]. The processed materials conserve their cross-sectional geometry [UTS01]. However, this process is only suitable for the forming of sheet metals. Moreover, a high channel of 90°, which represents the optimum angle for ECAP, is not applicable to the Con-shearing process [NAK98]. Such an arrangement would result in compression of the processed material rather than extrusion in the ECAP die. The optimum channel for Con-shearing is 65° [UTS04]. Furthermore, for the forming of higher strength

materials, larger feeding forces would be required, which simultaneously necessitate more satellite rolls. In such a case, the dimensions of the Con-shearing tool system would drastically increase which also raise the investment and operational costs.

Continuous confined strip shearing (C2S2) was proposed around the same time as Con-shearing [LEE01] and has many similarities with this process. By C2S2 process, a driven roll with special teeth on its surface is used to feed strip shaped materials through an ECAP-die with channel angles varying between 100° and 150°. The adjustment of the position of the lower die enables controlling the scalping depth of a C2S2 process (Figure 2-8). Beside grain refinement, C2S2 process is majorly used for the adjustment of texture orientation in aluminum alloys [KAN08, HAN02, HAN04].

Relatively high processing speeds up to 50 m/min can be realized with C2S2 processes. Additionally, C2S2 utilizes friction on the driven roll to feed the sheet metals into the ECAP die and minimizes simultaneously the friction losses in the entry section of the process. Therefore, a fairly homogeneous effective strain distribution is observed in the C2S2 samples. Hence, a high friction between the driven roll and the sheet metal eases the feeding of the material into the process. However, a high friction simultaneously decreases the tool life. Furthermore, for the ECAP die section, a low friction factor is still required in order to assure the reliability. Moreover, low channel angles on the ECAP die section drastically increase the torque requirement in the feeding roll and thus their avoidance is recommended. In addition, C2S2 process is only suitable for the forming of sheet metals [XU08].

Unlike C2S2 or Con-shearing, ECAP-Conform process makes use of the three surrounding surfaces of the groove in a center roll to feed the samples into an ECAP-die (Figure 2-8). The rotating center roll is enclosed in a stationary constraint die. That way, the material to be processed is grabbed from three sides. In such a configuration, higher forces can be applied onto the samples compared to the other continuous ECAP derivatives. Therefore, workpieces in the form of a rod with a square or rectangular cross-section can be formed by ECAP-Conform where higher forces are required to feed the material in the ECAP-die than with sheet metals [RAA04].

Compared to C2S2 and Con-shearing processes, forming with lower channel angles is possible with ECAP-Conform which yields in higher strains in one pass and thus increases the efficiency. Moreover, ECAP-Conform processed samples are fairly

homogeneous in cross-section as well as in length [XU10]. On the other hand, ECAP-Conform processed materials have mostly small cross-sections up to 81 mm^2 [POL11]. Recent studies show that samples with bigger cross-sections can be formed but only with a higher channel angle yielding in a lower accumulative strain per pass [GUN13]. Therefore, it is assumed that ECAP-Conform is suitable for the continuous production of high length-small cross-section materials.

Automated processes

A recently proposed spring-loaded ECAP technique addresses the efficiency problem of current SPD problems by increasing the output by automation (Figure 2-9.left). In this process, previously cut specimens are fed into the forming system while the case containing the sliding tool and the punch is retracted. In the pressed position of the case, the sliding tool forms the entry channel of the tool system. After pressing the specimen, the case is retracted to free the processed material [JIN11].

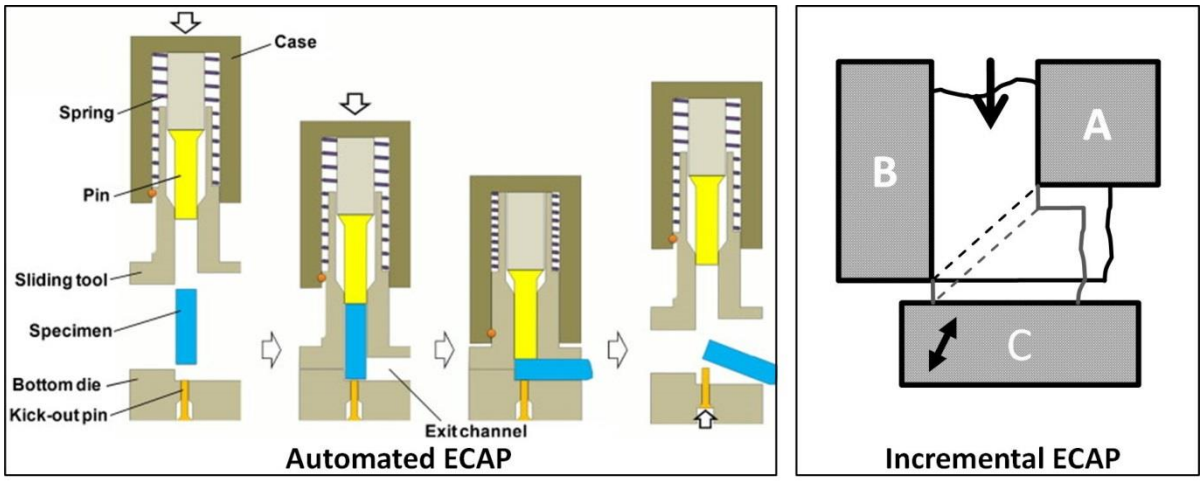

Figure 2-9 Schematic illustration of spring-loaded ECAP (left) [JIN11] and incremental ECAP (right) [ROS07] processes

Spring-loaded ECAP greatly increases the productivity of bulk UFG material manufacturing processes. The bolts, produced from materials which are first deformed with this technique are distinguished with a higher strength compared to their unprocessed counterparts [JIN12]. Although spring-loaded ECAP is a highly efficient process, it only enables the increase of the outcome of conventional ECAP. The specimen length is still limited by this technique to avoid buckling of the punch. Moreover, a small portion of the material with geometrical inhomogeneities at least at

the end section of every specimen has to be discarded. Therefore, spring-loaded ECAP can be efficiently utilized for a niche market, where short parts are required.

A novel approach to solve the friction problem in ECAP processes has been proposed by Rosochowski and Olejnik [ROS07]. They suggested forming the material gradually and called the new process incremental ECAP (I-ECAP). An I-ECAP tool system consists of a stationary die body and a moveable forming wall as well as a feeding unit (Figure 2-9.right). During I-ECAP, the moveable die wall is opened before forming so the material can be fed freely. After clamping the sample in the forming position, the moveable wall pushes the material into the groove of the stationary die body.

Since the relative movement between I-ECAP tool walls and the specimen is relatively small for every stroke, the friction is minimized by this process. Moreover, discontinuous contact enables the lubrication of tool surfaces during forming and thus further reduces the friction losses and increases tool life. Such a technique can be applied to rod type materials as well as sheet metals [OLE08, ROS10, ROS11]. Moreover, a multi-pass variant consisting of two forming sections in one tool system is also reported [ROS08a, ROS08b]. Therefore, incremental SPD methods have a great potential for the continuous production of bulk UFG materials.

2.2 Incremental Metal Forming

Incremental forming is the oldest known metal forming technique in the history of civilization. In prehistoric ages, it was used to produce simple tools, ceremonial items and primitive weaponry of copper [DER05]. With the development of new materials, such as bronze and Damascus steel, incremental forming methods began to be used in the manufacturing of comparatively more sophisticated items [SHE01]. Since the industrial utilization of this technique requires accurate control of the process as well as of the forming machinery, incremental forming methods were not able to compete with the newly developed comparatively simpler metal forming techniques of mass production, i.e. multi-stage closed-die forging, after the industrial revolution. As a result, this craft lost importance in the 20th century [GRO05a]. Due to the developments in process monitoring and controlling technology in the last decades, incremental forming processes are rescued from oblivion and are regaining their popularity.

A forming process is defined as an incremental metal forming process if within one production stage particular regions of a metal workpiece, which are relatively small compared to the whole part, experience more than one loading and unloading cycle due to the action of one set of tools [GRO07]. The different aspects of this definition should be clarified for better understanding. The tool set geometry does not represent the final geometry of the workpiece. On the contrary, the desired geometry in the workpiece is reached through many small forming steps. During an incremental forming process, particular regions of the workpiece which are in contact with the forming tools are formed. After forming, these regions loose contact with the tools. This loading and unloading cycle affects a relatively small section of the workpiece, but not the whole part. The desired geometry of the final part is reached while this forming region moves along the workpiece. If the final geometry for this particular region cannot be reached within one loading and unloading cycle, it can be repeated as many times as necessary within one production stage.

During the industrial revolution, incremental forming processes lost their competitiveness against other forging methods because the kinematic of the forming tools by incremental methods was comparatively more complex than those of the other mass production techniques, such as upsetting or deep-drawing. Even today, the complex tool kinematics is seen as one of the major disadvantages of these processes. Nevertheless, with the use of current technologies in monitoring and controlling, automation of the incremental forming machines has become possible since the last quarter of the 20th century. But still, the complete process and tool design requires the machine builder’s know-how. The whole forming process is divided into many small forming steps. This feature of this technique causes the repetition of similar tool movements until the desired geometry is obtained. This repetition results in an increased process time compared to the other single step processes. This feature is seen as the main disadvantage of the incremental forming processes.

Despite these disadvantages of incremental forming methods, some characteristics and advantages of these processes do exist. The forming forces are considerably lower in incremental techniques compared to single step methods. This feature makes them interesting for forming applications of long parts, where buckling mostly limits the part length. Due to the low forces, the forming tools as well as the forming machines are less loaded. Due to the low loads, the friction forces also decrease. As

a result, the tool life is prolonged. Simultaneously, the machine costs are lowered because lesser loading enables a compact design of functional parts.

Another advantage of incremental processes is the lower tooling cost. Tools are comparatively simple. A wide product range can be produced with no or minor changes in the tooling system. This is, for instance, very advantageous in those cases where the production needs to be flexible to respond to customer needs.

2.2.1 Classification of Incremental Forming Processes

Incremental forming processes can be categorized by the initial workpiece geometry into incremental sheet metal forming and incremental bulk metal forming. The incremental bulk metal forming can be roughly divided into forging and rolling processes. Thereby, the classification takes place according to the kind of tool motion. Processes with mainly translative tool movements are assigned to the forging processes, those with rotatory tool movements to rolling processes (Figure 2-10).

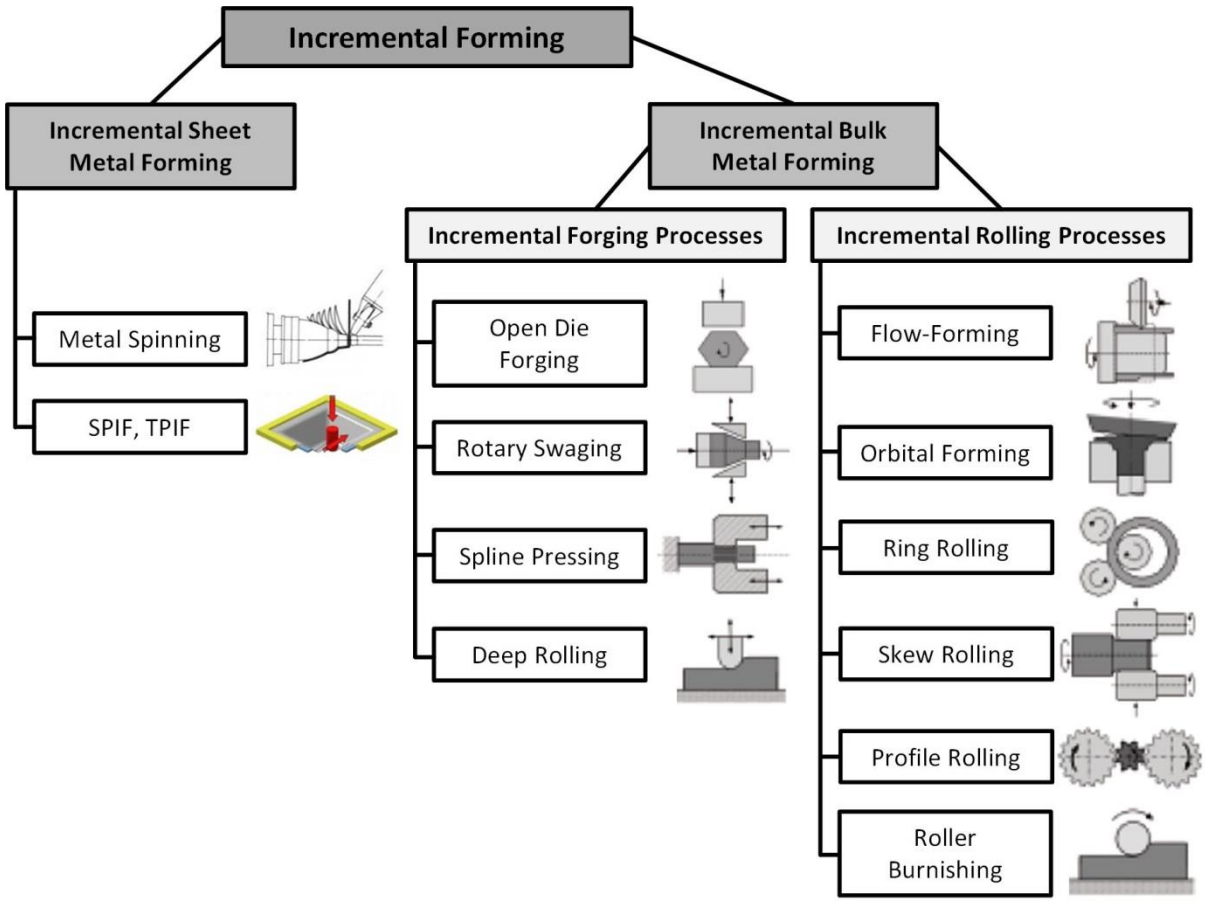

Figure 2-10 Classification of incremental forming methods [GRO07]

2.2.2 Rotary Swaging

According to the DIN 8583, rotary swaging belongs to the “Forming under compressive conditions” main group of forming processes and under this main group to the “Free forming” subgroup [DIN8583]. This process is an incremental bulk metal forming method, mostly used to produce tubes, bars and wires. However, the production of non-axisymmetric parts, such as screw drivers is also possible. The characteristic setup of a rotary swaging machine is shown schematically in Figure 2-11. During the swaging process, tool segments, which are arranged concentrically around the workpiece, perform high frequency radial movements with short strokes. Depending on the machine size and configuration, stroke frequencies may vary from 25 to 170 Hz with stroke lengths of 0.2 to 5 millimeters. The radial movement of the tool segments is for most of the machine types simultaneous. The tool segment number can vary from two to eight. In order to prevent the material to flow in the space between the tool segments, either the samples or the tool segments itself are rotated during swaging.

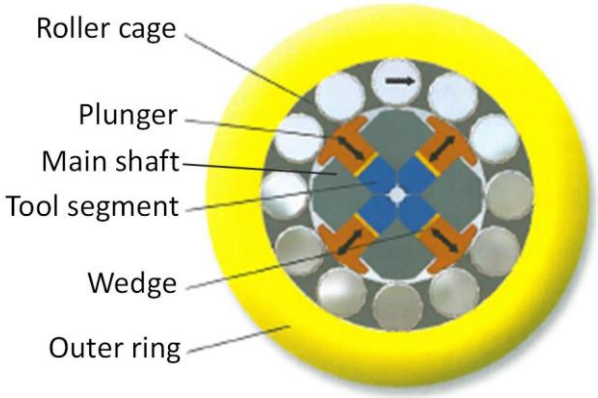

Figure 2-11 Setup of a rotary swaging machine [KIE03]

There are three major types of rotary swaging machines regarding the tool kinematics. By the internal rotating system machines, the outer ring is stationary and the main shaft is rotating. Such an application enables the production of long axisymmetric parts. On the other side, by the external rotating system machines, the outer ring rotates and drives the oscillation of the tool segments while the main shaft is stationary. Such an arrangement enables the forming of non-axisymmetric parts where the workpiece should not be rotated with respect to the tool segments. By the

double rotating system, both the outer ring and the main shaft rotate in opposite direction to increase the oscillation frequency.

Three major variants are known for rotary swaging (Figure 2-12). During infeed swaging, the workpiece is fed with a constant axial speed through the oscillating tool segments. On the other hand, during recess swaging, the oscillating tools perform a radial closing movement in addition to the oscillating movement while the workpiece is already positioned between opened tools. The swaging over mandrel is a further development of infeed and recess swaging. In that case, the workpiece is fed into the oscillating dies. However, before forming, a mandrel is placed into the pipe shaped material. Thus, during swaging, the outer section as well as the inner section can be formed. Depending on the geometry of the mandrel, different inner shapes are possible by this process variant.

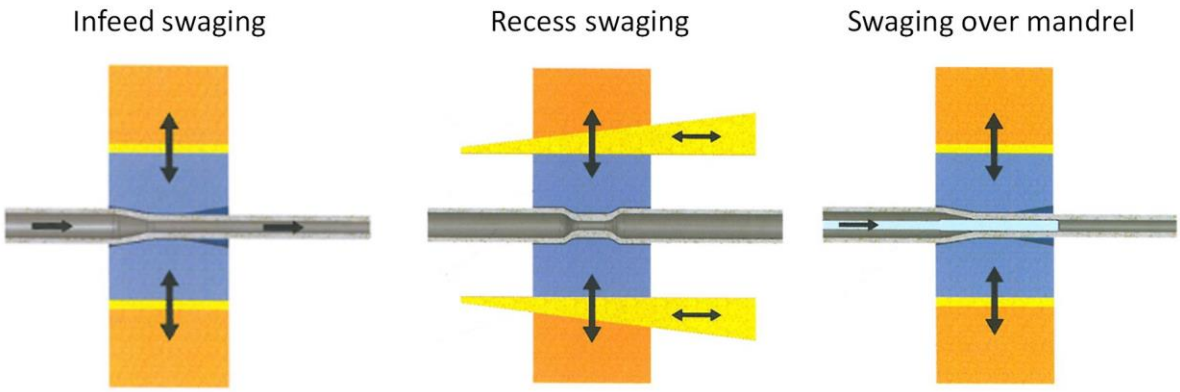

Figure 2-12 Different swaging methods [KIE03]

In addition to the relative rotation of workpiece and tool segments, the radius of the tool geometry has to be larger than the initial radius of the sample to prevent the formed material to flow into the space between the tools in opened position [HEI01]. The ratio of initial radius of workpiece (r_{wp}) to the tool radius (r_t) is called osculation (s) [KRÜ96]. For most cases, the osculation value is taken less than one. However, for the forming of thin walled pipes or non-axisymmetric parts, this value is mostly taken as one.

$$s = \frac{r_{wp}}{r_t} \leq 1 \qquad \textit{Equation 2-18}$$

Due to the oscillating movement of the dies with a high frequency, the forming takes place in many small processing steps in very short times, which enables high plastic strains within a single forming process. High plastic strains combined with the short forming cycles result in high plastic strain rates. Therefore, an adiabatic heating is mostly expected in the processed materials. The deformation is distributed almost evenly over the whole cross section of the workpiece [MUE97]. Hence, the increase in strength related to the strain hardening is homogeneous in the workpiece. Since the entire forming is divided into many steps, the required press forces are quite low [RAT06]. This feature enables a simple and compact design of the rotary swaging machine. Additionally, as the contact time between dies and workpiece is very short due to the oscillation movement, the friction is minimized during the forming [MUE97]. Therefore, a surface treatment of the billet or an active lubrication in the system is not necessary in most cases. The achievable tolerances in the outer section as well as in the inner section of the workpiece are extremely tight, corresponding to the tolerance classes IT 6 – 10 [GAE99]. Due to this feature, the formed parts are often ready to install without any additional operations. Therefore, the whole process chain up to the finished part can be shortened and costs can be reduced with the use of this forming method. Another advantage of the rotary swaging process lies in the simplicity of the forming dies. The form of the dies is not bound to the end geometry of the workpiece. Hence, smaller changes of the part can be realized with simple adjustments of the machine control without producing new dies. Thus, the process is suitable for mass production as well as small batch sizes.

2.3 Numerical Simulation and Modeling of Forming Processes

According to the guidelines of the Association of German Engineers (VDI-Verein Deutscher Ingenieure), a simulation is the reproduction of a process in a model which embodies its dynamic properties [VID93]. This model is used to investigate the insights of the process and the gained knowledge can be transferred to the reality.

Depending on the stage of design phase, simulations can be used for different purposes [WUN05]. While these can serve to investigate the feasibility and the potential problems in the pre-prototype phase, they are mostly used to examine the insights of an existing process after the successful implementation.

In metal forming, the term “simulation” is mostly used for the numerical investigation by means of the finite element method (FEM). Since the mathematical and

computational backgrounds of FEM are not the focus of this study, these can be referred from specialized literature [STE07].

2.3.1 Modeling Material Behaviour by Finite Element Simulations

Besides the mathematical parameters such as element formulation or matrix solver type, the modeling of the material's mechanical behaviour is the most significant factor influencing the results of the investigation, especially for metal forming operations. In this chapter, a short review will be given about the major models and methods to determine the parameters associated with these models.

Two basic approaches are material modeling and constitutive modeling. Material modeling implies the mathematical definition of the uniaxial flow behaviour for a specific material depending on the strain, strain rate and temperature. By this concept, the mathematical definition of flow stress differs from material to material. On the other hand, constitutive modeling involves the development of general equations for materials and defining the flow behaviour of the specific material by adjusting the model parameters using material test results [DIX11]. Major material models are summarized in Table 2-1.

Table 2-1 Major material models showing the dependency of flow stress

Empirical model	**Name**
$\sigma = \sigma_y + K\varepsilon^n$	Ludwik's expression
$\sigma = \sigma_y\,(1 + K\varepsilon)^n$	Swift's expression
$\sigma = \sigma_y + K\left(1 - e^{-(n\varepsilon)}\right)$	Voce's expression
$\sigma = \sigma_y \left(\frac{\varepsilon}{\varepsilon_0}\right)^n \left(\frac{\dot{\varepsilon}}{\dot{\varepsilon}_0}\right)^m \left(\frac{T}{T_0}\right)^\tau$	Power law model
$\sigma = (A + B\varepsilon^n) \cdot \left(1 + C \ln\left(\frac{\dot{\varepsilon}}{\dot{\varepsilon}_0}\right)\right) \cdot \left(1 - \left(\frac{T - T_0}{T_m - T_0}\right)^m\right)$	Johnson-Cook model

The first three models in Table 2-1 predict the strain hardening of the material without taking the effect of strain rate and temperature into consideration. Yield strength parameters for these models are derived from tensile testing. The other parameters are determined by adapting the analytically calculated flow curve on to the one derived from tensile testing. All these three models are capable of modeling the

material behaviour especially for low strain levels. However, for high plastic strain, their accuracy is doubtful [DIX08]. A novel approach to improve these models, especially for high strain levels suggests combining the tensile testing with upsetting to define the parameters [MÄN12]. By this method, first of all, the required material parameters are determined by means of tensile testing. Afterwards, upsetting experiments are conducted with the same material. Material data derived from tensile testing is implemented in a FE simulation model of this particular upsetting test. By incremental variation of the parameters, upsetting force or stress results obtained from FE simulation are adjusted to the ones from upsetting test. It is reported that this method delivers better results than simple tensile testing especially for bulk metal forming processes.

The last two models in Table 2-1 consider also the effect of strain rate and temperature. Both models predict the flow stress as a function of strain, strain rate and temperature. The main advantage of Johnson-Cook model over power law model is that it is implemented in nearly every FE-software.

Although these two models are well-accepted and numerically solid, the determination of the material parameters still represents a major challenge. They both are majorly used for the numerical simulation of metal machining processes where the strain rates and temperatures are high compared to cold bulk metal forming applications. Taylor's impact test, Hopkinson's compression or shear devices are used for the definition of material properties. Plastic strains nearing 4, strain rates as high as 2×10^4 s^{-1} and temperatures of 300°C can easily be reached with the mentioned testing methods [ARR13]. However, for the modeling of cold bulk metal forming processes, neither such high strains nor such high strain rates are required. Therefore, standard tensile testing or upsetting at room and at elevated temperatures can be used to determine the parameters.

2.3.2 Finite Element Simulation of SPD Processes

Over the past 15 years, researchers used different approaches for the simulation of SPD processes. These vary from each other in terms of used finite element software, solver type, modeling strategy, element type and formulation. An overview about their usage will be given in the following.

First investigation of ECAP process by means of FE method dates back to 1997. In this study, Prangnell et al. examined the effect of channel angle and friction on the

effective strain and material flow of an Al-0.15% Mg alloy with the aid of the commercial FE software DEFORM [PRA97]. They used a 2D approach assuming plain strain conditions. The same software and approach was also utilized in further studies of many researchers. Kim et al. investigated the effect of the outer corner angle on the strain homogeneity using also DEFORM software with 2D plain strain approach [KIM01]. In a later study, the same group examined the material behavior for a multi-pass ECAP-toll system where samples are formed two times [KIM02a]. The effect of the processing route in a sequential ECAP process, in particular the route C, was investigated also by Figueiredo et al. using 2D simulation models [FIG06].

The deformation behavior during conventional ECAP is investigated by Suh et al. for a frictionless condition by varying the outer corner angle using the explicit solver of the commercial software Abaqus and two dimensional plain strain approach [SUH01]. Their findings are extended by examining also the effect of friction in a later study using the same simulation approach [NAG04]. Kim et al. further extended the investigations by varying also the channel angle using similar FE approach [KIM02b]. The homogeneity of the strain distribution along the cross-section of the deformed material lied in the center of the evaluation for all of these FE-simulations.

The effect of a back-pressure was simulated by Son et al. using an in-house simulation software CAMPform-2D [SON06]. This group studied different versions of back pressure application with a 2D plane-strain approach. They used linear quadrilateral elements to model the sample.

Wei et al. was the first group which validated their FE-simulations with visio-plasticity (VP) experiments [WEI06]. They used 2D plain strain formulation of the commercial FE-software Abaqus to investigate the deformation behavior in the ECAP-processed CP-copper samples under variation of the outer corner angle. For validation purposes, this group used samples which were marked in their longitudinal cross-section and examined the deformation of these markings after forming with ECAP.

Zhao et al. was the first group to investigate the conventional ECAP process with the implicit solver of the FE-software MSC.Superform [ZHA05]. They examined the effect of channel angle and outer corner angle as well as process route on the strain distribution in the processed samples.

Since conventional ECAP is a three-dimensional process, it requires also 3D-simulations to investigate certain aspects, for instance the effect of processing route B. Xu et al. were the first ones who utilized 3D simulations to study the influence of the processing route, especially the route B on the strain distribution during conventional ECAP [XU06]. They used the commercial FE-software DEFORM 3D with tetrahedral elements and assumed a frictionless state for the process. In a later study, Mahallawy et al. investigated the effect of the same parameters on the strain homogeneity by taking into account the increase of the material strength after every forming pass in a sequential ECAP process using the same simulation software and parameters [MAH10].

Suo et al. additionally investigated the influence of the friction between ECAP-die surfaces and the workpiece on the deformation distribution by means of 3D-simulations [SUO06]. They used the explicit solver of the Abaqus software. In a later study, the same group also investigated the effect of channel angle and processing route using the identical simulation software and parameters [SUO07].

Although the strain distribution or, more explicitly, the homogeneity of the strain distribution was the main focus of the FE-simulations of conventional ECAP process, this technique is used also for other purposes. For instance, Kang and Kim developed in their study an empirical method to predict the average grain size of the severe plastic deformed materials after forming by ECAP process using the explicit solver of the FE-software Abaqus [KAN10]. They used the 2D plain strain approach in their simulations.

Zuyan and Zhongjin were the first ones who predicted the process loads with the aid of FE-simulations [ZUY99]. They used the 2D solver of the software package H-FORGE in their studies and investigated the influence of channel angle, friction factor, tool clearance and material strength on the maximum press loads during one step and two step conventional ECAP. In a later study, Li et al. examined additionally the effect of the outer corner angle on press loads by using the 2D explicit solver of the Abaqus software [LI04].

Jiang et al. used 3D algorithms to predict the loads for a sequential four pass ECAP process [JIA08]. They used the DEFORM software in conjunction with four node tetrahedral elements. After every forming pass, the material is characterized with

tensile testing. Afterwards, these test results are implemented in the FE-model. That way, they were able to predict the press load increase in consecutive ECAP passes.

Beside conventional ECAP, FE-simulations are also used for design and analyze purposes of derivative ECAP processes. Rosochowski and Olejnik defined the correlation between the channel length and the strain distribution for a multi-pass ECAP with two forming sections in one tool system [ROS02]. They used the explicit solver of Abaqus. The sample is modeled with plane strain, bilinear, quadrilateral elements with reduced integration formulation. In this study, the research group also verified the simulation results with VP-experiments. Similarly, Djavanroodi and Ebrahimi investigated the same process with the 3D solver of the software package DEFORM [DJA10]. They varied channel angle and channel length in the simulations and examined their effect on the strain distribution and process loads.

Deformation behavior by C2S2 process is analyzed by Wei et al. using a 2D approach with the finite element code DEFORM [WEI09]. This group investigated the effective stress and strain distribution as well as the torque required to drive the feeding roll in the process by varying the channel angle and friction coefficient between the die surfaces and the sample.

Incremental-ECAP was simulated by Rosochowski and Olejnik to investigate the feasibility of this process and to define the design guidelines [ROS07]. The same group also examined a multi-pass version of the I-ECAP containing two forming sections in one tool system [ROS08b]. They used for both simulations the explicit solver of the FE-software Abaqus.

Since the deformation of the tools is only in elastic state and therefore can be neglected, it is a common practice to model the tools as a rigid body in the FE-simulations of SPD processes. Moreover, another approach which is widely accepted is to simulate the processes in 2D in order to minimize the modeling effort and calculation time. 3D simulations are mostly used in cases, where the real process cannot be modeled with the simplified 2D approaches.

2.3.3 Finite Element Simulation of Incremental Bulk Metal Forming Processes

The basic features of incremental bulk metal forming processes generate major challenges for the numerical simulation of these. First of all, the end form of a product

is reached only after many similar deformation steps by incremental bulk metal forming processes. From the numerical simulation point of view, this aspect necessitates to model the deformation with very high number of time steps which results in high computation times. Another disadvantage of the cyclic loading and unloading is that it causes a more significant adiabatic heating in the processed materials than in steady-state deformation processes. Additionally, the incremental characteristic results in a more sophisticated kinematics for incremental bulk metal forming processes. This feature mostly requires a more complex modeling of the tool and workpiece movements than single step forming operations and necessitates the usage of small codes called subroutines in addition to the commercial FE-software. Moreover, the deformation zone in every single deformation step is small compared to the overall sample dimensions. Hence, a fine mesh should be used to achieve accurate results [HOF00]. Furthermore, the contact between the tools and the workpiece, especially for rotary swaging, is temporarily lost during every single forming cycle.

Because of these characteristics of incremental bulk metal forming processes, the numerical simulation of these requires computational times that reaches several months on state of the art computers. Accordingly, result data may reach hundreds of GBytes [GRO07].

Due to the above mentioned reasons, the advancement in numerical simulation applications of incremental bulk metal forming processes addresses mostly the efficiency problem.

The dynamic explicit modeling enables very high computational savings compared to the static implicit simulations for ring rolling process [XIE00]. Although this approach can predict the product geometry accurately, there is a great deviation in terms of process forces. This deviation results on the one hand from mass scaling and on the other hand from neglecting the thermal effects. The aggressive use of mass scaling which is required to accelerate the numerical simulation, leads to high deviations in the process force predictions [PAU06]. The coupled thermo-mechanical simulation of the same process is capable of an accurate temperature prediction throughout the workpiece. Moreover, it also reduces the deviation in the process forces [MIN06].

The usage of Arbitrary Lagrangian-Eulerian (ALE) formulation is appropriate for the numerical simulation of incremental bulk metal forming processes. That formulation

enables the division of the numerical problem into two different reference frames, one involving the material related data and the other one the computation. That way, a moving fine mesh can be utilized in the PDZ and a coarser mesh outside of it [DAV03]. Such an approach reduces the simulation time at cost of reduced accuracy caused by the mapping of material and computational mesh after the deformation increments [DAV02].

Another approach to speed-up the numerical simulation of incremental bulk metal forming is to use a hybrid mesh consisting of two distinct meshes constructed for the material and for computational purposes. In that case, the mesh that contains the material, stress, strain and displacement data moves along with the PDZ while the other, mostly coarser mesh containing the field variables such as temperature is stationary [YEA03]. The hybrid mesh approach is mostly used for the numerical simulation of ring rolling process. It also enables the speed-up of simulation. However, the accuracy outside the PDZ is mostly questionable for this approach [LIM98].

A novel approach to accelerate the numerical simulation of incremental bulk metal forming processes is to use the similarities inside the process cycle. Such an algorithm was developed to investigate the gear rolling process where the produced part contains many geometrically identical sections [GRO05b]. Rotary swaging is another field of application for that method.

All of the above mentioned approaches, except the last one about the similarity algorithm, to decrease the simulation time are applied to ring rolling process where the deformation cycle number is relatively small and the numerical simulations tend to converge more easily compared to the other incremental bulk metal forming methods. However, for the simulation of processes with more deformation cycles such as rotary swaging, simple and more stable implicit approaches have been used.

2D models are mostly utilized to save simulation time for the simulation of rotary swaging processes. A thermo-mechanical coupled 2D analysis is used to investigate the feasibility of axial-radial forming, a derivative of rotary swaging. This analysis, which uses the implicit solver of commercial FE-software MSC.Marc shows good agreement with the experimental results except the last few seconds of the deformation process [SCH95]. On the contrary, the numerical results of Rathmann for a 2D mechanical analysis of an infeed swaging process with the same software

deviate significantly from the experimentally obtained ones [RAT06]. This deviation, however, is improved with the 3D modeling of the investigated process, yet still comprises a distinct shift from experimental results. These deviations by both investigations have two reasons, on the one hand the osculation on the forming tools, on the other hand the pure mechanical modeling. On the first study of Schmoeckel and Speck, despite the 2D modeling, the force requirement is overestimated only on the last few seconds of the process where the material has filled the cavity in the tools and osculation starts to take effect on the real process. By the second study of Rathmann, the osculation is effective from the beginning of the forming. So, the process forces are highly overestimated by the numerical simulation. Therefore, the implementation of the 3D modeling improves the accuracy because it incorporates the effects of the osculation. However, since the temperature generation is neglected, a small deviation from experimental results is present.

Considering both, the effects of temperature generation and the osculation, significantly improves the accuracy of the numerical simulation of rotary swaging process at cost of calculation time. Rong et al. investigated the infeed swaging of a magnesium bar at elevated temperatures in a thermo-mechanically coupled analysis using a 3D model by the MSC.Marc software [RON07]. They report a very good correlation between the numerical analysis and experiments in terms of temperature development on the specimen and part geometry.

3 Motivation, Objectives and Approach

3.1 Motivation

State of the art demonstrated in the previous chapter reveals that, despite their outstanding mechanical properties, the commercial usage of UFG materials produced by SPD processes is still limited to a few high-end applications where the cost of the material plays an insignificant role in the buying decision. There has been a tremendous effort to improve the SPD processes and boost the commercialization of UFG materials. A few of these attempts were successful, yet developed processes are only applicable to workpieces in small dimensions. Therefore, although the first reports about SPD processes dates back to 1970s, their commercial boom has not been reached yet. The main problems of SPD processing are related to the friction losses during deformation. Incremental bulk metal forming processes are known to be capable of optimizing the friction. Accordingly, there is a great potential to improve current SPD processes by combining them with incremental bulk metal forming methods.

3.2 Objectives

The main objective of the current study is to investigate the feasibility of a continuous and hence an efficient SPD process based on the combination of the conventional ECAP and the incremental bulk metal forming of rotary swaging. Simultaneously, the principles of forming of materials with the developed process should be developed. The developed fundamentals will be validated with model experiments.

The process related parameters such as forming forces, sample temperature, plastic strain distribution in the deformed material are in the focus of the study at hand rather than the mechanical and microstructural properties of the materials after SPD with the developed process.

The gained knowledge should provide an insight into the process characteristics and should give the opportunity to improve the combined SPD process by defining the

correlations between the deformation related parameters. The defined relations will not only open the opportunity to enhance the developed process but also conventional SPD methods.

3.3 Approach

Within the framework of the current study, a new SPD process based on conventional ECAP and rotary swaging should be developed. This process is called “Equal Channel Angular Swaging” (ECAS). Two different materials will be used in the investigations; commercially pure copper (Cu-ETP) and low carbon cold forging steel (C4C). These two materials are selected not because of the difference in their microstructure but in their mechanical properties.

A four step approach will be followed in the investigations. After introduction of the ECAS process concept as well as mechanical and tribological characterization of the materials, formulas predicting the force requirement to process samples with ECAS method will be defined using the slip-line field theory similar to conventional ECAP. However, unlike current equations for the ECAP process, the developed formulas will take the effect of friction on the different channel walls of the tool system and the correlation between the back pressure and the contact stresses into consideration. Derived analytical formulations should enable a quick evaluation of possible further developments of ECAS process depending on the mechanical material properties, channel angle, friction coefficient and sample dimensions as well as forming tool dimensions.

In the second step, first FE-simulation models will be generated. The effect of the geometrical parameters of the tool system (channel length and arc of curvature) on the plastic strain distribution, material flow and temperature development on the processed samples will be investigated. In the light of the results of these first FE simulations, a tool system will be designed and manufactured to conduct model experiments.

In a later step, derived analytical formulas and the FE-simulations will be validated with experiments. All experiments will be conducted on the existing rotary swaging machine at the Institute for Production Engineering and Forming Machines (PtU). These model experiments serve also as the feasibility study for the ECAS process.

Moreover, the FE-simulations will be optimized using the results of the experiments by varying the simulation related parameters.

In the last step, after validation of the numerical simulations, the effect of different process parameters such as feeding speed, feeding type, friction coefficient and temperature on force requirement, strain distribution and temperature development in ECAS process will be investigated with the aid of FEA. The results of these simulations should give suggestions for the improvement of the developed process. The approach used in the studies is demonstrated in Figure 3-1 schematically.

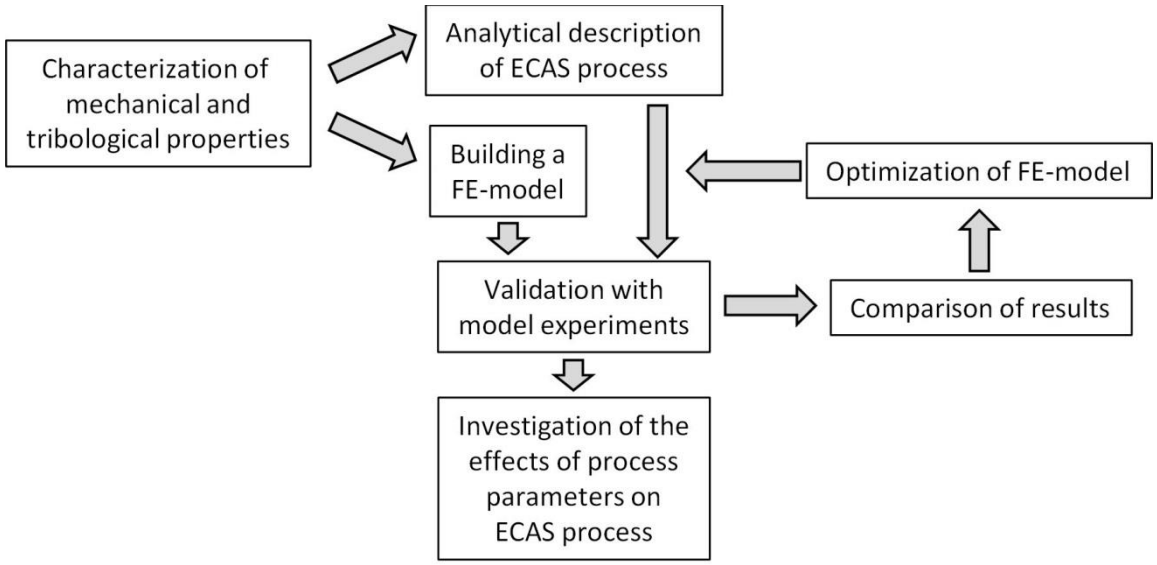

Figure 3-1 Approach of the studies

4 Equal Channel Angular Swaging (ECAS) Process

Before getting started with the investigations, the ECAS process concept and the rotary swaging machine on which this process will be performed will be explained briefly. The ECAS process bases upon the combination of conventional ECAP and the incremental bulk metal forming method of rotary swaging. During the proposed ECAS process, two forming tool halves, which are concentrically arranged around the workpiece, perform high frequency radial movements with short strokes, while samples are pushed through these (Figure 4-1). Due to this oscillation motion, the contact time and the relative movement between the tool and the workpiece are very small within a stroke cycle. This feature enables the feeding of the material while the tools are open. Moreover, the discontinuous contact enables the permanent lubrication of the tools and the workpiece. Another important aspect of ECAS is that the samples are not pushed against stationary tool walls. Since the oscillation direction nearly coincides with the pushing direction, the workpiece is pulled by the tools during forming.

By the proposed ECAS process, the tool contours are building an eccentric channel, which consists of three different sections (Figure. 4-1, lower-left). Therefore, the material undergoes two-times a simple shear deformation while passing the channels. The entry, middle and exit channel are designated with numbers 0, 1 and 2, respectively. Unlike the previous studies, where the channel length is defined as the channel offset, this length is defined as the width of the rectangular portion of the channel in the cross-section, where the light grey sections in Figure 4-1.lower-left are excluded. The length of the individual channels is denoted by the capital letter “L” and a subscript afterwards. The yielding lines generated by the channel intersections are demonstrated with dotted lines in Figure 4-1.lower-left and denoted by roman numbers. In order to prevent any collision with the forming machine, the channel angles on both deformation zones are equal. Hence, the sample enters and exits the forming machine along parallel axes.

The forming channel, which is built by the groove in the tools, is divided exactly in the middle section along the axial direction (Figure 4-1.lower-right). Therefore,

deformation of rectangular as well as round samples is possible with ECAS process. Nevertheless, in the current study, only the deformation of round bars with a diameter of 20 mm will be investigated.

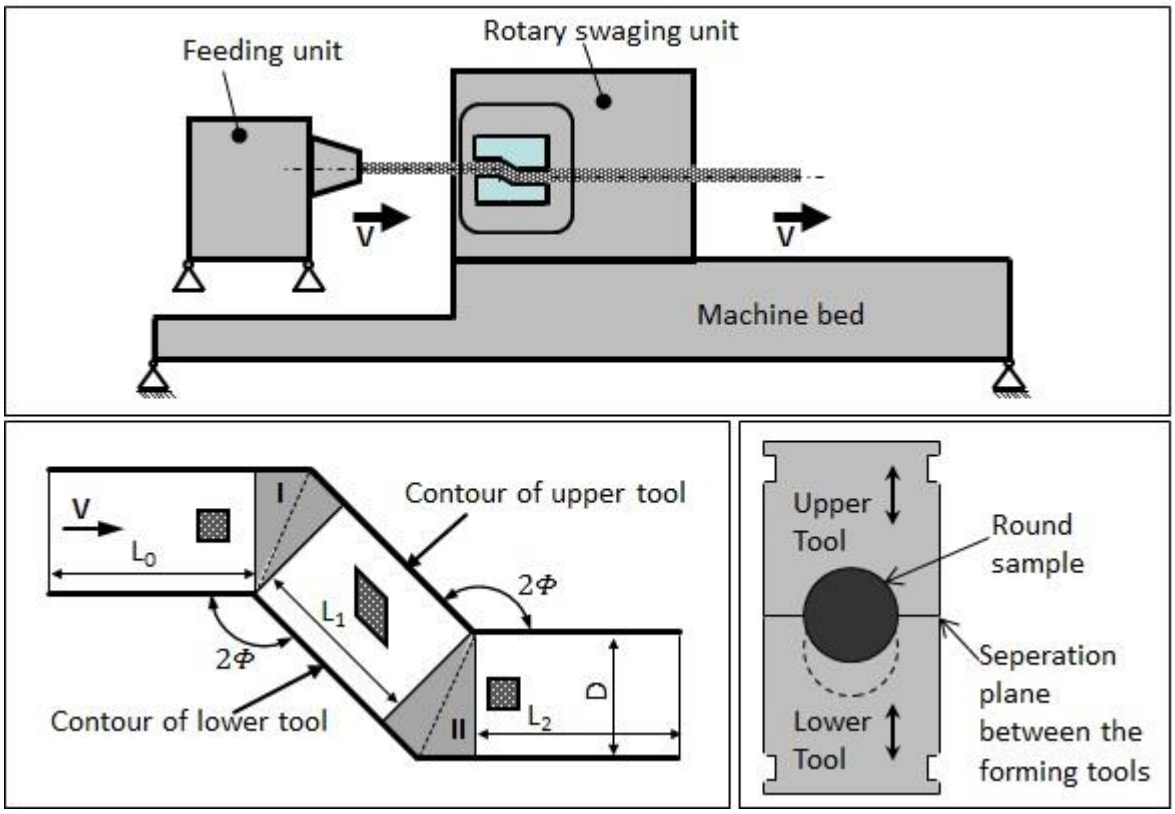

Figure 4-1 Schematic illustration of the rotary swaging machine (up), geometrical parameters of the tool system (down, left) and tool arrangement of ECAS process (down, right)

The model experiments will be conducted on the rotary swaging machine existing at the Institute for Production Engineering and Forming Machines. It is an external rotating system machine of the company Heinrich Müller Pforzheim (HMP). This machine is designed to accommodate four tools. However, in the current study, only two forming tools will be used. The free slots will be filled with dummy parts.

The machine is equipped with a programmable logic control (PLC) unit which undertakes position and velocity control of the axial and radial axes as a main function. The clamp unit is fixed to an axial feeding system consisting of two spindles. Combined with the PLC, it enables an accurate positioning of the workpieces while providing high forces in axial direction.

The characteristics of the rotary swaging machine are summarized in Figure 4-2.

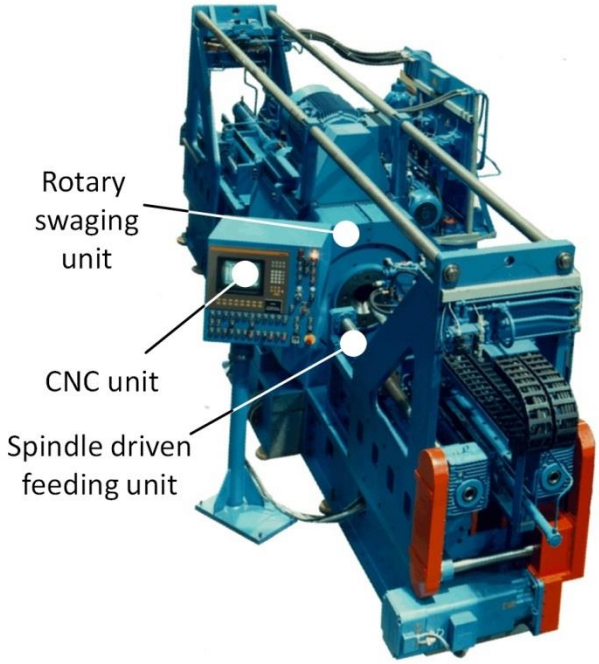

UR8-4DD-55LH-CNC

Machine specifications:

Motor capacity (forming):	30 kW
Motor capacity (axial feeding):	15 kW
Tool stroke:	0.7 mm
Swaging frequency:	30 Hz
Max. radial load:	1000 kN
Max. axial load:	400 kN
Radial feed rate:	0 – 0.15 m/min
Axial feed rate:	0 – 3 m/min
Rotary feed:	108 1/min
Number of tools:	4

Figure 4-2 Characteristics of the rotary swaging machine used in the study

5 Properties of Used Materials

5.1 Mechanical Properties

In the investigations, it is intended to consider the effects of both, strain rate and temperature on the yield strength of materials. The Johnson-Cook material model enables an easy prediction of the yield strength dependent on these parameters. Moreover, the Johnson-Cook material model is implemented in most FE-software and hence doesn't require an additional programming. Therefore, this constitutive model is used to define yield strength of the used materials. A two-step approach, which was proposed by Mänz is followed to determine the material model related parameters [MÄN12]. Accordingly, flow curves determined with tensile testing are optimized with upsetting tests and their numerical simulation.

Tensile specimens according to DIN 50125 have been used to characterize the materials at room temperature. Strain rate is set to 10^{-2} s^{-1}. Additionally, cylindrical specimens with a diameter of 7 mm and a height of 10.5 mm are used in upsetting tests to investigate the strain rate and temperature effect. A commercial lubricant containing MoS_2 Beruforge 150D of Bechem is used to coat the specimens before testing. Therefore, only a small bulging is observed on deformed samples (Figure 5-1).

Figure 5-1 Geometry of the upsetting test specimens

First tests are conducted with strain rates 10^{-2} s^{-1}, 10^{-1} s^{-1} and 10^{-0} s^{-1} at room temperature. Afterwards, the temperature is varied for the strain rate of 10^{-0} s^{-1} from 25°C to 175°C in 75°C steps. All specimens are formed to their half height; up to a theoretical plastic strain of 0.69. Subsequently, upsetting tests are numerically simulated using the flow curve obtained from tensile testing. The parameters of the Johnson-Cook formulation are optimized to fit simulated upsetting forces to the measured ones. Obtained parameters for both materials are shown in Table 5-1.

Table 5-1 Parameters of the Johnson-Cook material model for used materials

Parameter	**Cu**	**C4C**
A – Yield strength [MPa]	335.43	424.88
B – Strain hardening effect [MPa]	15.82	91.67
n – Strain hardening exponent	0.175	0.198
C – Strain rate sensitivity	0.0112	0.0124
$\dot{\varepsilon}_0$ – Reference strain rate	1	1
T_{room} – Room temperature [K]	298	298
T_{melt} – Melting temperature [K]	1356	1803
m – Thermal softening exponent	0.98	0.83

Flow curves extrapolated with the Johnson-Cook model using the optimized parameters are shown in Figure 5-2 and 5-3.

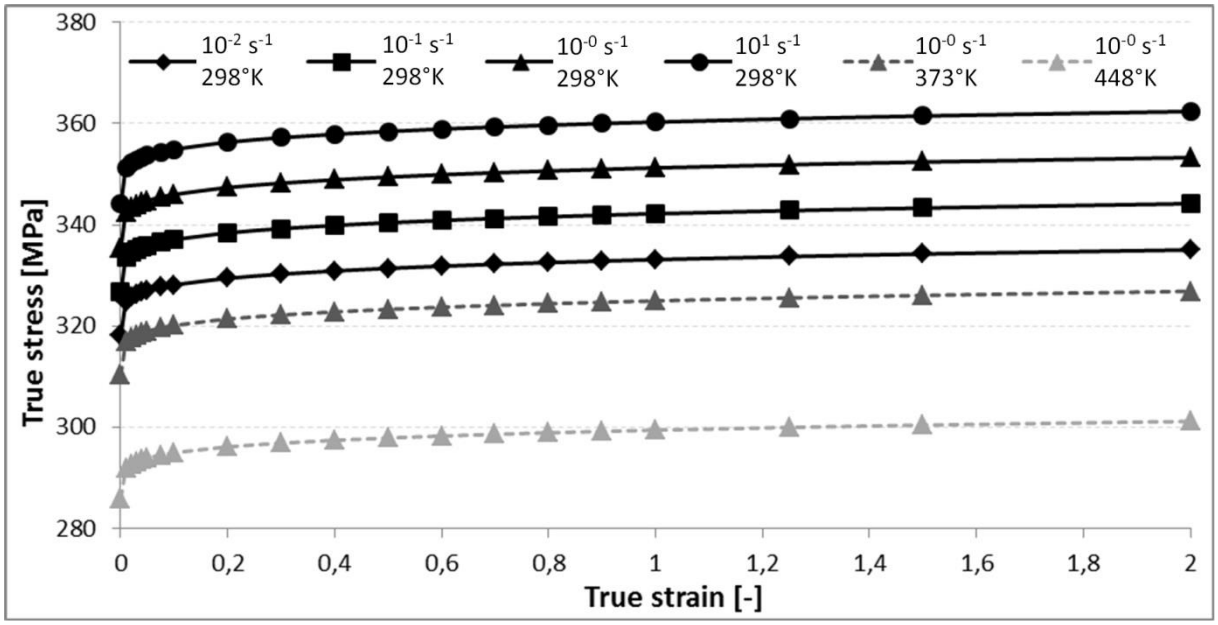

Figure 5-2 Extrapolated strain rate and temperature dependent flow curves of Cu

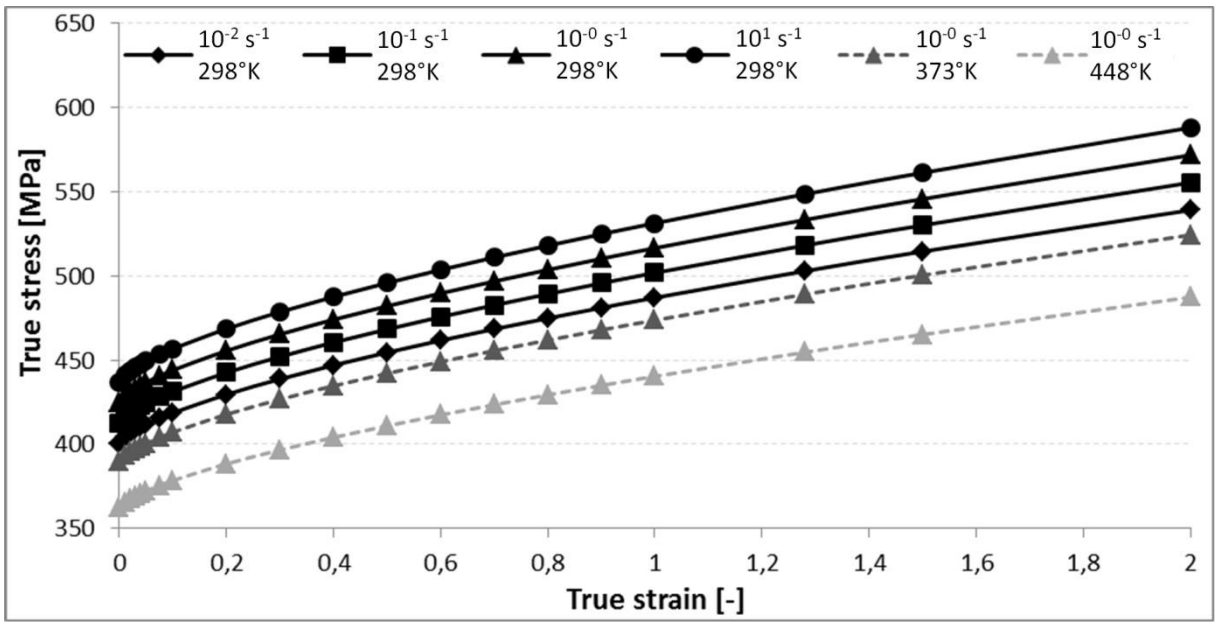

Figure 5-3 Extrapolated strain rate and temperature dependent flow curves of C4C

The common point of both materials in the investigated range is that the temperature has a more significant effect on yield strength than strain rate. Increasing the temperature by 150°C results in a decrease of 49.5 MPa and 62.7 MPa by copper

and steel, respectively, while decreasing the strain rate from 10^0 s^{-1} to 10^{-2} s^{-1} causes a reduction of only 17.3 MPa and 24.26 MPa, respectively.

5.2 Tribological Properties

Tribological conditions between work piece and tools heavily influence material flow and force requirement in SPD processes. Therefore, the properties of the tribological system are of high importance. In the present study, the friction coefficients of the investigated materials are determined with the Sliding Compression Test (SCT) [GRO13a, GRO13b].

By the SCT, cylindrical samples are compressed with a punch. During the compression, the material flows into the specially formed engraving of the punch. The applied force is kept constant during the entire test. Thus, the contact normal stress is constant as well. After compression is complete, the sliding plate is moved transversely with a predefined velocity under the formed specimen. By measuring the forces on the sliding plate and the punch, friction forces and friction coefficients can be determined.

In the current study, cylindrical specimens with a diameter of 15 mm and a height of 10 mm are used for friction coefficient determination purposes. Samples of both materials are sandblasted before testing. Since the samples are formed in many consecutive steps, it is common practice to use liquid lubricants in incremental bulk metal forming processes. Therefore, extrusion oil SSP 70 of Zeller+Gmelin will be used in the investigations. Samples are dipped into this oil before SCT. Copper samples are compressed at room temperature with a constant force of 300 kN corresponding to a mean contact normal stress of 800 MPa. Steel samples are compressed also at room temperature with a constant force of 400 kN corresponding to a mean contact normal stress of 1050 MPa. After the compression, the sliding plate is pushed with a constant velocity of 10 mm/s for 6 seconds. Afterwards, all tests are repeated at a temperature of 348°K. The friction coefficients over the sliding distance are shown in the Figure 5-4.

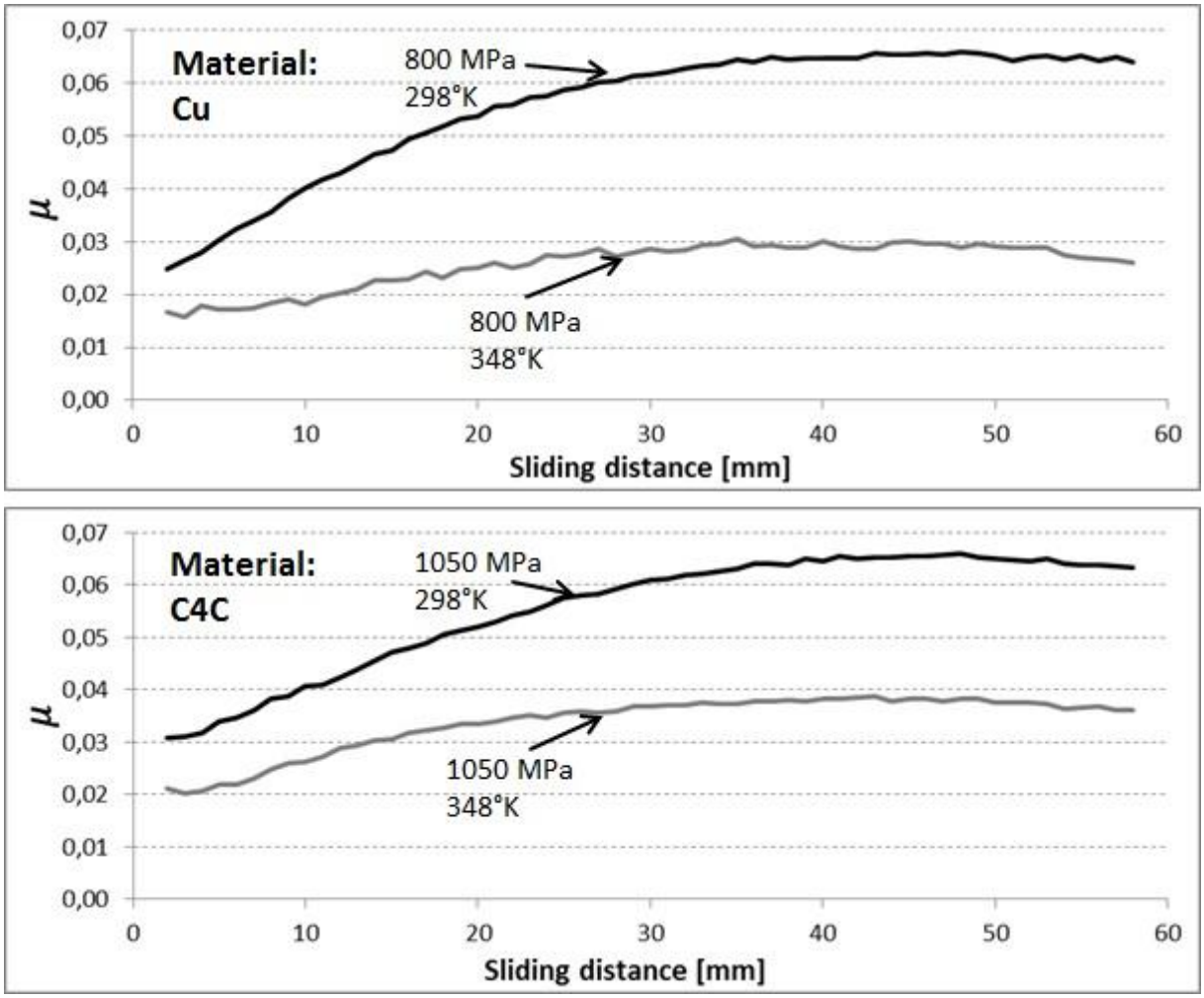

Figure 5-4 Friction coefficient over sliding distance for Cu and C4C

Friction coefficients for both materials and temperatures start with a comparatively small value. However, as sliding of the plate proceeds, these values increase and reach a stagnation point eventually. Moreover, friction coefficients tend to drop at the end of the SCT. The increase at the beginning of the tests points out a dependence of the friction coefficient on the amount of lubricant in the system. While the sliding plate advances, the liquid lubricant under the sample escapes from the contact area. Furthermore, lubricant in front of the sample is swept away by the sample itself. Thus the friction force increases. On the other hand, friction related increase of the temperature results in a decrease at the end of the SCT [ZAN14].

6 Mechanics of Severe Plastic Deformation Processes

As stated in Chapter 2.1.1, the plastic strains and forces developing during deformation by ECAP process has been investigated in many studies. The strain development is defined basically dependent on the tool geometry of the ECAP system. The effect of material properties, friction or temperature is not considered by the analytical descriptions. Therefore, the validity of the existing formulas for the ECAS process will be proven by model experiments and FE-simulations. Development of new theories describing plastic strains is not the subject of the study at hand.

On the other hand, the force requirement by ECAP deformation is defined dependent on mechanical properties of the used material and friction as well as the geometry of the tool system and sample. However, in the previous studies, only a single forming zone is investigated. Since it is intended to use an ECAS tool system with two forming sections in it, present formulations to describe the force requirement cannot be used in the current study. Moreover, the friction effect is considered only in case of a dead metal zone formation and for punch pressures which exceeds the yield strength of the deformed material. Therefore, an improvement of existing formulations is also necessary.

To be able to compare both SPD processes, first the formulations will be developed for ECAP and later for ECAS. For a better comparison with the former studies, a slip-line field (SLF) approach consisting of a single slip line which was used in the first analytical investigations of ECAP will be also used in the current study. A round bar geometry will be investigated. The following assumptions are made for the SLF formulation:

- The deformation is plain strain.
- No dead metal zone is formed during deformation.
- No back pressure is applied onto the samples.

- The channels are completely filled with the sample. There is no clearance between the tool channel walls and the sample.
- There are two deformation zones with equal channel angles in a single tool system. The deformation follows the route C.
- The round geometry of the samples is represented by its rectangular equivalent which has the same cross sectional area as the round one (Figure 6-1). In the current study, the equivalent width (w_{eq}) of the sample is 15.7 mm.
- Friction is assumed to be constant throughout the channels.
- The investigated materials are considered as perfectly plastic without strain hardening inside a plastic deformation zone.
- Temperature effects are neglected. It can only be incorporated by adjusting the shear yield strength of the material according to a separate temperature calculation.

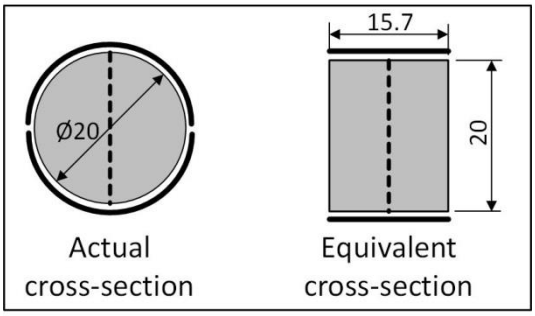

Figure 6-1 Schematic illustration of the cross-section of the investigated samples

Three different channel angles, 105°, 120° and 135° will be investigated with the derived formulas.

6.1 Loads on ECAP-Process

In order to be able to evaluate the effect of the second forming within one ECAP tool system, first the process with one forming section (1 turn ECAP) will be investigated. Before getting started, abbreviations used in this chapter will be explained shortly for a better understanding. Some of those are also shown in the schematic illustration of 1 turn ECAP process in Figure 6-2. The capital letter “F” is used to describe the force. The first subscript by this description denotes the side of the tool wall where the force is acting (upper or lower). If the force is a resulting force of normal and friction forces,

the phrase “resulting” follows the subscript indicating the side of the wall. In case that investigated force is not a resulting force, the second subscript denotes the channel number where it is acting (“0” for entry channel, “1” for the middle channel and “2” for the exit channel). The third subscript indicates the direction of the particular force component (“X”, “Y”, “Xi” or “Yi”). The last subscript, if present, states the yielding line from which the force results (First “I” or second “II” yielding line). Moreover, “μ” stands for the friction coefficient and “λ” for the angle between the normal and friction force. Furthermore, “k” is the shear yield strength of the material and “P” is the pressure. Additionally, “D” denotes the diameter of the sample.

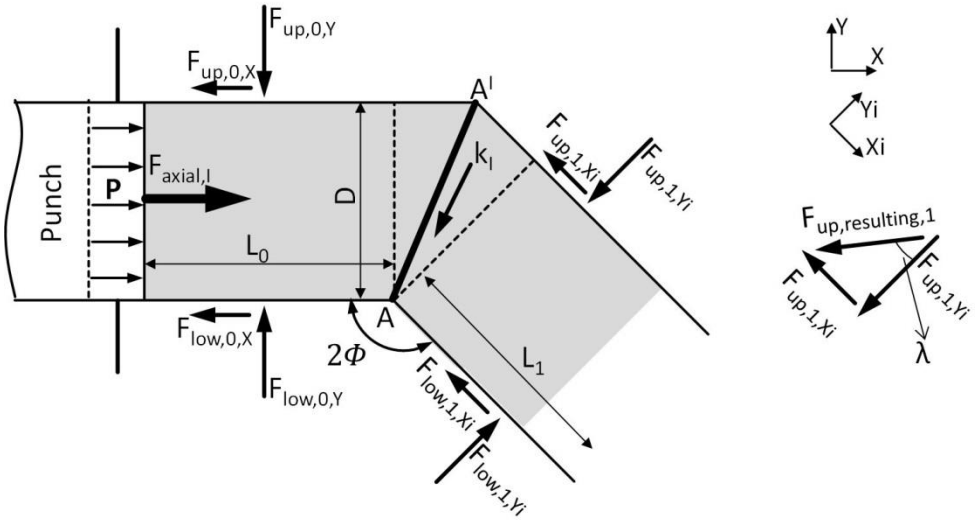

Figure 6-2 Schematic illustration of the forces in single turn ECAP

By conventional ECAP, the only driving force in the deformation system is the one in pushing direction. For standardization purposes, it will be called axial force (F_{axial}). The deformation along the yielding line (AA^I in Figure 6-2) is a result of it. In order to preserve the force balance in the tool system, the component of the reaction force on the opposite wall of the middle channel (For 1 turn ECAP, it is also the exit channel) in the axial direction ($F_{up,resulting,1,X}$) together with the friction losses in the entry channel ($F_{up,0,X}$ and $F_{low,0,X}$) should be equal to this pushing force ($F_{axial,I}$). Moreover, in order to be able to form the material, the component of $F_{up,resulting,1}$ in the yielding direction should be equal to the yielding force along the first deformation line AA^I which is (Figure 6-3):

$$F_{yielding,I} = \frac{k_I \cdot D}{\sin \phi} \cdot w_{eq} \qquad \textit{Equation 6-1}$$

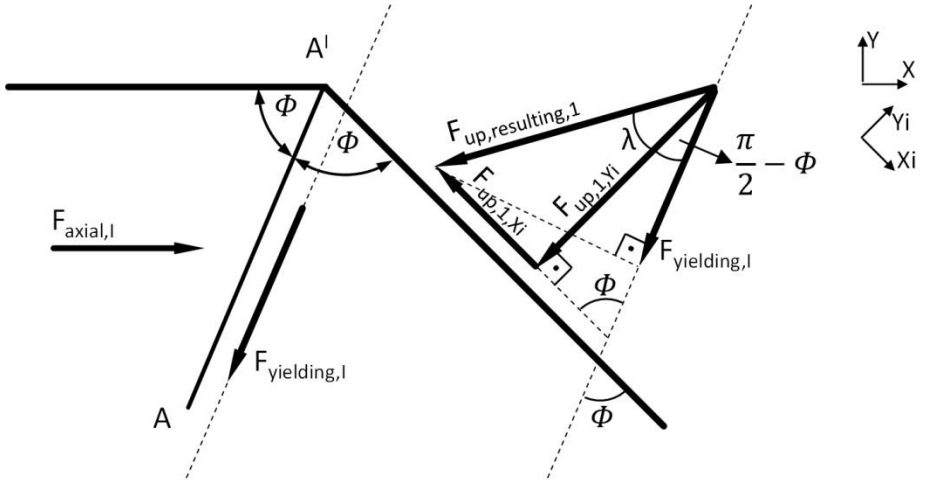

Figure 6-3 Schematic illustration of the force components on the upper side of the ECAP tool

The component of $F_{up,resulting,1}$ in the yielding direction is shown schematically in Figure 6-3.

$$F_{up,resulting,1} \cdot \cos\left(\frac{\pi}{2} - \phi + \lambda\right) = F_{yielding,I} \qquad \textit{Equation 6-2}$$

$$F_{up,resulting,1} \cdot \sin(\phi - \lambda) = \frac{k_I \cdot D}{\sin \phi} \cdot w_{eq} \qquad \textit{Equation 6-3}$$

$$F_{up,resulting,1} = \frac{k_I \cdot D}{\sin \phi \cdot \sin(\phi - \lambda)} \cdot w_{eq} \qquad \textit{Equation 6-4}$$

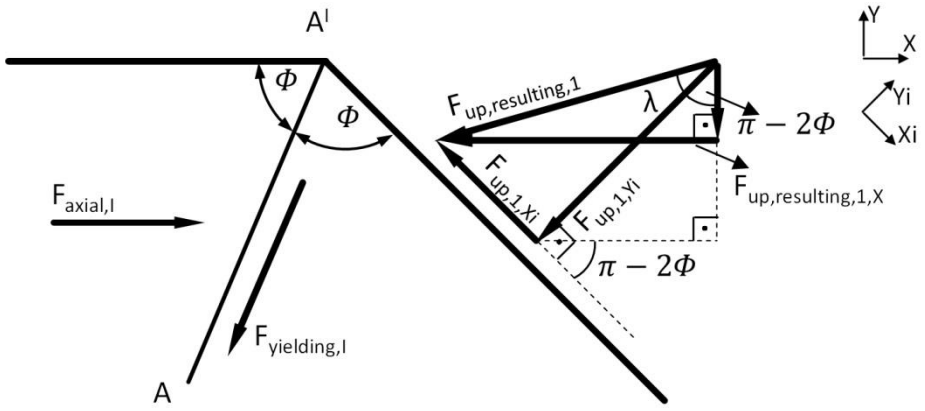

Figure 6-4 Schematic illustration of the force components of $F_{up,resulting,1}$

The component of $F_{up,resulting,1}$ in the feeding direction ($F_{up,resulting,1,X}$) should be equal to the fraction of $F_{axial,I}$ which is related to the forming of the material (Figure 6-4).

$$F_{axial,I} = F_{up,resulting,1,X} \qquad \textit{Equation 6-5}$$

$$F_{axial,I} = F_{up,resulting,1} \cdot \sin(\pi - 2\phi + \lambda) \qquad \textit{Equation 6-6}$$

$$F_{axial,I} = F_{up,resulting,1} \cdot \sin(2\phi - \lambda) \qquad \textit{Equation 6-7}$$

$$F_{axial,I} = \frac{k_I \cdot D \cdot \sin(2\phi - \lambda)}{\sin\phi \cdot \sin(\phi - \lambda)} \cdot w_{eq} \qquad \textit{Equation 6-8}$$

For the frictionless case, Equation 6-8 reduces to:

$$F_{axial,I} = \frac{k_I \cdot D \cdot \sin 2\phi}{\sin^2 \phi} \cdot w_{eq} \qquad \textit{Equation 6-9}$$

$$F_{axial,I} = 2 \cdot k_I \cdot D \cdot \cot\phi \cdot w_{eq} \qquad \textit{Equation 6-10}$$

Equation 6-10 is equal to the one for a single turn ECAP process proposed by Segal et al. [SEG94].

In case of friction, the forces normal to the channel walls (Y-direction) are caused by two reasons: First, by the radial pressure resulting from F_{axial} and $F_{up,resulting,1,X}$.

Secondly, by the force component of $F_{up,resulting,1}$ in Y-direction. In order to sustain the force equilibrium throughout the tool system, this second component should be compensated by the lower wall of the entry channel. Friction forces directed in the opposite of the feeding arise from these normal forces.

The pressure in the entry channel ($P_{0,I}$) is:

$$P_{0,I} = \frac{F_{up,resulting,1,X}}{D \cdot 2 \cdot w_{eq}} \qquad \textit{Equation 6-11}$$

$$P_{0,I} = \frac{k_I \cdot \sin(2\phi - \lambda)}{2 \cdot \sin\phi \cdot \sin(\phi - \lambda)} \qquad \textit{Equation 6-12}$$

Therefore, the normal force acting on both walls of entry channel are:

$$F_{up,0,Y} = P_{0,I} \cdot L_0 \cdot w_{eq} \qquad \textit{Equation 6-13}$$

$$F_{up,0,Y} = \frac{k_I \cdot L_0 \cdot \sin(2\phi - \lambda)}{2 \cdot \sin\phi \cdot \sin(\phi - \lambda)} \cdot w_{eq} \qquad \textit{Equation 6-14}$$

Accordingly, the friction force on the upper wall of the entry channel is:

$$F_{up,0,X} = F_{up,0,Y} \cdot \mu \qquad \textit{Equation 6-15}$$

$$F_{up,0,X} = \frac{k_I \cdot L_0 \cdot \sin(2\phi - \lambda)}{2 \cdot \sin\phi \cdot \sin(\phi - \lambda)} \cdot w_{eq} \cdot \mu \qquad \textit{Equation 6-16}$$

Unlike the upper wall, the lower wall of the entry channel compensates also the $F_{up,resulting,1,Y}$ which is:

$$F_{up,resulting,1,Y} = F_{up,resulting,1} \cdot \sin\left(2\phi - \lambda - \frac{\pi}{2}\right) \qquad \textit{Equation 6-17}$$

$$F_{up,resulting,1,Y} = \frac{k_I \cdot D \cdot (-\cos(2\phi - \lambda))}{\sin\phi \cdot \sin(\phi - \lambda)} \cdot w_{eq} \qquad \textit{Equation 6-18}$$

Therefore, $F_{low,0,Y}$ is:

$$F_{low,0,Y} = P_0 \cdot L_0 \cdot w_{eq} + F_{up,resulting,1,Y} \qquad \textit{Equation 6-19}$$

$$F_{low,0,Y} = \frac{k_I \cdot L_0 \cdot \sin(2\phi - \lambda)}{2 \cdot \sin\phi \cdot \sin(\phi - \lambda)} \cdot w_{eq} + \frac{k_I \cdot D \cdot (-\cos(2\phi - \lambda))}{\sin\phi \cdot \sin(\phi - \lambda)} \cdot w_{eq} \qquad \textit{Equation 6-20}$$

Accordingly, the friction force on the lower wall of the entry channel is:

$$F_{low,0,X} = \left[P_0 \cdot L_0 \cdot w_{eq} + F_{up,resulting,1,Y}\right] \cdot \mu \qquad \textit{Equation 6-21}$$

$$F_{low,0,X} = \left[\frac{k_I \cdot L_0 \cdot \sin(2\phi - \lambda)}{2 \cdot \sin\phi \cdot \sin(\phi - \lambda)} + \frac{k_I \cdot D \cdot (-\cos(2\phi - \lambda))}{\sin\phi \cdot \sin(\phi - \lambda)}\right] \cdot w_{eq} \cdot \mu \qquad \textit{Equation 6-22}$$

Finally, the force required to push the sample through the ECAP die is:

$$F_{axial,I} = F_{up,resulting,1,X} + F_{up,0,X} + F_{low,0,X} \qquad \textit{Equation 6-23}$$

Although it is unlikely that a part of the sample material is outside the die and pushed with a punch into it in ECAP, in order to enable a consistent comparison, it will be assumed that the length of the entry and (for the two turn ECAP system) the exit channel is 65 mm and the middle channel is 15 mm in length. The entry channel is completely filled with sample material. For the evaluation of ECAP, in order to be independent from the sample cross section, punch pressure is mostly used for comparison purposes. Moreover, to be able to compare different materials, a dimensionless number is obtained by dividing the punch pressure through shear yield strength. In addition, since the shear yield strength of one material (k) is half of the yield strength according to Tresca yield criterion, this dimensionless number is $P/2k$. Figure 6-5 displays the predictions for single turn ECAP process according to Equation 6-23.

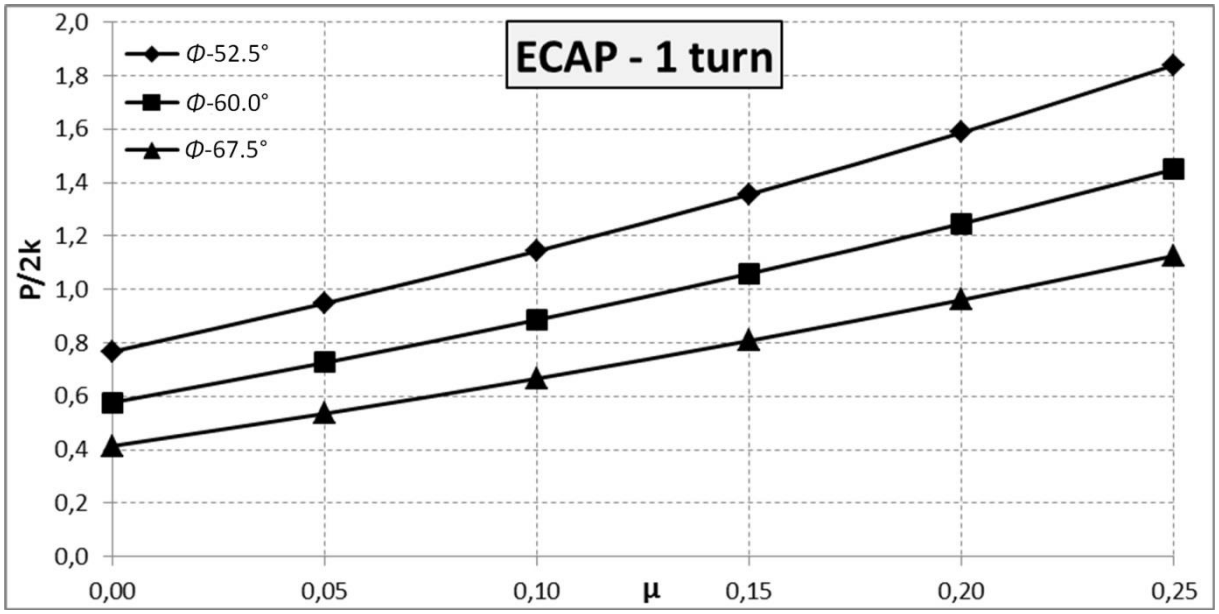

Figure 6-5 Punch pressure predictions for single turn ECAP

As can be seen by Figure 6-5, friction has a negative effect on punch pressure in conventional ECAP. Furthermore, it is clear that the punch forces are rising exponentially as the friction coefficient increases.

For the calculation of the force requirement in a two turn ECAP system, it is assumed that the sample has passed the second yielding line completely and the entry as well as the middle channel is completely filled (Figure 6-6).

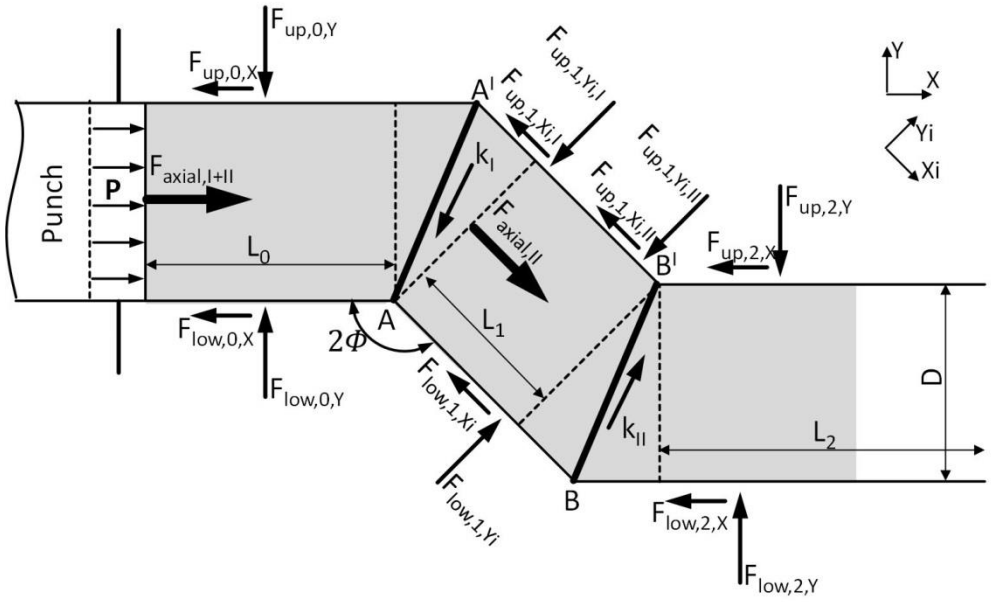

Figure 6-6 Schematic illustration of the forces in two turn ECAP

In this case, calculations will start with the second yielding line and go backwards. The required forces can be calculated similar to the ones for the first yielding line. So, the forces $F_{yielding,II}$, $F_{low,resulting,2,Xi}$, $F_{low,1,Xi}$, $F_{up,1,Xi,II}$ and $F_{axial,II}$ become:

$$F_{yielding,II} = \frac{k_{II} \cdot D}{\sin \phi} \cdot w_{eq} \qquad \textit{Equation 6-24}$$

$$F_{low,resulting,2,Xi} = \frac{k_{II} \cdot D \cdot \sin(2\phi - \lambda)}{\sin \phi \cdot \sin(\phi - \lambda)} \cdot w_{eq} \qquad \textit{Equation 6-25}$$

$$F_{low,1,Xi} = \frac{k_{II} \cdot L_1 \cdot \sin(2\phi - \lambda)}{2 \cdot \sin \phi \cdot \sin(\phi - \lambda)} \cdot w_{eq} \cdot \mu \qquad \textit{Equation 6-26}$$

$$F_{up,1,Xi,II} = \left[\frac{k_{II} \cdot L_1 \cdot \sin(2\phi - \lambda)}{2 \cdot \sin \phi \cdot \sin(\phi - \lambda)} + \frac{k_{II} \cdot D \cdot (-\cos(2\phi - \lambda))}{\sin \phi \cdot \sin(\phi - \lambda)}\right] w_{eq} \cdot \mu \qquad \textit{Equation 6-27}$$

$$F_{axial,II} = F_{up,resulting,2,Xi} + F_{low,1,Xi} + F_{up,1,Xi,II} \qquad \textit{Equation 6-28}$$

It is assumed that $F_{axial,II}$ is acting on the entry channel as a back pressure. Furthermore, forces related to the first yielding along the AA' line acting on the upper wall of the middle channel are not affected by $F_{axial,II}$.

Therefore, $F_{axial,I+II}$ can be expressed as follows:

$$F_{axial,I+II} = F_{axial,II} + F_{up,resulting,1,X,I} + F_{up,0,X} + F_{low,0,X} \quad \textit{Equation 6-29}$$

In equation 6-29, $F_{axial,II}$ and $F_{up,resulting,1,X,I}$ remain unchanged. However, since $F_{axial,II}$ is causing an additional back pressure in the entry channel, $F_{up,0,X}$ and $F_{low,0,X}$ increase drastically. The additional pressure ($P_{0,II}$) related to $F_{axial,II}$ can be calculated as follows:

$$P_{0,II} = \frac{F_{axial,II}}{D \cdot 2 \cdot w_{eq}} \quad \textit{Equation 6-30}$$

Therefore, the forces acting normal to the entry channel walls related to the pressure inside the channels and corresponding friction forces become:

$$F_{up,0,Y} = \left(P_{0,I} + P_{0,II}\right) \cdot L_0 \cdot w_{eq} \quad \textit{Equation 6-31}$$

$$F_{up,0,X} = \left(P_{0,I} + P_{0,II}\right) \cdot L_0 \cdot w_{eq} \cdot \mu \quad \textit{Equation 6-32}$$

$$F_{low,0,Y} = \left[\left(P_{0,I} + P_{0,II}\right) \cdot L_0 \cdot w_{eq}\right] + F_{up,reulting,1,Y,I} \quad \textit{Equation 6-33}$$

$$F_{low,0,X} = \left[\left[\left(P_{0,I} + P_{0,II}\right) \cdot L_0 \cdot w_{eq}\right] + F_{up,reulting,1,Y,I}\right] \cdot \mu \quad \textit{Equation 6-34}$$

Figure 6-7 displays the predicted $P/2k$ values by Equation 6-29 for two turn ECAP.

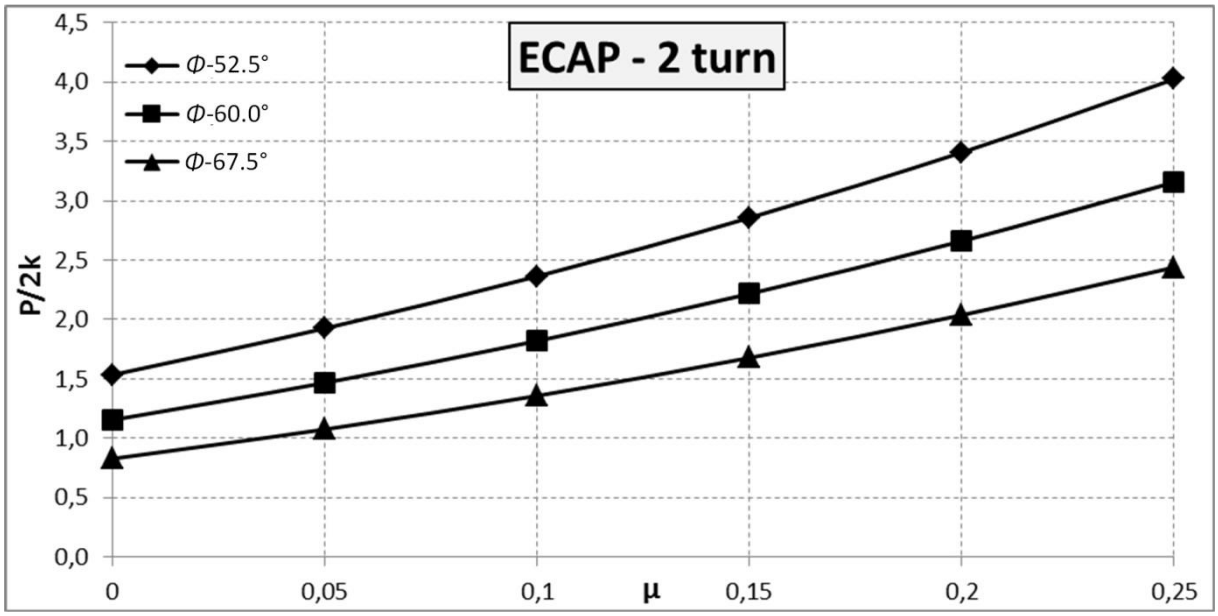

Figure 6-7 Punch press predictions for two turn ECAP

The pressures rise exponentially as for the case of single turn ECAP. However, due to the increase in the axial pressure inside the entry channel, the punch pressures are more than doubled.

6.2 Loads on ECAS-Process

For ECAS process, there are two different force sources; radial one in the direction of tool oscillation and the axial one in the feeding direction of the sample (Figure 6-8). In the calculations, it will be assumed that the radial forces are responsible for the whole deformation. Axial forces only compensate the redundant force components in the feeding direction. Moreover, for the analytical investigation, since the feeding motion in every load cycle is small, the sample will be assumed stationary in axial direction when the tools reach the bottom dead center.

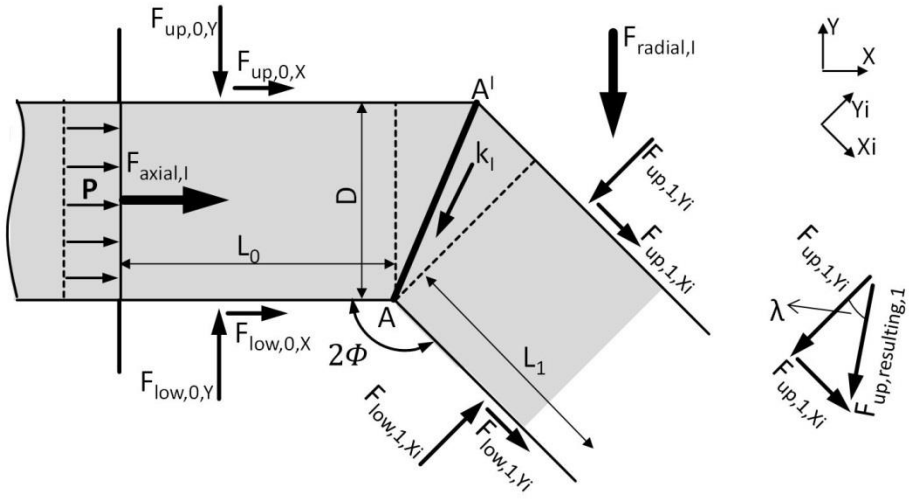

Figure 6-8 Schematic illustration of the forces in single turn ECAS

Unlike ECAP, due to the kinematics of the tools, friction is acting on the sample's feeding direction in ECAS, not on the opposite direction. Thus, it eases the feeding and reduces the axial forces. This aspect is seen as the most significant advantage of ECAS process over ECAP concerning the force requirement. As in the previous chapter, first, single turn ECAS will be considered in analytical investigations.

The yielding force $F_{yielding,I}$ remains the same as in ECAP in the previous chapter. Similarly, this yielding is a consequence of the resulting force on the upper wall of the middle channel. Therefore, its component in the yielding direction should be equal to $F_{yielding,I}$ (Figure 6-9):

$$F_{up,resulting,1,I} \cdot \cos\left(\frac{\pi}{2} - \phi - \lambda\right) = F_{yielding,I} \qquad \textit{Equation 6-35}$$

$$F_{up,resulting,1,I} \cdot \sin(\phi + \lambda) = \frac{k_I \cdot D}{\sin\phi} \cdot w_{eq} \qquad \textit{Equation 6-36}$$

$$F_{up,resulting,1,I} = \frac{k_I \cdot D}{\sin\phi \cdot \sin(\phi + \lambda)} \cdot w_{eq} \qquad \textit{Equation 6-37}$$

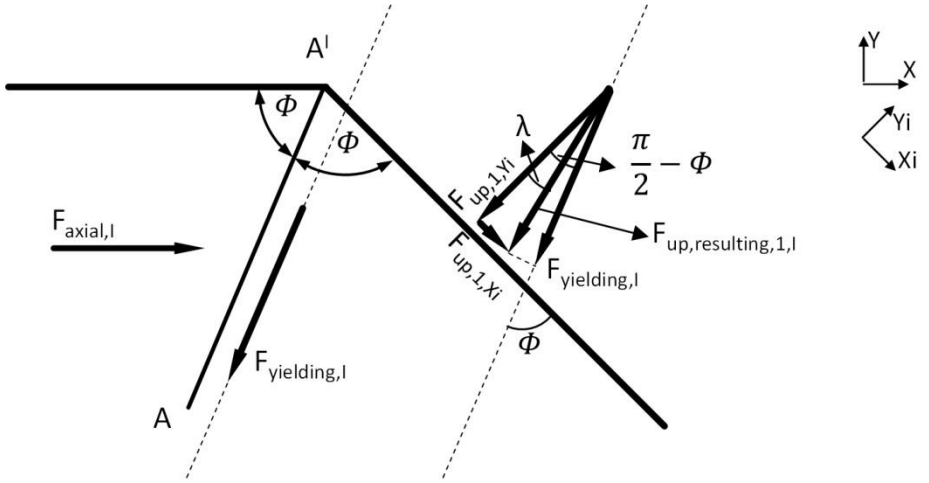

Figure 6-9 Schematic illustration of the force components on the upper side of the ECAS tool

This force ($F_{up,resulting,1,I}$) is the result of the radial force ($F_{radial,I}$) applied by the tool (Figure 6-10):

$$F_{radial,I} = \frac{F_{up,resulting,1,I}}{\sin\left(2\phi + \lambda - \frac{\pi}{2}\right)} \qquad \textit{Equation 6-38}$$

$$F_{radial,I} = \frac{k_I \cdot D}{\sin\phi \cdot \sin(\phi + \lambda) \cdot (-\cos(2\phi + \lambda))} \cdot w_{eq} \qquad \textit{Equation 6-39}$$

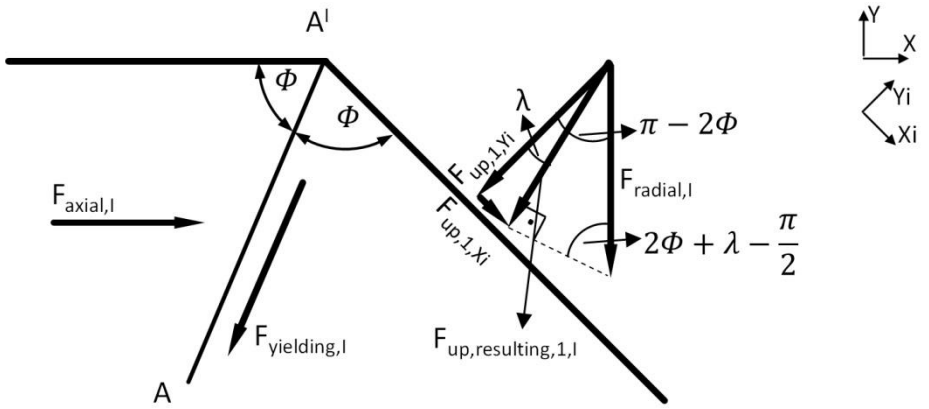

Figure 6-10 Schematic illustration of the $F_{radial,I}$

Moreover, the component of $F_{up,resulting,1,I}$ in feeding direction ($F_{up,resulting,1,X,I}$) should be compensated by the axial force (Figure 6-11):

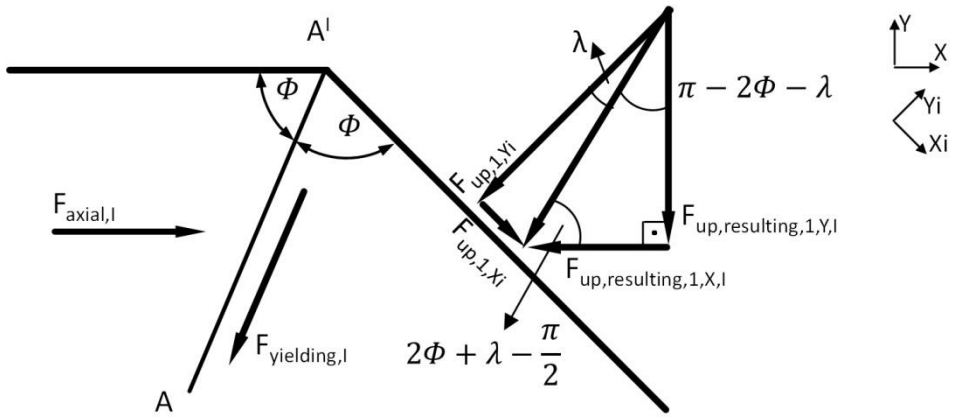

Figure 6-11 Schematic illustration of the force components of $F_{up,resulting,1,I}$

$$F_{low,0,Y} = F_{up,resulting,1,X,I} = F_{up,resulting,1,I} \cdot \cos\left(2\phi + \lambda - \frac{\pi}{2}\right) \qquad \textit{Equation 6-40}$$

$$F_{up,resulting,1,X,I} = \frac{k_I \cdot D \cdot \sin(2\phi + \lambda)}{\sin\phi \cdot \sin(\phi + \lambda)} \cdot w_{eq} \qquad \textit{Equation 6-41}$$

Furthermore, when the tools reach the bottom death center, the component of $F_{up,resulting,1,I}$ in Y-direction should be compensated by the lower wall of the entry channel ($F_{low,0,Y}$).

$$F_{up,resulting,1,Y,I} = F_{up,resulting,1,I} \cdot \sin\left(2\phi + \lambda - \frac{\pi}{2}\right) \qquad \textit{Equation 6-42}$$

$$F_{up,resulting,1,Y,I} = \frac{k_I \cdot D \cdot (-\cos(2\phi + \lambda))}{\sin\phi \cdot \sin(\phi + \lambda)} \cdot w_{eq} \qquad \textit{Equation 6-43}$$

The resulting friction force on the same channel is:

$$F_{low,0,X} = F_{low,0,Y} \cdot \mu \qquad \textit{Equation 6-44}$$

$$F_{low,0,X} = \frac{k_I \cdot D \cdot (-\cos(2\phi + \lambda))}{\sin\phi \cdot \sin(\phi + \lambda)} \cdot w_{eq} \cdot \mu \qquad \textit{Equation 6-45}$$

At this point, it will be assumed that the radial pressure in the entry channel caused by the axial forces doesn't apply on the walls of the same channel unless this pressure causes a plastic deformation in the sample. This assumption is legitimate

because the deformation in the yielding line causes an elastic displacement in the forming machine and tools. Since ECAS tools are made out of two separate pieces and are not fixed together in order to enable the oscillation movement, it is reasonable to assume that the elastic displacement caused by the yielding force is higher than the elastic expansion of the sample. Therefore, it will be assumed that the walls of the entry channel aren't in contact with the sample because of the radial pressure.

Finally, the axial forces $F_{axial,I}$ to hold the sample fixed during deformation become:

$$F_{axial,I} = F_{up,resulting,1,X,I} - F_{low,0,X} \qquad \textit{Equation 6-46}$$

$$F_{axial,I} = \frac{k_I \cdot D \cdot \sin(2\phi + \lambda)}{\sin\phi \cdot \sin(\phi + \lambda)} \cdot w_{eq} - \frac{k_I \cdot D \cdot (-\cos(2\phi + \lambda))}{\sin\phi \cdot \sin(\phi + \lambda)} \cdot w_{eq} \cdot \mu \qquad \textit{Equation 6-47}$$

Figure 6-12 displays the predicted $P/2k$ values in axial and radial direction for single turn ECAS.

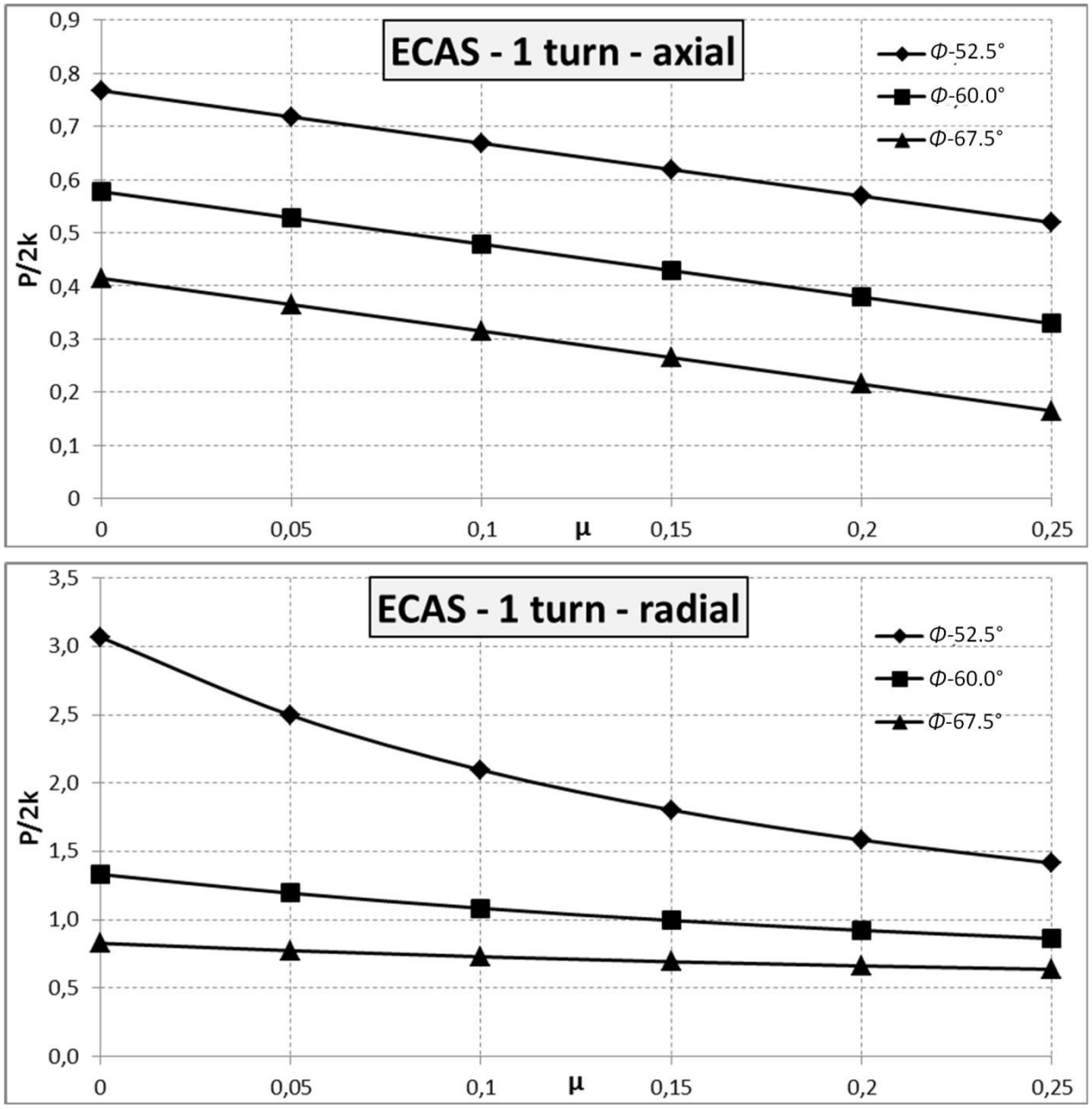

Figure 6-12 Pressure predictions in axial and radial direction for single turn ECAS

It is clear that friction plays a major role in the force requirement for a ECAS process. However, unlike ECAP, it eases the deformation and reduces the forces in the axial direction. An important aspect is that the pressure values are equal to the ones of a ECAP process for the frictionless case.

Nonetheless, the radial forces which are primarily responsible for the deformation are distinctively higher than the axial ones. Moreover, there is an abrupt increase when the channel angle (2ϕ) nears 90°. This is because of the fact that the tools can

transfer only forces normal to their contacting walls. As the channel gets steeper, the angle between the normal of the contacting tool wall and radial oscillation direction increases. As a result, to acquire the same value, a higher force should be applied. Theoretically, it is impossible to deform materials with a channel angle (2ϕ) of 90° by ECAS. This is a major disadvantage of this process.

The same approach as in the single turn ECAS can be used in the calculation of the forces emerging by its two turn variant. However, unlike conventional ECAP, the radial pressure inside the channels doesn't have any effect on the forces in ECAS if the sample material remains elastic outside the plastic deformation zone. Hence, a second forming within a single tool system would simply duplicate the force requirement compared to the single turn ECAS. Nevertheless, since the material hardens after the first deformation zone, an increase of the material strength and as a result also in the force requirement is expected. Consequently, the loads, displayed in Figure 6-13 can be calculated with the following formulas:

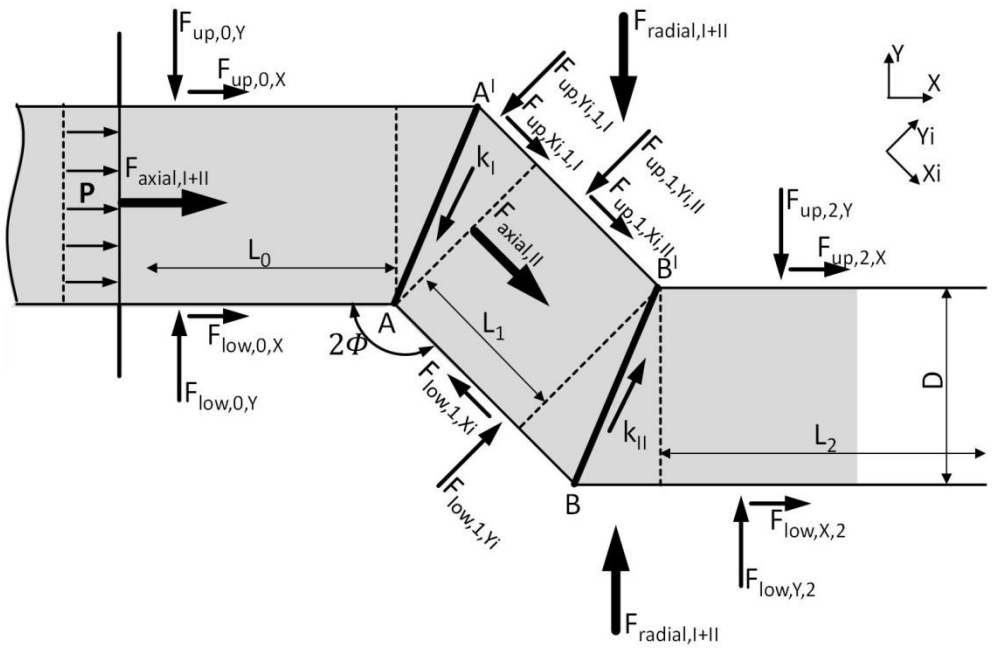

Figure 6-13 Schematic illustration of the forces in two turn ECAS

$$F_{up,1,Xi,II} = \frac{k_{II} \cdot D \cdot (-\cos(2\phi + \lambda))}{\sin\phi \cdot \sin(\phi + \lambda)} \cdot w_{eq} \cdot \mu \qquad \textit{Equation 6-48}$$

$$F_{axial,II} = \frac{k_{II} \cdot D \cdot \sin(2\phi + \lambda)}{\sin\phi \cdot \sin(\phi + \lambda)} \cdot w_{eq} - \frac{k_{II} \cdot D \cdot (-\cos(2\phi + \lambda))}{\sin\phi \cdot \sin(\phi + \lambda)} \cdot w_{eq} \cdot \mu \quad \textit{Equation 6-49}$$

$$F_{radial,II} = \frac{k_{II} \cdot D}{\sin\phi \cdot \sin(\phi + \lambda) \cdot (-\cos(2\phi + \lambda))} \cdot w_{eq} \quad \textit{Equation 6-50}$$

Consequently, the total force in both directions can be calculated by simply adding these values to Equation 6-39 and Equation 6-47.

$$F_{axial,I+II} = \frac{(k_I + k_{II}) \cdot D \cdot \sin(2\phi + \lambda)}{\sin\phi \cdot \sin(\phi + \lambda)} \cdot w_{eq} - \frac{(k_I + k_{II}) \cdot D \cdot (-\cos(2\phi + \lambda))}{\sin\phi \cdot \sin(\phi + \lambda)} \cdot w_{eq} \cdot \mu \quad \textit{Equation 6-51}$$

$$F_{radial,I+II} = \frac{(k_I + k_{II}) \cdot D}{\sin\phi \cdot \sin(\phi + \lambda) \cdot (-\cos(2\phi + \lambda))} \cdot w_{eq} \quad \textit{Equation 6-52}$$

$P/2k$ values in axial and radial direction predicted using Equation 6-51 and Equation 6-52 are shown in Figure 6-14.

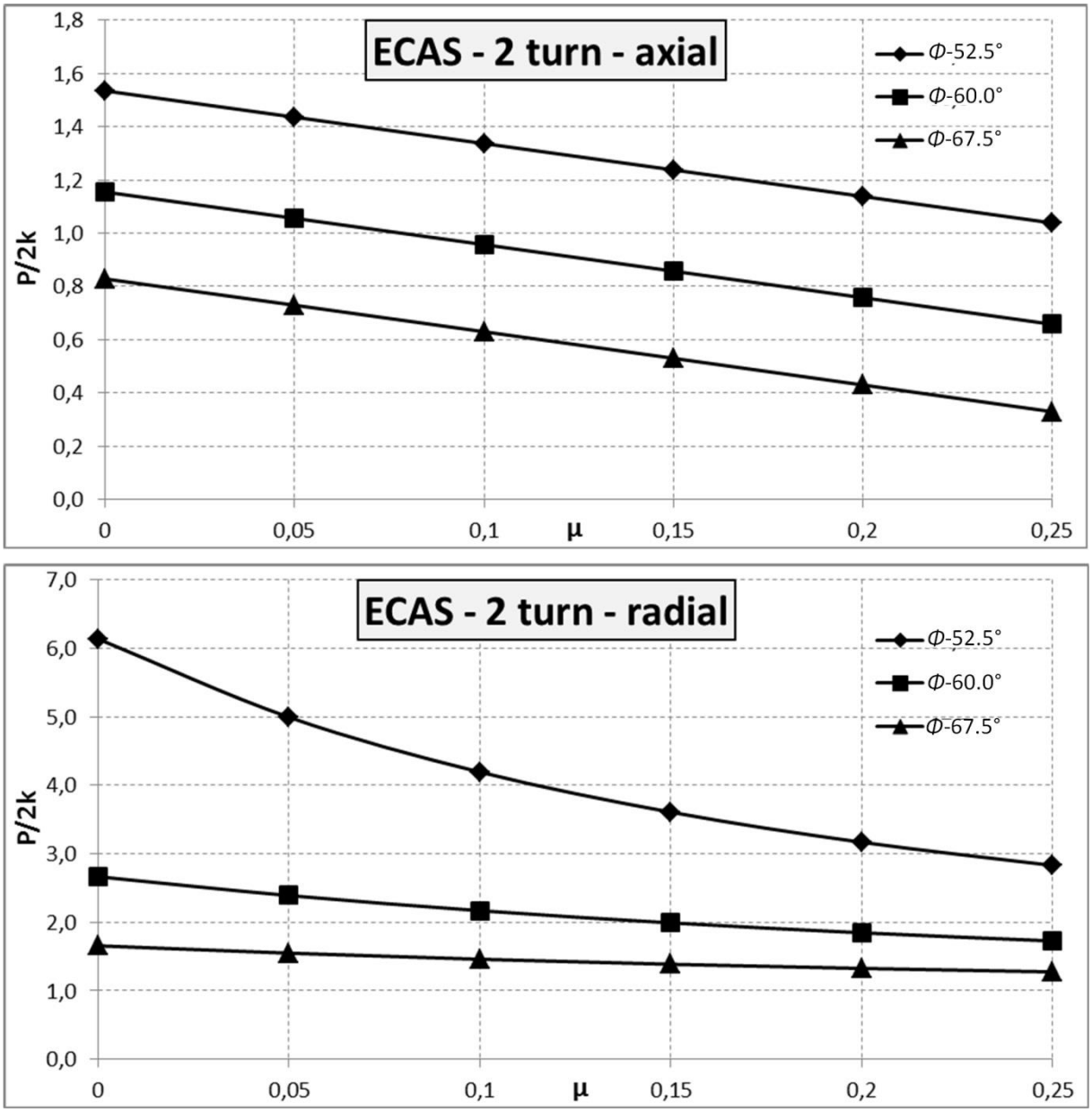

Figure 6-14 Press predictions in axial and radial direction for two turn ECAS

As in the case of single turn ECAS, the pressures in both axial and radial directions decrease while the friction coefficient increases in two turn ECAS process. Besides the fact that the radial pressures are extremely higher than the axial ones and the ECAS process is inefficient in terms of overall pressure requirement compared to ECAP, the axial pressure in the feeding direction is considerably lower. Since a major prerequisite for a continuous forming operation is a low force requirement in the feeding direction, ECAS process has a high potential for the continuous and thus

cost efficient production of UFG materials. An important aspect is that the pressures in the axial direction for a channel angle (2ϕ) of 120° is lower than the yield strength of the material by friction coefficients higher than 0.07. Thus, in order to prove the validity of the derived formulas, an ECAS tool system with a channel angle of 120° will be used in this study. The validation will be done by using FE-simulations and model experiments in the next chapters.

7 Finite-Element-Simulation of ECAS-Process

In order to validate the equations derived in Chapter 6, a model experiment will be designed. However, as mentioned in the previous studies about ECAP, the geometrical parameters, especially the channel length and outer corner radius have a significant effect on the plastic deformation and strain homogeneity [ROS02 and DJA10]. Therefore, it is planned first to investigate the effects of channel length and outer corner radius on the deformation by ECAS using FE simulations. Nevertheless, different FE approaches have been utilized in the past. Before starting the parameter study, it will be investigated which approach, 2D or 3D is more appropriate for the numerical analysis of an ECAS process. The material copper will be used in this comparison study.

7.1 Determination of Finite Element Simulation Strategy

The coupled thermo-mechanical FE model of the ECAS process is generated with the commercial software package of MARC/Mentat 2010. In the first approach, the cross section of the billet in longitudinal direction perpendicular to the radial movement is modeled in 2D. In the second approach, the billet is modeled in 3D. Due to the symmetry of the process, only half of the billet is modeled in order to save computation time.

In both simulation models, the tools are assumed to be rigid with heat conduction capabilities. The length of the entry, middle and exit channels are 65 mm, 15 mm and 65 mm, respectively. Since the production of channel intersections with sharp corners is technologically very difficult, a chamfer radius of 1 mm is defined at both inner and outer corners of the forming tools.

As the numerical simulation of incremental bulk metal forming processes are highly time consuming (see Chapter 2.3.3), two regions with different mesh sizes are defined in the deformable sample (Figure 7-1). The first one is the region where the sample is deformed and has accordingly a finer mesh. The second one connects this first section with the push mechanism and has a coarser mesh. Moreover, in the first

simulations to compare the 2D and 3D approaches, a rather coarse mesh of 2mm by 2mm is used in the deformation region of the sample. The 2D model is divided into 750 four-node, quadrilateral, plain-strain elements with full integration. In the 3D model, 4200 eight-noded, isoparametric, arbitrary hexahedral elements with also full integration formulation are used. It is intended to use a finer mesh in the later investigations.

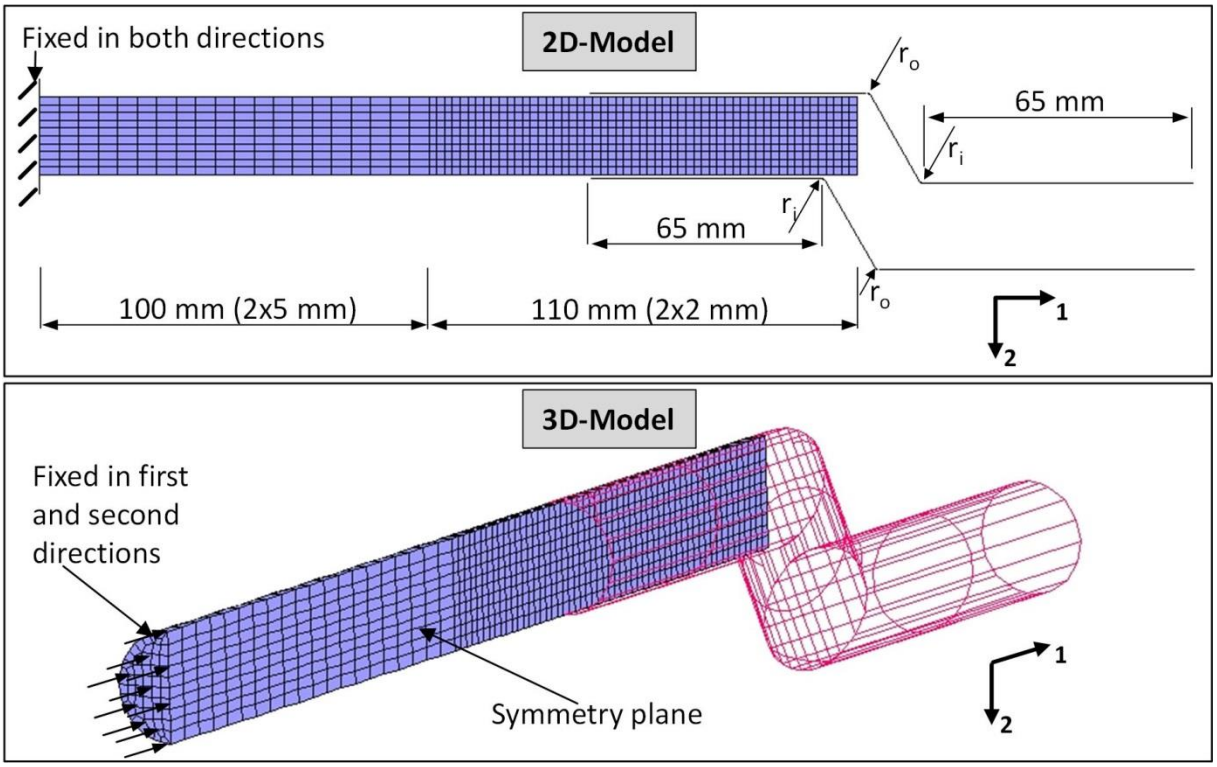

Figure 7-1 2D and 3D models of ECAS process

In both models, the oscillation movement of the tools is modeled with a sinusoidal function [TUR11]. The frequency and the amplitude of this motion are 30 Hz and 0.7 mm, respectively. Since there was no standard option for the modeling of such a movement in the used program, this function was implemented in the model with the MOTION subroutine. Contrary to the real process, the rod material is fixed at the open end and the tools are driven over it with a constant axial speed of 1 mm/s in combination with the oscillation. Every forming cycle is represented with 80 increments. In order to reduce the result file size, only the data by every 80th increment, by which the tools reach the bottom dead center, is saved.

The properties of the material are defined according to the Johnson-Cook model explained in Chapter 5.1. The heat transfer characteristics and the mechanical properties of the used material are assumed to be as follows [DKI12, MIR10]:

Table 7-1 Heat transfer characteristics and mechanical properties of investigated materials

Parameter	**Cu**	**C4C**
ρ – Density [kg/m^2]	8960	7873
c – Specific heat [J/kg K]	384.4	466
k – Thermal conductivity [W/m K]	395	43
h – Heat transfer coefficient [W/m^2 K]	4	4
ζ_d – Deformation heat dissipation [-]	0.85	0.85
ζ_f – Friction heat dissipation [-]	0.85	0.85
E – Young's modulus [GPa]	110	210
ν – Poissons's ratio [-]	0.3	0.3
μ – Friction coefficient [-]	0.065	0.065

The FE analyses are carried out with the implicit solver of MARC/Mentat 2010. All the simulations are conducted on Dell Power Edge R410 servers with Intel Xeon X5660 2.8 GHz processors.

The deformation, temperature distribution, the process forces and the simulation time in 2D simulations are compared with the 3D ones. Figure 7-2 demonstrates the mesh deformation of both modelling strategies.

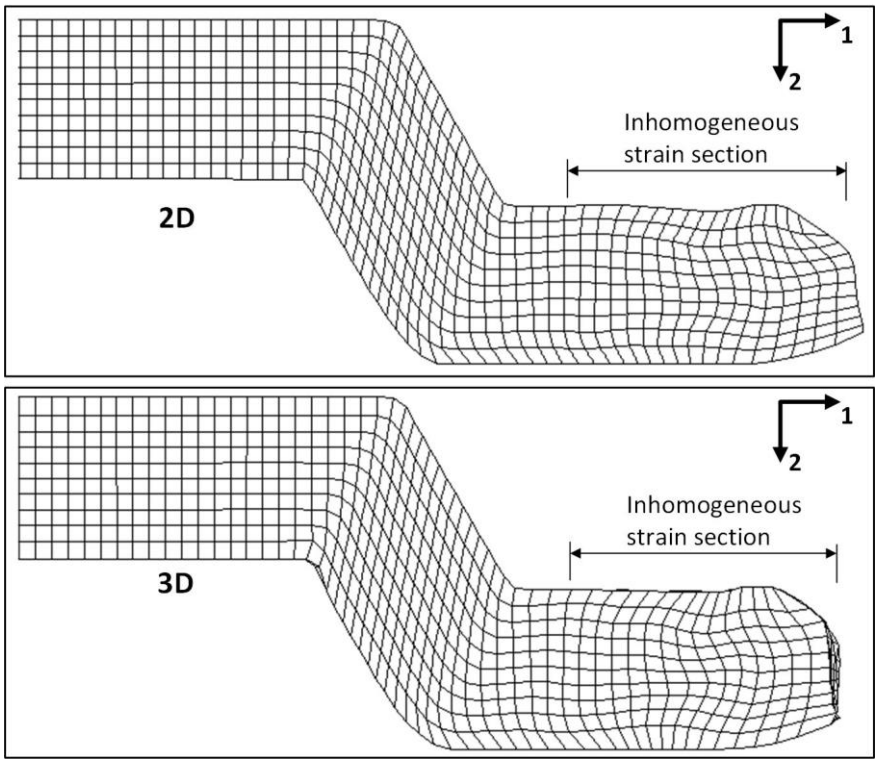

Figure 7-2 Mesh deformation in 2D and 3D models of ECAS process

The deformation characteristics of both strategies are fairly similar along the cross-section in lateral direction. The mesh deformation after the first yielding line (I) in the middle channel is homogeneous and resembles simple shear. However, in the exit channel after the second yielding line (II), the deformation starts to deviate from the expected simple shear pattern, especially in the vicinity of the upper and lower tool boundaries in both cases. An inhomogeneous section follows this partially regular zone.

A small deviation is observed in the strain distribution in the exit channel (Figure 7-3). The total equivalent plastic strains (TEPS) of the 3D simulations shown in this figure are larger than the TEPS values of the 2D ones especially in the first and last two millimeters of the evaluation path. This deviation is presumably caused by higher straining of the outer section of the samples in the third direction by the 3D simulations. Since a plain strain formulation is assumed in 2D simulation, such an additional straining doesn't exist in 2D approach. Despite these differences in the TEPS values, the mesh deformation is alike by both simulation approaches. This similarity of the mesh deformation can be observed when the shear strain values in the 12-direction is inspected. The shear strain values shown in Figure 7-3 are almost

identical for both cases except the upper and lower end of the sample. However, the deviations in these sections are not as high as the TEPS distributions.

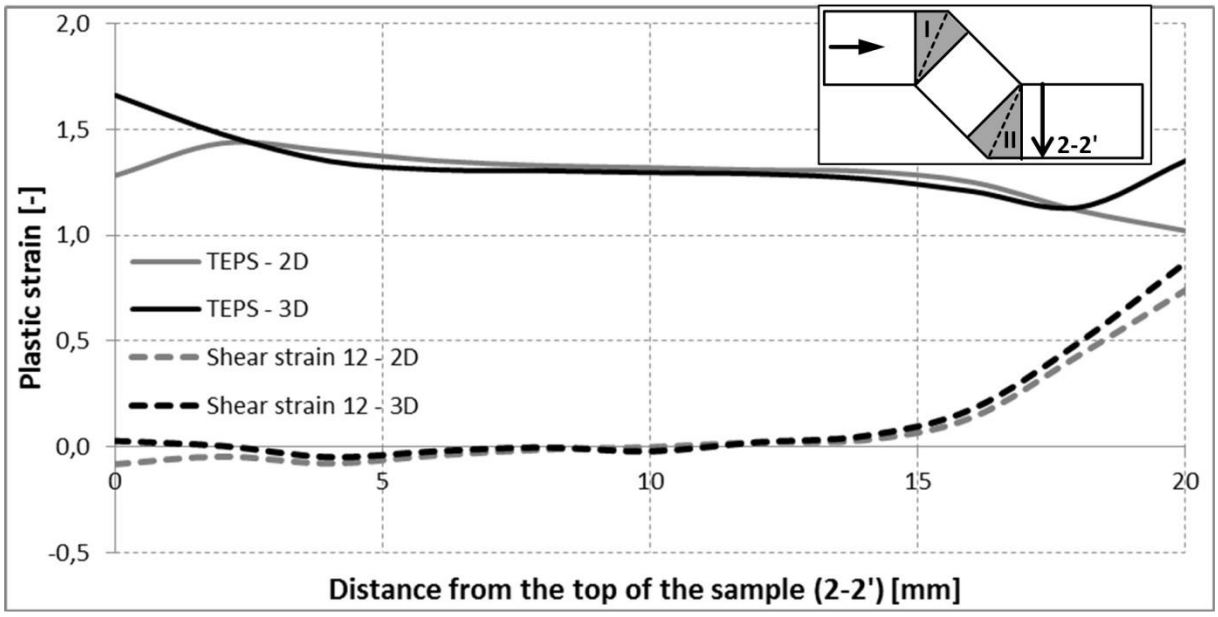

Figure 7-3 Comparison of plastic strains in 2D and 3D FE simulations in the exit channel

A more distinctive deviation is observed by the comparison of the temperature distribution in the samples (Figure 7-4). As mentioned in Chapter 6, an equivalent cross-section is defined for 2D modelling of ECAS process. However, although the cross sectional area is equal to the real one by this definition, the contact area of the tool surfaces are just half of the real one. As a result, the heat transfer between the tool walls and the sample surface is less in the 2D model compared to the 3D one. Nevertheless, the difference in the maximum values is only 18°C between 2D and 3D simulations. On the other hand, the temperature difference in the sample inside the exit channel is more distinctive.

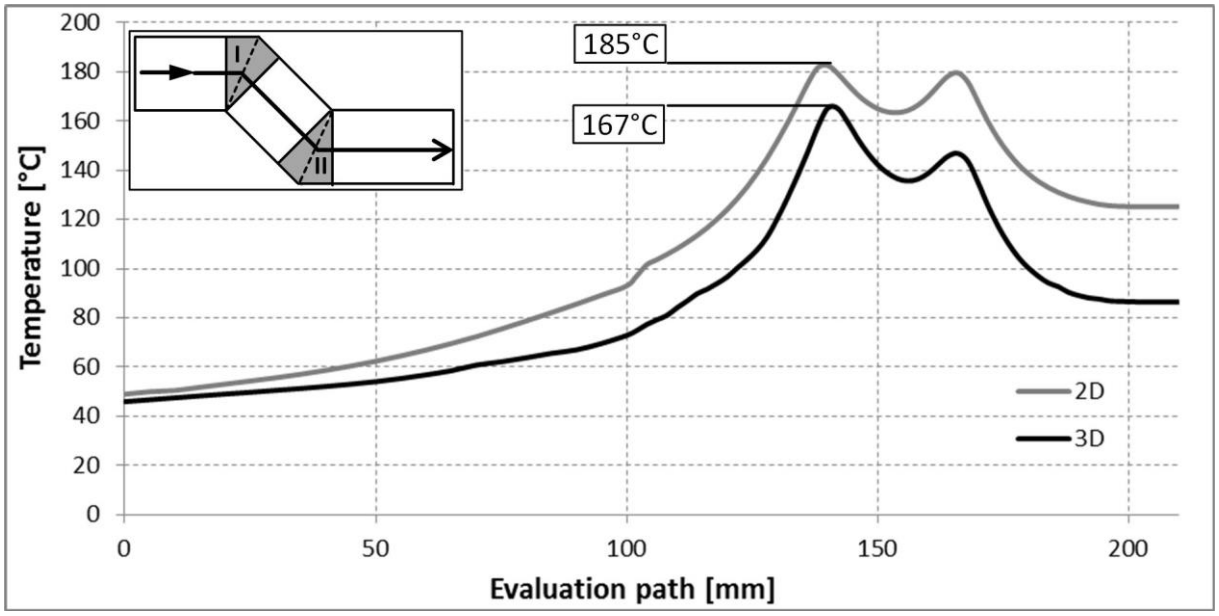

Figure 7-4 Comparison of temperatures in 2D and 3D FE simulations

The process forces required to form the samples are nearly equivalent for both simulation approaches (Figure 7-5). The major differences occur when the round workpiece first touches the tools. In 3D simulations, since the roundness of the sample isn't neglected, the sections outside the lateral cross section come into contact with the tools. Accordingly, a smaller portion of the material is formed at the beginning. Therefore, a smoother increase in forces is observed in axial and radial directions. However, as the process proceeds, this difference starts to equalize. Overall, predicted forces at the end of the process are nearly equal.

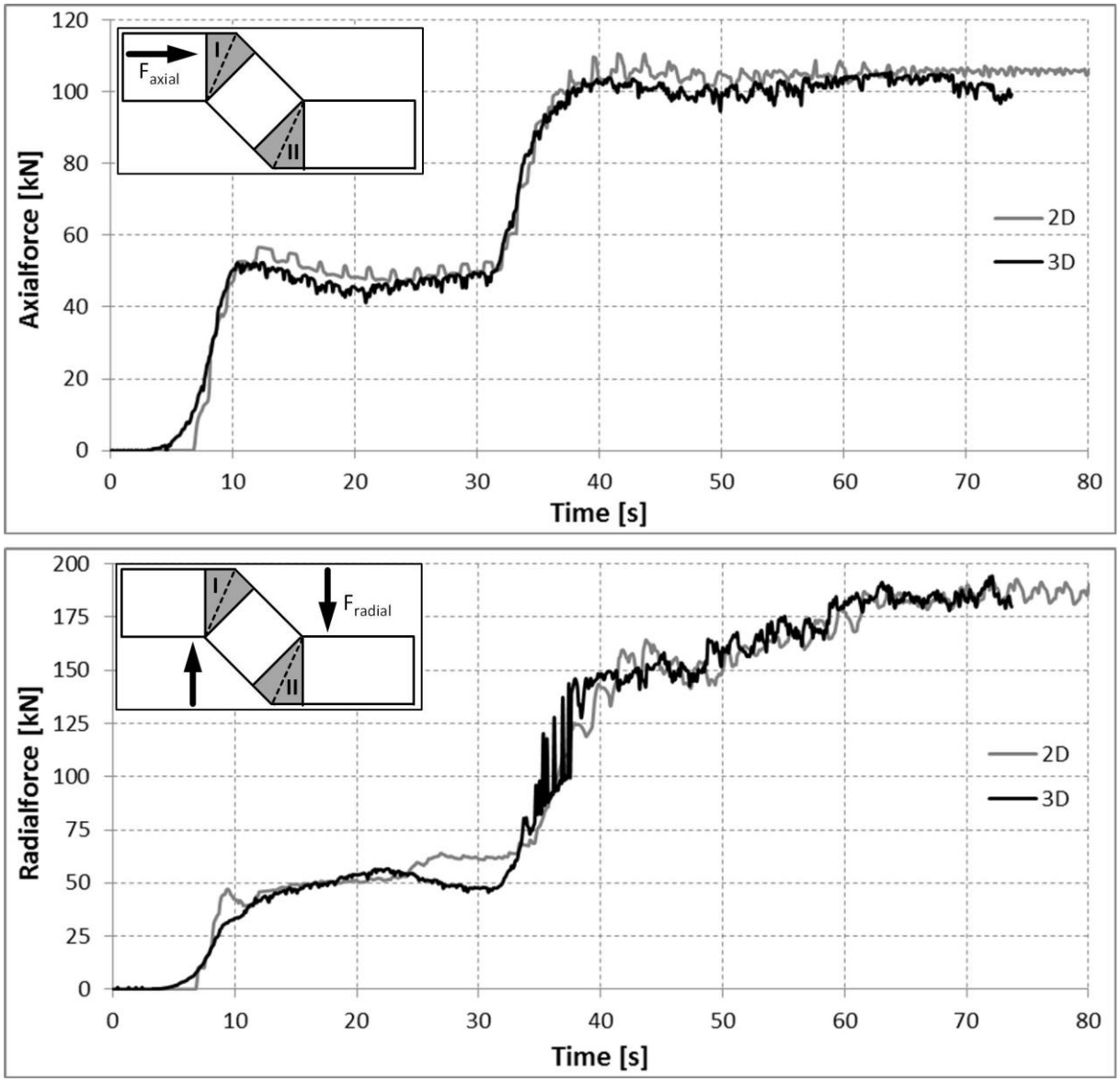

Figure 7-5 Comparison of process forces in 2D and 3D FE simulations

The comparison of both approaches prove that 2D and 3D FE simulations deliver similar results regarding mesh deformation, temperature and process force. However, the major difference between these two is the simulation time. While the computation of the 3D FE model requires approximately 38 days, the 2D simulation is finished within 5 hours. Thus, the usage of the 3D approach for a parameter study is not feasible. Therefore, 2D FE simulation models will be used in the later investigations of ECAS processes.

7.2 Effect of Channel Length

Firstly, the effect of the channel length on mesh deformation, temperature development and process forces will be investigated with the aid of FE simulations. The process parameters in Table 7-1 together with the material parameters defined in Chapter 5 are used. The 2D modeling approach is implemented. However, unlike the previous chapter, a finer mesh of 1mm by 1mm is utilized. In order to ease the visual evaluation, flow lines of 2 mm by 2 mm are defined. Both materials, copper (Cu) and low carbon steel (C4C) are investigated. The length of the entry and exit channels (L_0 and L_2) is kept constant at 65 mm in all models. The length of the middle channel (L_1) is varied between 5 mm and 20 mm with 5 mm steps.

The mesh deformation after ECAS processing with copper samples is demonstrated in Figure 7-6. In the first variation with a middle channel length of 5 mm, the deformation is inhomogeneous. After the second yielding line, the exit channel isn't filled with material completely. Accordingly, a regular shear pattern can be observed neither after the first, nor after the second yielding line. Increasing the channel length L_1 to 10 mm leads to a more homogeneous deformation. However, a regular shear pattern isn't present after the second yielding in this case. Further increasing L_1 to 15 or 20 mm provides a uniform deformation after first and second yielding line, especially in the middle of the sample. As explained in Chapter 6.2, the deformation along the second yielding line causes a force component on the middle channel of the upper tool. By short channels, this force component overlaps with the one caused by the first yielding of the material. Such an overlapping results in inhomogeneities by the force distribution and induces a bending rather than shearing along the second yielding line in the tool. With this feature, ECAS process agrees well with the former studies about the effect of the channel length on the strain distribution in the ECAP-processed samples. Similar results are obtained also from the simulations with the material C4C. These results are demonstrated in the Appendix A.

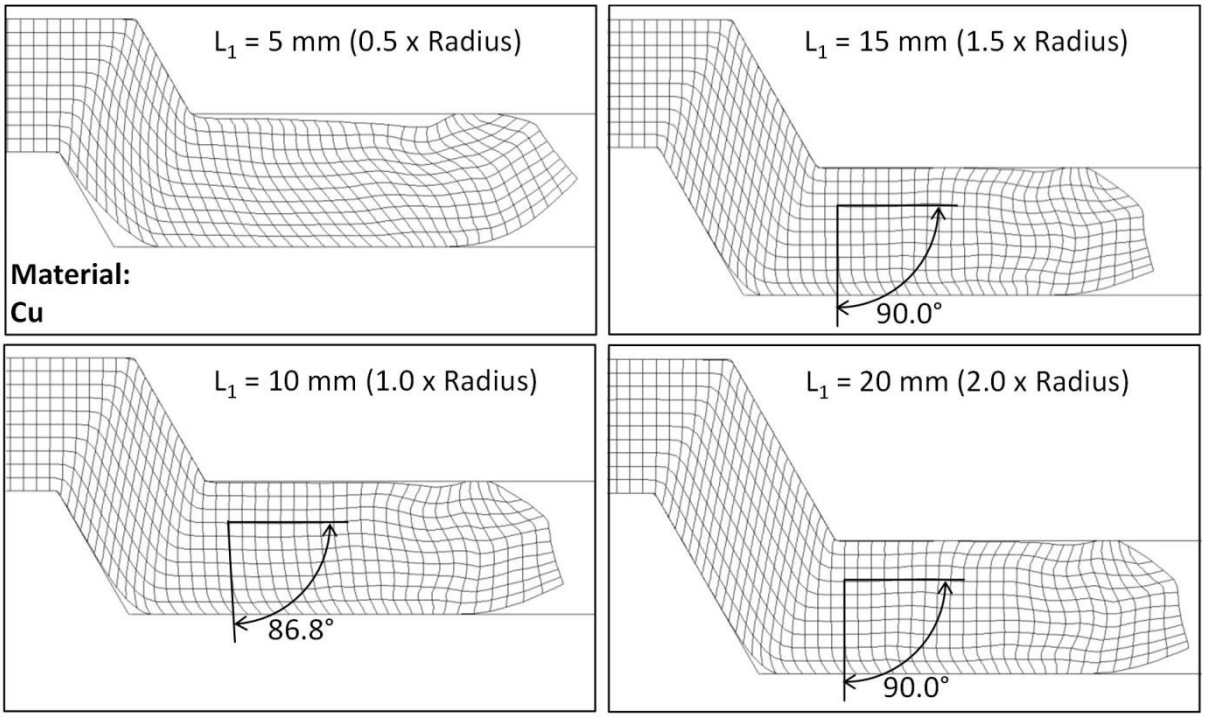

Figure 7-6 Comparison of mesh deformation in copper

Similar results are obtained when the shear plastic strain is investigated in the middle and exit channel (Figure 7-7). The strain inhomogeneity in the case of the middle channel length of 5 mm reveals itself as an irregular deviation from the analytically predicted values according to Equation 2-6. Although the shear strain distribution appears regular for the other three variants, the one with a length of 10 mm deviates slightly from the other two in the lower section of the sample. The deformation inhomogeneity for the same case causes also a partial strain recovery after the second yielding line. Another important aspect is that even the strain values of the homogeneous deformation deviate from the analytically predicted ones. This deviation is presumably caused by the fact that the material isn't deformed along a single shear line as assumed by the definition of Equation 2-6. A small curvature should be formed at the outer corner of the material which results in a decrease of the strain values. Similar results are also valid for the low carbon steel. Corresponding diagrams are demonstrated in Appendix A.

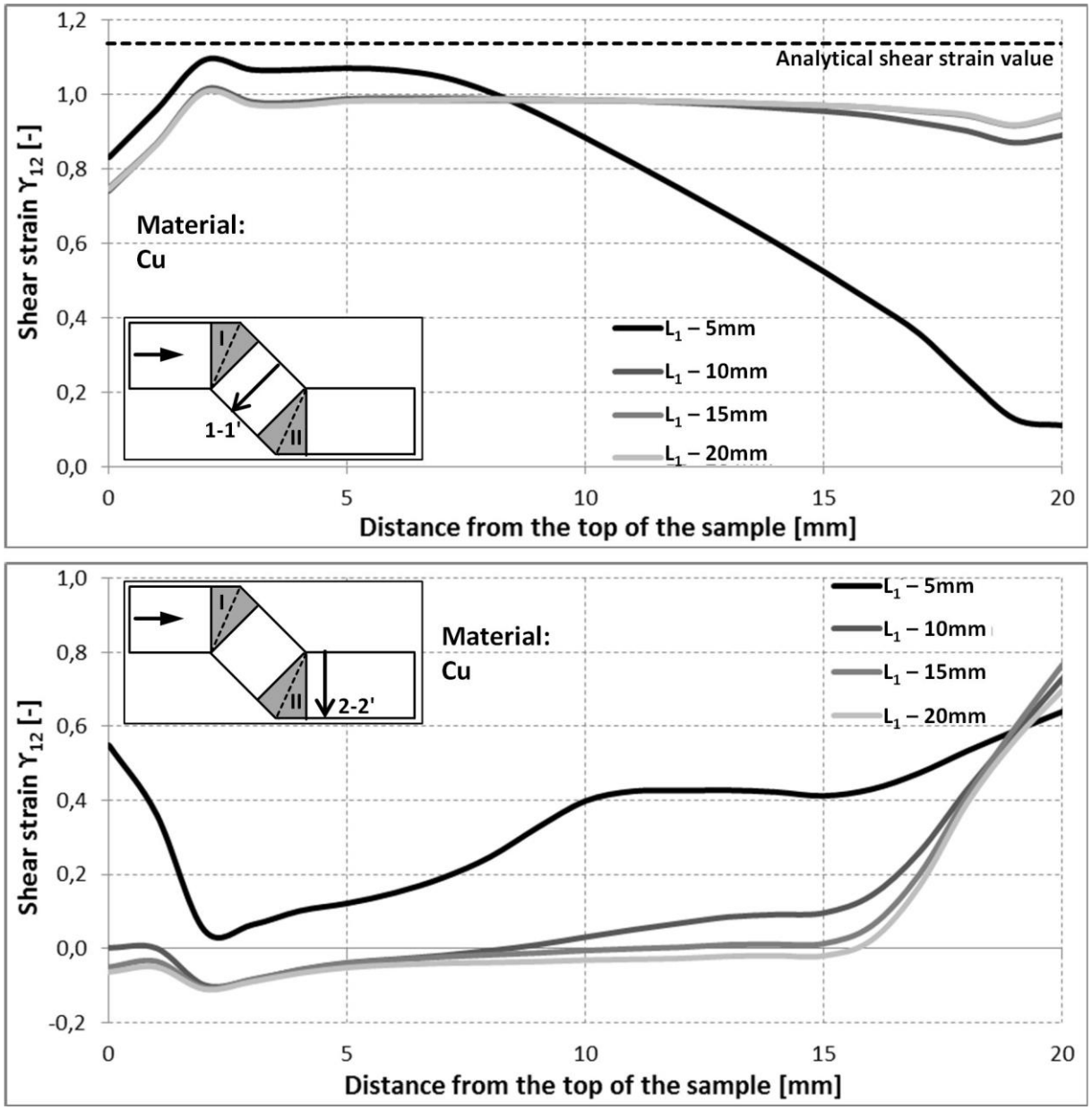

Figure 7-7 Comparison of shear strains from the middle (upper diagram) and exit channel (lower diagram) in copper

The plastic deformation and friction cause an increase in the temperature in the materials during the ECAS processing. It is observed that the temperature distribution inside the sample along an evaluation path in the middle of its lateral cross section follows the same pattern as the one in Figure 7-4. To ease the evaluation, the maximum temperatures in the sample are shown in Table 7-2.

Table 7-2 Maximum temperatures in copper and low carbon steel samples after channel length variation

Material	L_1			
	5 mm	10 mm	15 mm	20 mm
Cu	193.0°C	189.7°C	185.9°C	181.1°C
C4C	383.1°C	385.2°C	370.6°C	354.8°C

In copper samples, the maximum temperature varies between 193.0 and 181.1°C. Since the increase of the channel length increases also the contact heat transfer area, it basically reduces the temperature in the samples. Same heat transfer situtaion is also valid for the low carbon steel. However, due to the lower thermal conductivity of steel, temperatures at the fixed edge of the sample barely rise and a sharper increase is observed in the deformation zones. Accordingly, the maximum temperatures are higher than copper. Furthermore, investigation of the temperature development inside the samples reveals important facts about the ECAS process. Especially by low carbon steel, such high temperatures would cause blue brittleness and would initiate cracks in samples. Therefore, for a successful implementation of ECAS process, an active cooling system is inevitable.

Force distribution in both, axial and radial direction agrees well with the previous findings about the deformation (Figure 7-8). By a middle channel length of 5 mm, force levels are lower than other variations. The reason for this is that the middle and exit channels are not fully filled. By higher channel lengths, although the plastic strain distribution may vary, the tools are completely filled with sample material. Therefore, same force levels are observed by the middle channel lengths higher than 5 mm. The maximum axial and radial forces are by about 112 and 158 kN, respectively.

While the force distribution behaviour in axial direction is similar to the copper material, different force patterns in radial direction are observed by the forming of the low carbon steel samples (Figure 7-9). Although the force levels in that direction are nearly equal for channel lengths of 15 and 20 mm, they tend to increase as the forming process proceeds after the second yielding line. This increase is associated with the higher strength and the lower thermal conductivity of steel. These both characteristics cause higher and more confined temperature regions in the vicinity of the forming zones compared to copper samples. Accordingly, radial forces required

to deform the material drop. Such a decline results in a decrease in the friction related axial forces which pulls the sample in the feeding direction. Therefore, as the temperature increases, the sample material in the entry channel of the tool halves tend to expand more and more in the radial direction. This expansion is balanced by the tool walls which result in higher forces in radial direction. Since the temperature distribution is more uniform and maximum values are less than by steel, such an effect is not observed during the deformation of copper material.

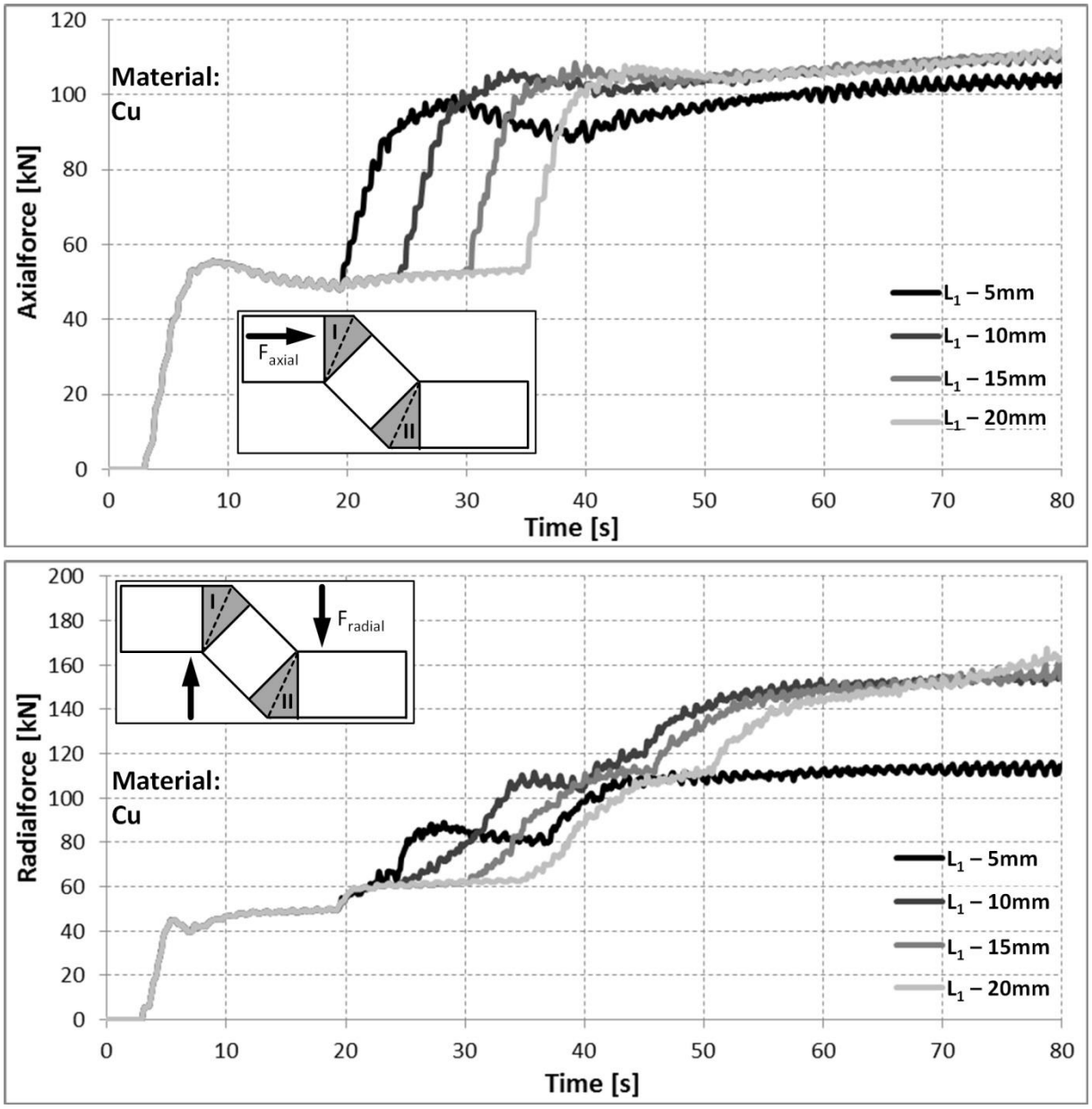

Figure 7-8 Comparison of process forces in axial (upper diagram) and radial direction (lower diagram) in copper

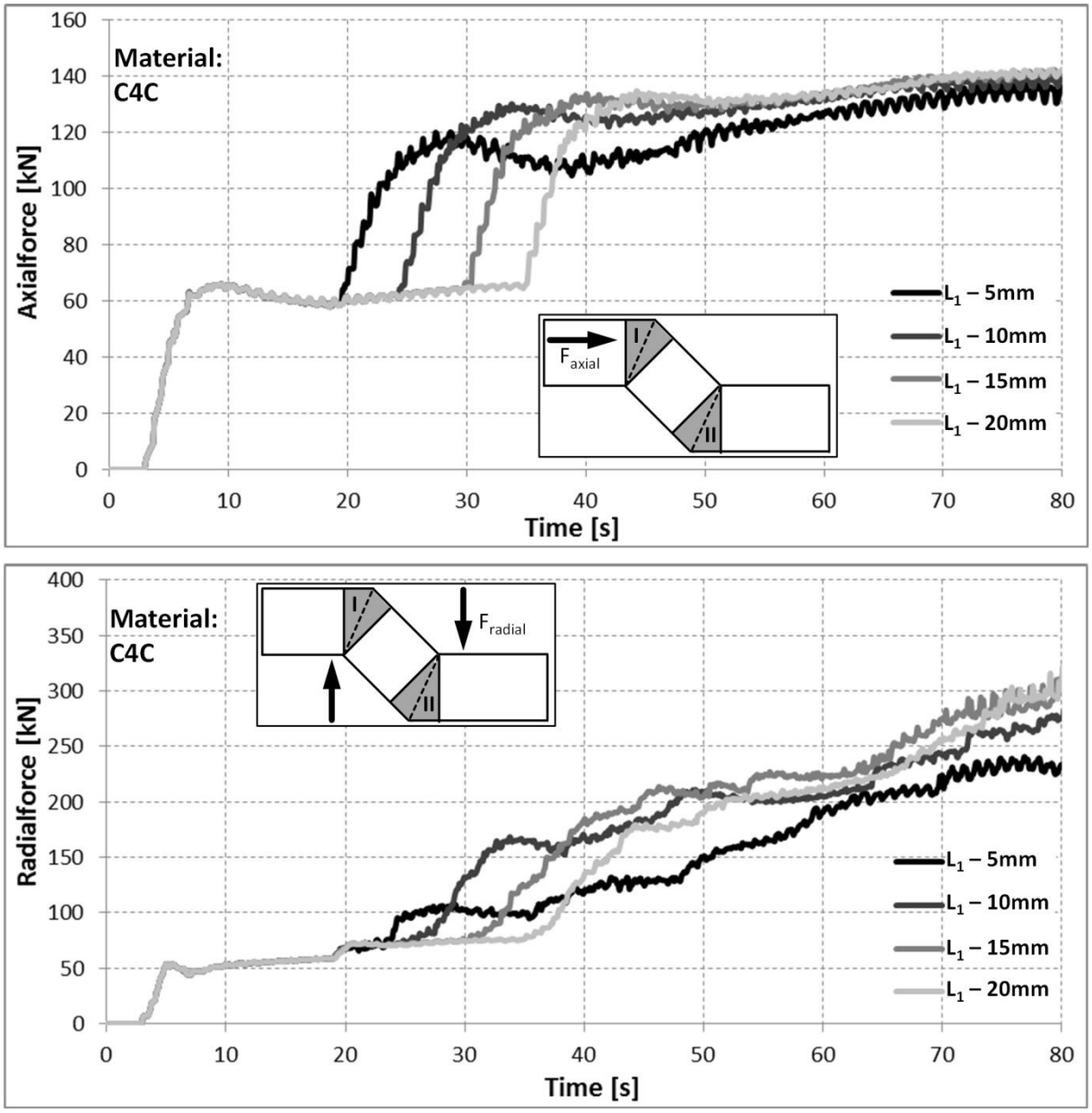

Figure 7-9 Comparison of process forces in axial (upper diagram) and radial direction (lower diagram) by low carbon steel

To sum up, while the length of the middle channel has a considerable effect on the deformation and force requirement in ECAS process, the temperature distribution inside the sample is less affected by it. Increasing this length over 10 mm ensures a homogeneous strain distribution and more stabilized forming forces, especially in the axial direction. On the other hand, increasing it from 15 mm to 20 mm doesn't have an improving effect. Such an increase would result in higher tool material and

machining costs. Therefore, the length of the middle channel is selected 15 mm which is 1.5 times the sample cross-section radius.

7.3 Effect of Outer Corner Radius

In the second step of the variations, the effect of outer corner radius on the deformations, temperature development and process forces are investigated with the aid of FE simulations. Same process and material as well as numerical modeling parameters as in the previous chapter are used. The length of the entry (L_0), middle (L_1) and exit channel (L_2) is kept constant at 65, 15 and 65 mm, respectively. The outer corner radius is varied between 1 and 7 mm with 2 mm steps. These variations correspond to arc of curvatures (2φ) of 2.5°, 7.7°, 13.1° and 18.8°, respectively.

The mesh deformation after ECAS processing with copper samples is demonstrated in Figure 7-10. By all variants, the exit channel of the tools is completely filled with the sample. Moreover, a regular shear pattern is observed in all workpieces, especially in the middle section of all channels, except the last variation. Apparently, the outer radius variation affects the deformation only on the upper side of the samples. However, as the radius is increased to 7 mm, this effect on the upper section spreads out over the entire cross section of the workpiece. It hinders the full recovery of the mesh after the second yielding line. As a result, a small inhomogeneity is observed in the deformation. Same results are obtained also from the numerical simulations with low carbon steel material (see Appendix A).

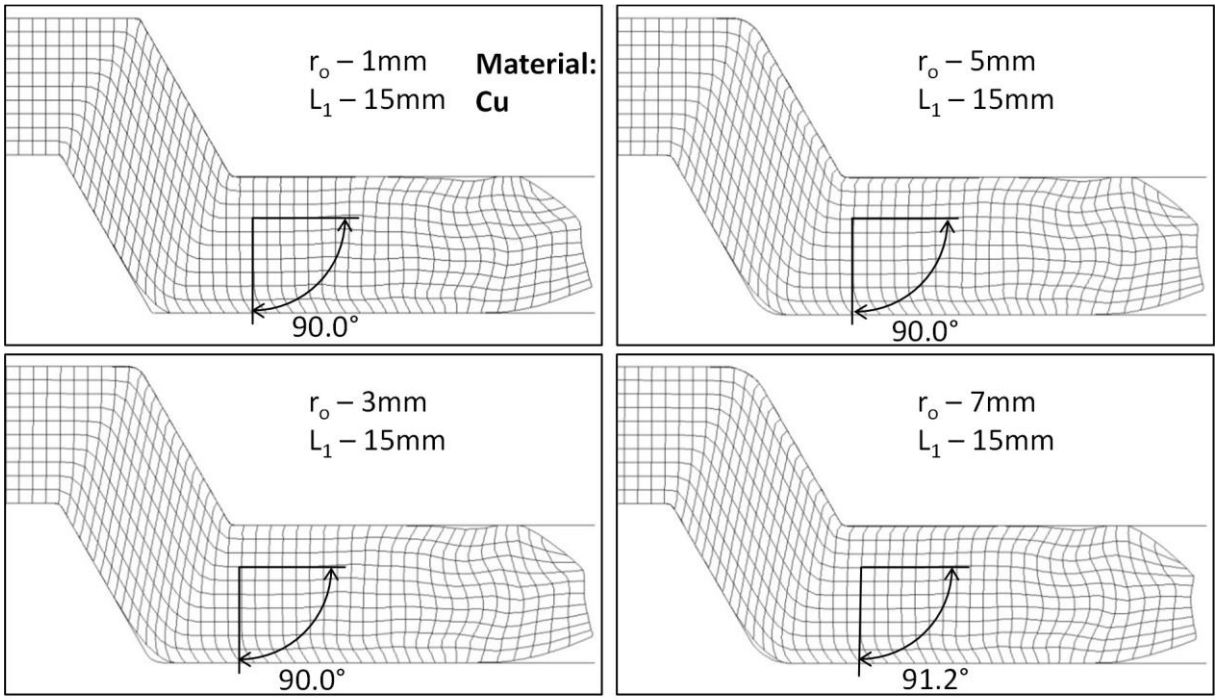

Figure 7-10 Comparison of mesh deformation by copper after outer corner radius variations

Similar conclusions can be drawn from the inspection of shear strain distributions in the middle and exit channels (Figure 7-11). As the outer corner radius increases, the shear strains on the upper section of the workpiece starts to deviate from the values in the steady state section in both channels. However, it has no effect on the shear strains on the lower section. It is reasonable because in all variations, the outer corner of the second yielding line isn't filled with workpiece material (compare with Figure 7-10). Moreover, due to the deviation in the mesh deformation by the radius of 7 mm, the shear strain values in the exit channel are slightly lower for this radius.

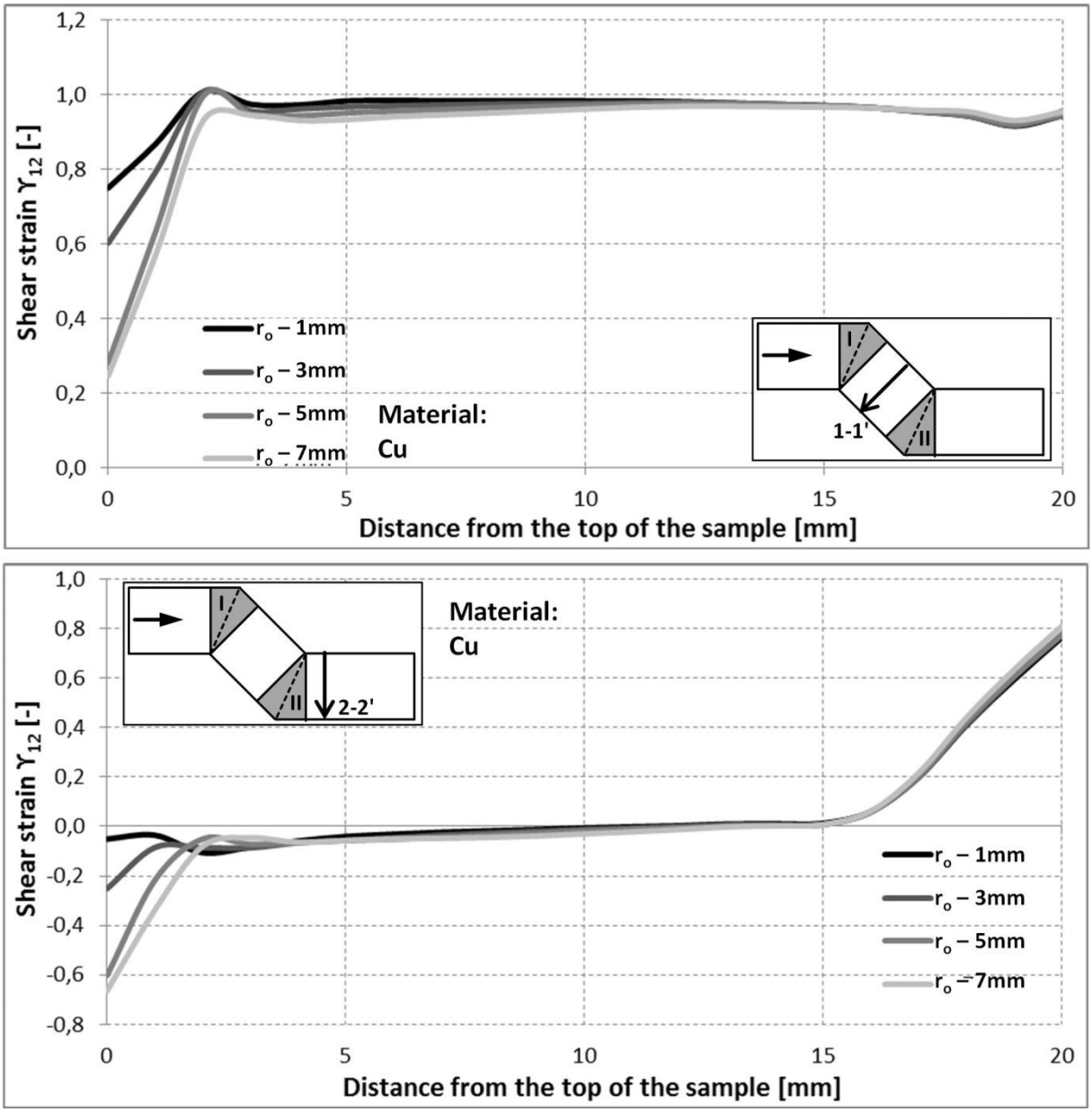

Figure 7-11 Comparison of shear strains from the middle (upper diagram) and exit channel (lower diagram) by copper material after outer corner radius variations

The temperature distribution inside the sample along the evaluation path in the middle of its lateral cross section follows the same pattern as in the previous chapters. To ease the evaluation, the maximum temperatures in the sample are shown in Table 7-3.

While the maximum temperatures vary between 185.9 and 163.2°C in copper samples, it is between 369.3°C and 386.3°C in low carbon steel. For both materials, increasing the outer corner radius from 5 mm to 7 mm reduces the maximum temperatures in the workpiece. This slight drop is associated with the decrease in the overall deformation in the material. For other radii, no significant change is observed.

Table 7-3 Maximum temperatures by copper and low carbon steel samples after outer corner radius variations

	r_o			
Material	1 mm	3 mm	5 mm	7 mm
Cu	185.9°C	177.2°C	173.3°C	163.2°C
C4C	370.6°C	386.3°C	380.8°C	369.3°C

The variation of outer corner radius doesn't have a significant effect on the axial and radial force behaviour in copper samples. A slight reduction in the maximum axial forces is observed when the outer radius is increased (Table 7-4).

Table 7-4 Maximum forces in axial and radial direction during ECAS processing of copper and low carbon steel samples in outer corner radius variation

Material		r_o			
		1 mm	3 mm	5 mm	7 mm
Cu	axial	111.7 kN	109.3 kN	106.1 kN	103.1 kN
	radial	165.1 kN	153.5 kN	158.2 kN	159.1 kN
C4C	axial	142.7 kN	141.0 kN	135.3 kN	131.4 kN
	radial	326.4 kN	352.7 kN	212.0 kN	208.9 kN

On the other hand, it has a considerable effect in the deformation of low carbon steel samples. The maximum forces in axial direction drops while outer radius increases, just like in the deformation of copper samples. Nevertheless, by the radius of 5 and 7 mm, the continuous increase in the radial forces is avoided. For both of these radii, the forces reach a steady state as the ECAS process proceeds after passing the second deformation zone (Figure 7-12). This is associated with the decrease of the axial forces. As the axial forces drop, the elastic expansion of the workpiece in the

radial direction decreases. After a certain point, this radial expansion doesn't have to be compensated by the tool walls of the entry channel section. Therefore, a steady state is obtained by outer corner radii equal or higher than 5 mm in the investigated low carbon steel.

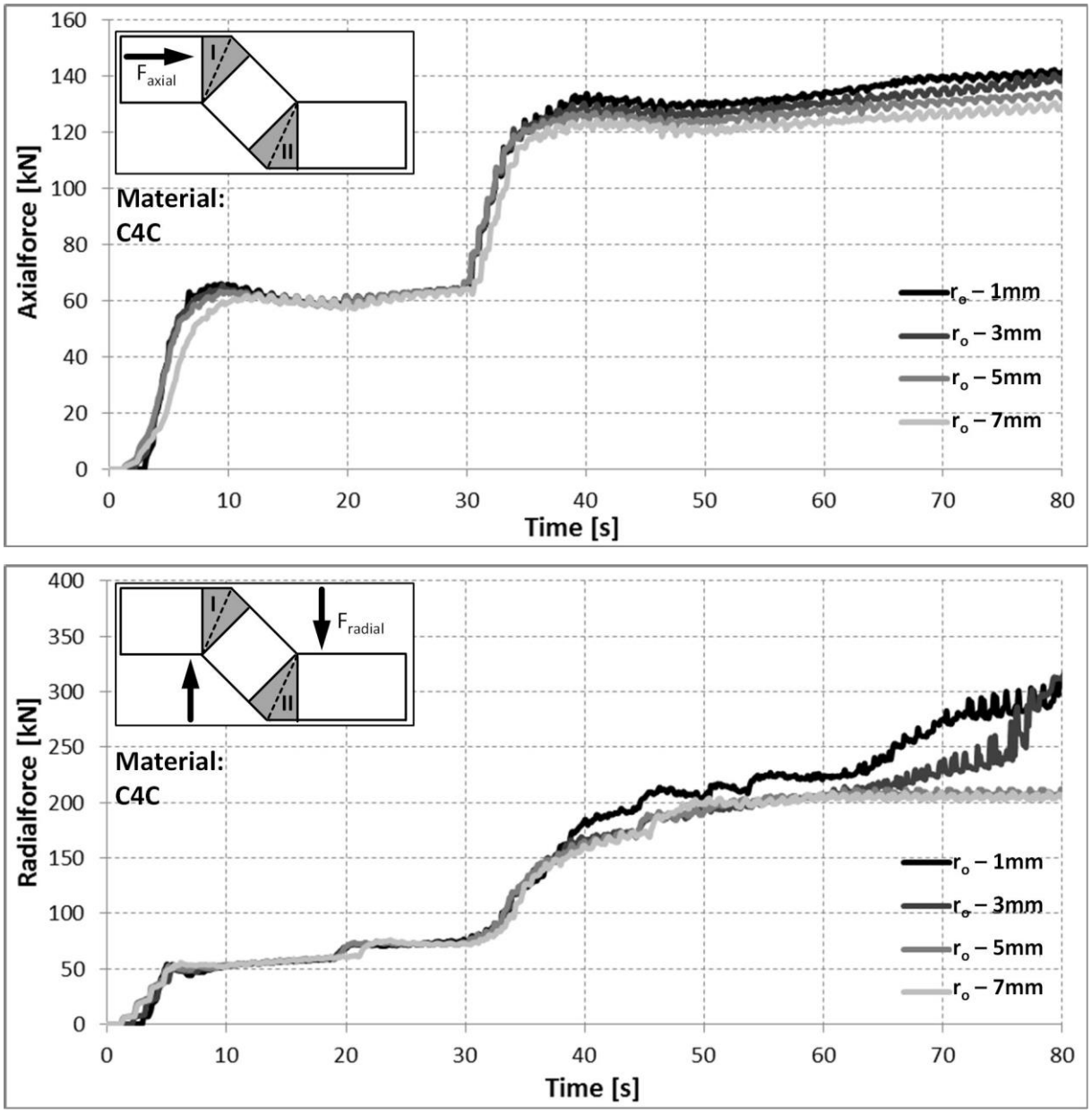

Figure 7-12 Comparison of process forces in axial (upper diagram) and radial direction (lower diagram) in low carbon steel

In conclusion, while the increase of the outer corner radius causes an additional inhomogeneity in the plastic shear strain distribution in both materials, especially in

the upper section of the workpieces, such an increase results also in a drop of the forming forces. As the radius of 5 mm ensures a steady radial force behaviour especially in low carbon steel samples without compromising the homogeneity of the plastic strains in the middle section of the samples cross section, this radius is selected for further studies.

8 Experimental Investigations of ECAS-Processes

The derived analytical formulations and finite element simulations from previous chapters should be validated with model experiments. For validation purposes, an ECAS tool system has been designed using the findings of the numerical investigations of Chapter 7. The designed tools are shown in Figure 8-1.

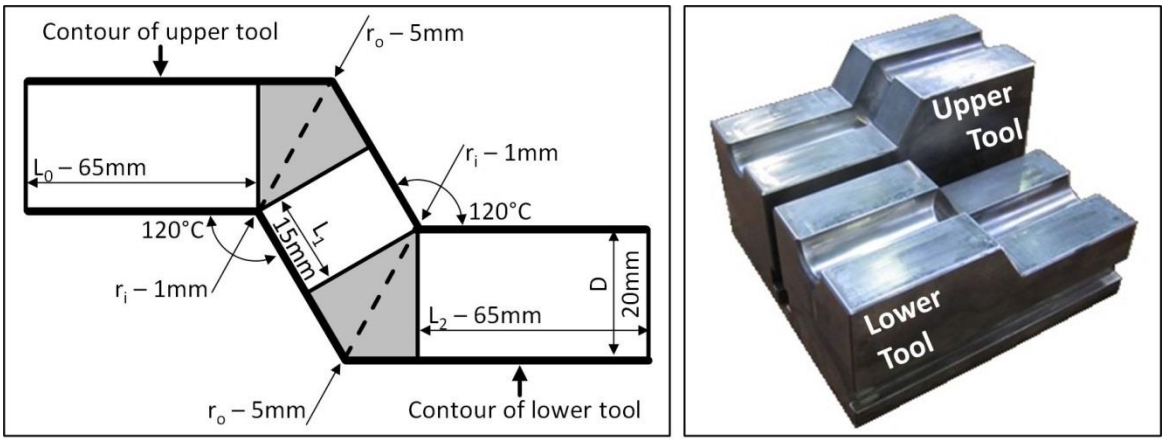

Figure 8-1 Schematic illustration of geometrical characteristics of ECAS tool system (left) and manufactured tool halves (right)

The tool system enables a two-step deformation within one forming step. All three channels intersect with the same channel angle (2ϕ) of 120°. This feature ensures that the workpiece enters and exits the deformation system along the same axis and prevents any collision with the forming machine. The overall length of the tools is 150 mm. The entry (L_0), middle (L_1) and exit channels (L_2) are 65 mm, 15 mm and 65 mm, respectively. The outer corner radius has been selected 5 mm which corresponds to an arc of curvature of 13.1°. In order to ease manufacturing, the inner corner radius has been selected as 1 mm. The forming channel has a circular cross section with a diameter of 20 mm. A ledeburitic 12 % chrome steel, X153CrMoV12 (1.2379) has been selected as tool material. After machining the tool geometry, the tool steel is hardened to 60 HRC. The forming surfaces are hand polished after hardening.

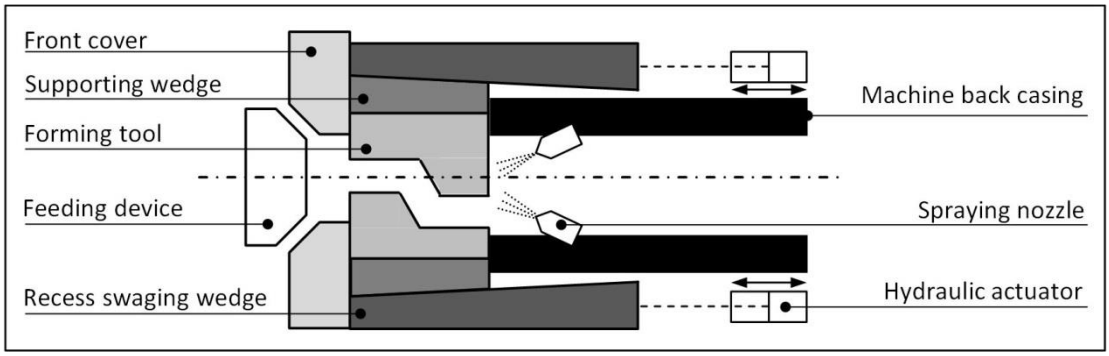

Figure 8-2 Schematic illustration of forming tools and periphery equipment assembly by the rotary swaging machine

As revealed by the numerical investigations in Chapter 7, for a successful implementation of the ECAS process with the rotary swaging machine at PtU, the workpieces have to be actively cooled. However, the existing machine lacks a cooling system. Therefore, the rotary swaging machine is equipped with an external cooling unit. Although it is intended to cool the samples from both sides, entry and exit, the entry section is covered by the clamp of the feeding unit during deformation. It leaves the exit section as the only possibility for cooling. Due to the tight design of the rotary swaging machine, the space around the exit channel is hardly accessible. Therefore, already installed pneumatic pipes are used to cool and lubricate the forming system. Cold extrusion oil SSP 70 of Zeller+Gmelin has been used in all experiments. The flow rate of the coolant/lubricant was 2.5 l/min.

Round bars of both materials, copper and low carbon steel, are used in the experiments. All workpieces were 320 mm in length. 110 mm of every sample is used to clamp those in the feeding device. The sample outside the clamp has the same length as in the numerical simulations. The feeding distance is kept constant at 80 mm in all experiments. Due to the geometrical restrictions of the rotary swaging machine, a further feeding of the 320 mm long samples was not possible. The feeding speed was 1 mm/s.

Forming forces, temperature development in the workpiece and material flow were in the center of the investigations as evaluation variables. It is also intended to prove the feasibility of ECAS process and the validity of the developed analytical hypothesis with model experiments.

8.1 Results of Experiments with Copper Roundbars (Cu-ETP)

The severe plastic deformation of the copper samples by ECAS was possible with the developed tool system. No cracking on the outer surface of the workpieces or any adhesion traces on tool surfaces are observed after forming. The undeformed portion of the round bars outside the tools remained intact without any sign of buckling after processing by ECAS with the forming parameters defined in the previous chapter.

The first experiments prove the feasibility of ECAS processes. However, for a better understanding of forming mechanics and limitations, the process forces and material flow as well as the temperature development will be investigated in detail in the following subchapters.

Process Forces

A slightly modified version of the strain gauge based force measurement equipment developed in previous studies has been used in the current investigations [RAT06]. The capacity of the system is improved to 400 kN in axial and 800 kN in radial direction. For an accurate representation of the cyclic deformation of the workpieces, all measurements are conducted with a sampling rate of 4800 Hz. In this manner, every forming cycle is represented with approximately 160 measurement points. The results are displayed in Figure 8-3. While the sensor setup to measure the axial forces required a pretension till about 20 kN, only a small amount of pretension was necessary in the modified system for the measurement of radial forces. Therefore, the measurements in axial direction start after force levels reach 20 kN. Since all measurement data including the loading and unloading cycle are shown in the following figure, the results appear as blocks rather than curves.

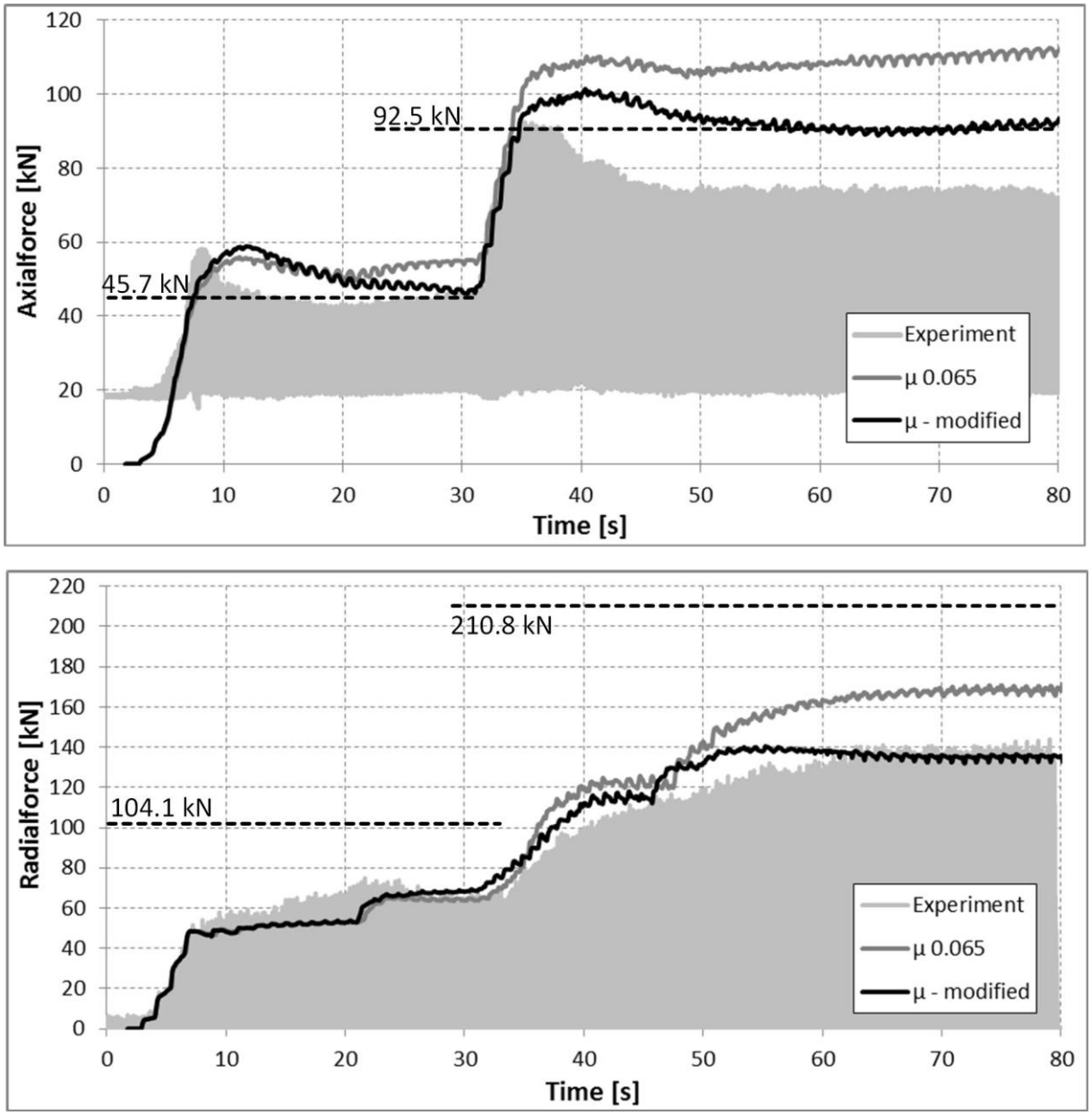

Figure 8-3 Measured, numerically simulated and analytically predicted (dashed lines) process forces required to deform copper workpieces (Feeding speed 1 mm/s)

The forming at the first yielding line starts with a sudden increase in axial forces up to 58 kN. This increase corresponds to the phase, where majorly the side edges of the round samples are in contact with the tools. Shortly after, the axial force levels stabilize at about 45 kN. The deformation along the second yielding line starts also with an abrupt increase reaching 96 kN and stabilizes afterwards at 77 kN. Since the tool geometry in the second forming zone is the same as the first one, it would be

expected that axial forces doubles after the workpiece crosses the second yielding line. However, with values of 77 kN, it is less than twice of the forces in the first deformation zone. It could be related to the temperature increase in the workpiece during the deformation process. Nevertheless, in such a case, same decrease in the force levels would be expected also in radial direction. The first deformation in the tool causes radial forces of maximum 74 kN. As the workpiece passes the second forming zone, this value increases to 143 kN. Although the force levels clearly doesn't double, the difference is much less than the ones in axial direction. Therefore, it is assumed that the increase in the temperature isn't the only reason for such a drop in the force levels.

In the previous studies about conventional ECAP, the friction is believed to be the most significant factor influencing the deformation. For a better understanding of the force requirement in ECAS process, a finite element analysis has been conducted. The effect of friction has been investigated by varying the friction coefficient. In the FE simulations, the same modeling approach from Chapter 7 has been used except the deformation and friction heat conversion factor. As ECAS process is cooled, the related dissipation factors are assumed to be 0.35. The rest of the generated heat is absorbed and transferred by the liquid coolant/lubricant. As demonstrated in Chapter 6.2, the coulomb friction coefficients by copper samples varied between 0.025 and 0.065. Accordingly, in the first and second simulation, the friction coefficient is assumed to be constant throughout the process at 0.025 and 0.065, respectively.

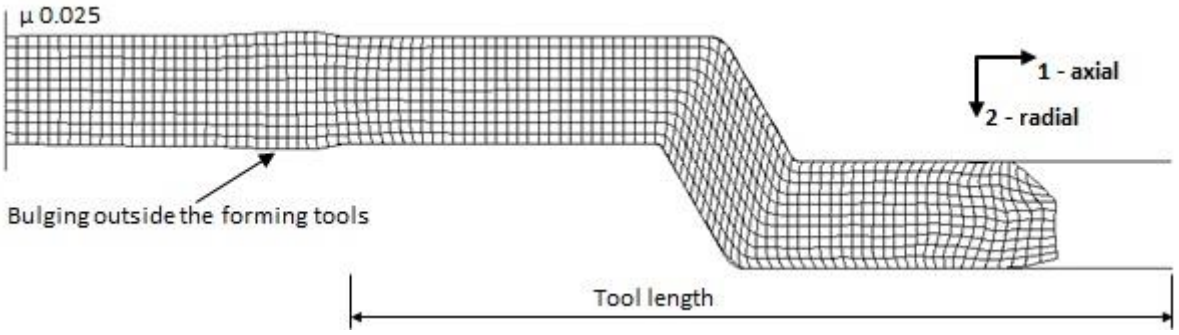

Figure 8-4 Bulging occurrence in the finite element simulation with a friction coefficient of μ - 0.025

As demonstrated in Figure 8-4, the lower friction coefficient caused a bulging in the workpiece between the tools and feeding device. This failure is caused by the high forces in axial direction. Although it is a process error, this misstep reveals important

facts about the mechanics of ECAS. As mentioned in Chapter 6.2, friction eases the forming in ECAS process. Due to the kinematics of the tools, it helps to pull the workpieces into the deformation zone and reduces required forces in axial direction. As predicted by the derived formulas, by a friction coefficient of 0.025, the pressures in the axial direction should be higher than the yielding limit of the material and should result in a plastic deformation in the workpiece sections, which are not confined by the forming tools. Thus, it is shown that the assumption about the pulling effect of friction in ECAS processes is true.

The forming with a constant friction coefficient of 0.065 was possible without any failure in the workpiece. The forces predicted by this numerical simulation are demonstrated in Figure 8-3 together with the measured ones. First of all, the numerically calculated axial forces in the first deformation zone are lower than the measured ones. Moreover, the decrease in the force levels after the first contact can’t be depicted. Furthermore, the forces occurring after the second yielding line are overestimated by the numerical simulations. Additionally, the drop after the workpiece’s end passes the second deformation zone can’t be depicted by this finite element analysis.

Numerically calculated forces in radial direction are underestimated in the first deformation zone and overestimated in the second one. The deviation of the numerically predicted forces from the measured ones is about 16%.

These two numerical simulations indicate that the friction has a significant effect on the feasibility of ECAS. Moreover, it is clear that the process can’t be modeled with constant friction factors throughout the whole deformation. The sliding compression test results from Chapter 5.2 gives important clues about the friction factor change during course of the deformation. As revealed by these test, the friction factor is rather low at the well lubricated state. However, as the sliding proceeds, a significant increase in the friction factor is observed. This increase is related to the fact that the liquid lubricant is pressed outside the contact zone while the specimen slides above the tool surface. Although the rotary swaging machine used in the experiments is continuously lubricated, the tight design of the same machine enabled the installation of the lubricant spraying nozzles only on the exit side of the process. Therefore, this lubrication system has a greater cooling effect rather than lubrication. Thus, in a later finite element model, varying friction coefficients are defined.

As the middle channel wall of the upper tool and the exit channel wall of the lower tool have the most significant effect on the forces, the friction coefficients are varied only on these tool walls. Other surfaces are assumed to have a constant friction coefficient of 0.065. Since the tool surfaces are sufficiently lubricated before starting the forming, the friction coefficient on these both channel walls is assumed as 0.025 before the workpiece comes to first contact with these. After this first contact, the friction coefficient is linearly increased up to 0.095 in the next 20 mm of the feeding and kept constant afterwards. The predicted results with this modified friction concept are also demonstrated in Figure 8-3.

With the use of the modified friction concept, the force distribution can be represented more precisely compared to the first two simulation models with constant friction coefficients. Axial forces predicted with the later simulation reach the same level as the measured ones after the workpiece comes into contact with the tools for the first time. Afterwards, a continuous decrease is observed in the simulated values till the measured force levels are reached. However, the drop in the forces is slower than in the real process. Similarly, the maximum axial forces at the second forming zone are equal to the measured values. Moreover, the decrease after the process reaches steady state can be depicted. Nevertheless, this decrease in the numerical calculations deviate from the real process and is overestimated by 18%.

Additionally, numerically calculated radial forces using the modified friction concept can also better represent the measurements than the constant friction coefficient models. The estimated radial forces are closer to the real ones in the first deformation zone. Moreover, calculated forces in the steady state zone after the second deformation section are nearly identical to the measured ones with a deviation of just above 1%. Furthermore, the force trend can be predicted more precisely with the use of the modified friction concept.

The previous investigations indicate that the friction is a major factor influencing the feasibility and the forces required to deform workpieces by ECAS processes. As assumed by the analytical formulas in Chapter 6.2, unlike ECAP, friction aids the forming and pulls the samples inside the process rather than generating a resistance to the deformation. In the investigated version of ECAS, the tribological conditions vary as the forming proceeds and reach a steady state eventually.

In the last step of force evaluation, the measured loads are compared with the ones predicted with the analytical formulas derived in Chapter 6.2 (Equation 6-39, Equation 6-47, Equation 6-51 and Equation 6-52). In the calculations, it assumed that the temperature of the sample is 100°C and the friction coefficient is constant at 0.095. Analytical estimations are also displayed in Figure 8-3 together with the measurements and numerical simulation results. The analytically predicted forces are shown as dashed lines.

While the axial forces in the first deformation zone are predicted precisely, the radial forces in the same region are overestimated by about 40%. After the second deformation zone, the deviation is even higher. Its values in axial and radial direction are 20% and 48%, respectively. In order to evaluate these deviations, the material flow during ECAS processing should be investigated more closely. Copper samples taken from different stages of the process, starting from the first deformation zone and reaching to the steady state section after the second deformation, are shown in Figure 8-5.

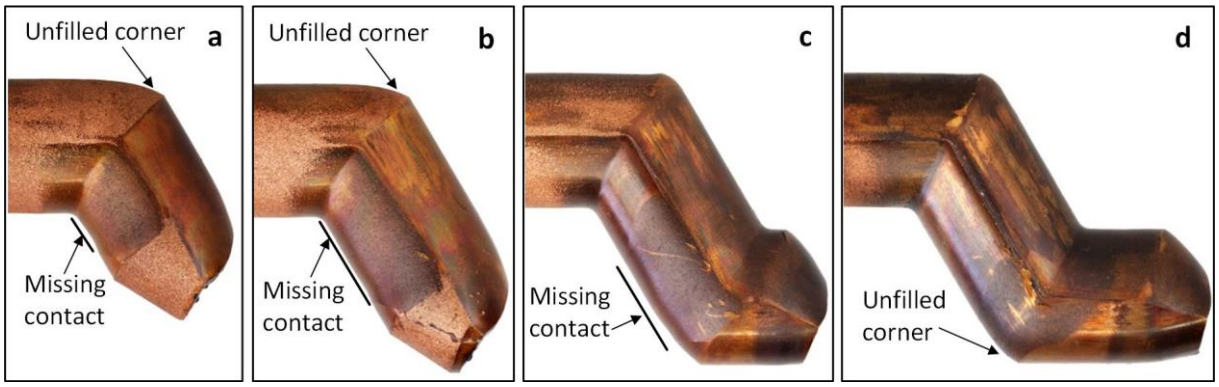

Figure 8-5 Copper samples taken from different stages of ECAS process

By the derivation of analytical formulas, it is assumed that the tool geometry is completely filled and the deformation takes place along a single yielding line. However, these highly conservative assumptions are not valid for the real process. As shown in Figure 8-5.a, the workpiece is partly bent rather than completely sheared at the beginning of the process. Accordingly, an unfilled corner section is present around the intersection of the entry and middle channel of the upper tool. As a result, the highly idealized analytical formulas overestimate the process loads. Nevertheless, the combination of bending and shearing as the major deformation mode at the beginning of the process doesn't explain the accurate axial force

prediction. By the same explanation, the axial forces should be also overestimated. Nonetheless, as described earlier, the friction coefficient increases during the process. At the beginning of the deformation, the friction forces, which reduce the axial forces, in the vicinity of the entry channel of the lower tool should be still comparatively small. The combination of these two effects results in an accurate prediction of the axial loads.

As the workpiece reaches the second deformation zone, the unfilled corner on the first yielding line starts to close (Figure 8-5.c). After the sample reaches the steady state deformation, the first corner gap closes completely and the deformation mode along the first yielding line becomes majorly simple shear (Figure 8-5.d). However, in this case, an unfilled corner gap builds at the outer corner of the lower tool. Accordingly, the major deformation mode along the second yielding line becomes a combination of bending and simple shear. As a result, the process loads are overestimated by the derived analytical formulas. Moreover, since the progress in the deformation results in an increase of the friction coefficient, the predicted axial forces are also overestimated in this case.

In conclusion, the derived analytical formulas are capable of defining the correlations between the forming loads and the resulting friction forces as well as their effect on the overall deformation loads. However, as the assumptions used by the derivation of these analytical formulas are highly idealized, predicted forming forces are overestimated compared to the real process.

Workpiece Temperature

During severe plastic deformation of metallic materials, the temperature of the samples should be kept under the recrystallization temperature in order to enable an effective grain refinement. Moreover, forming temperatures above 300°C causes blue brittleness in low alloy steels which result in cracks in the deformed materials. Therefore, the temperature development during ECAS processes is of high importance and it is investigated by means of measurements and finite element simulations.

However, real-time measurement of the temperature on spots near the deformation zone or exactly at the deformation zone represents a major challenge. Since the workpiece is confined by the tools during forming, optical systems cannot be used for this purpose. Moreover, application of a sensor onto the workpiece enables data

gathering only from positions remote from the deformation zone. Furthermore, the integration of sensors into the workpiece or tool results either with tool breakage or with buckling of the sample. Thus, temperature indicating sticks are used for the measurement (Tempil Tempstik®). These sticks are from a crayon like material and are used mostly to check the temperature by welding operations. Every stick has a specific temperature on which its color is changed irreversibly. Although the temperature distribution over the deformed samples cannot be obtained by using these sticks, they provide a quick and reliable solution to test whether a specific temperature is exceeded or not. To this end, samples are marked with temperature indicating sticks with different specific temperatures and formed afterwards. Although this marking is erased when the particular section of the workpiece enters the deformation zone, this concept enables the determination of the temperatures near the deformation region inside the entry channel of the tools. The results are displayed in Figure 8-6 together with the temperature distribution obtained from numerical simulations with the modified friction concept.

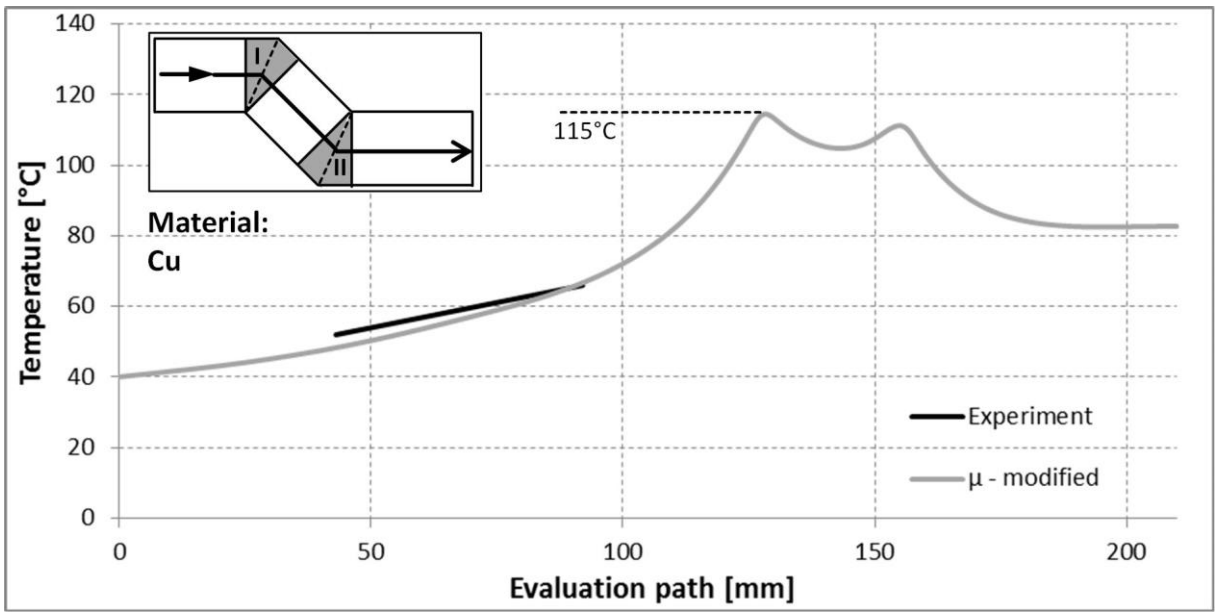

Figure 8-6 Numerically simulated and measured temperatures on copper samples

Temperature indicating sticks used by the measurement ranged in the specific temperatures from 52°C to 450°C. The measurement of the temperatures as close as 10 mm to the first deformation zone was possible. Since excessive contact stresses act on the last section of the entry channel, markings in this last 10 mm were erased. In the experiments with copper samples, the stick with specific temperature of 79°C

didn’t change its color. The numerical simulation predicts for the particular spot where the last marking is observed a temperature of 84°C. The second measurement spot indicates a temperature of 66°C. This value agrees well with the numerical simulation. Nevertheless, the last measurement spot marks a higher temperature than the numerically calculated one. Experimentally acquired temperature data slightly deviate from the numerical ones. However, these are both at the same level. Therefore, it is concluded that the finite element simulations are accurate enough to predict the temperature distribution in the copper samples with the defined simulation parameters.

The finite element simulation of the ECAS process predicts the maximum temperature on the first deformation zone. In this case, the maximum value is 115°C. Since this temperature is less than the recrystallization temperature of copper, an efficient grain refinement is expected in the copper samples.

Material Flow

In order to verify the material flow in the FE-simulations, model experiments are conducted with marked copper samples. Therefore, 320 mm long round copper bars are split in the middle surface by machining and then marked with a square grid of 2 mm by electrochemical etching. Afterwards, these two parts are put together and the material is formed by ECAS with a constant feeding speed of 1 mm/s.

The results of the experiments together with the numerically simulated mesh are demonstrated in Figure 8-7.The entry channel L_0 is not fully shown in this figure for a better visualization. The regularly distributed markings in the middle channel indicate a homogeneous shearing of the material along the first yielding line. However, as the sample reaches the second yielding line, the lower section of the workpiece tend to be bent rather than simply sheared. Although in an insignificant manner, a similar effect is also observed on the upper section of the material. Nevertheless, the regular mesh in the middle section of the sample in the exit channel indicates that the deformation is mostly recovered along the second yielding line. The square shape of the grid is preserved after the forming with a little deviation. The deformation in the experiments resembles the one from FE simulations.

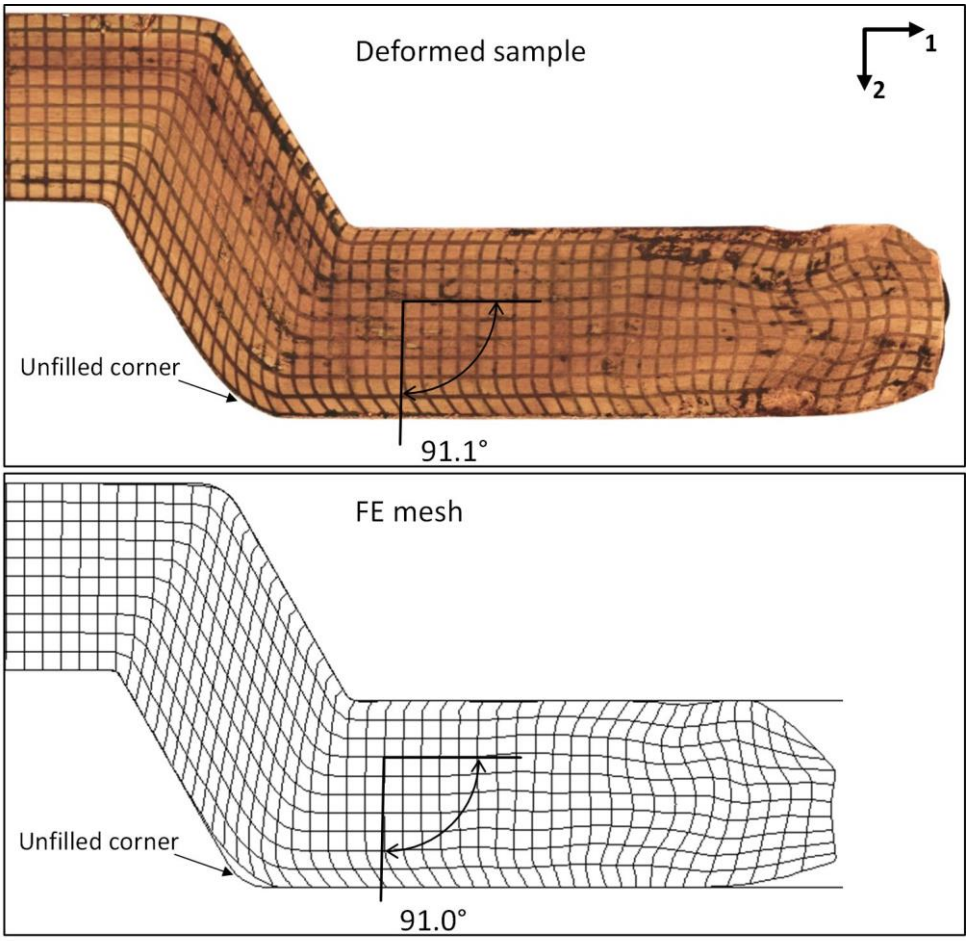

Figure 8-7 Material flow in produced and numerically simulated workpieces

Similar results are observed by investigating the plastic strain distribution in finite element simulations. The strains in the exit channel of the tool are demonstrated in Figure 8-8.

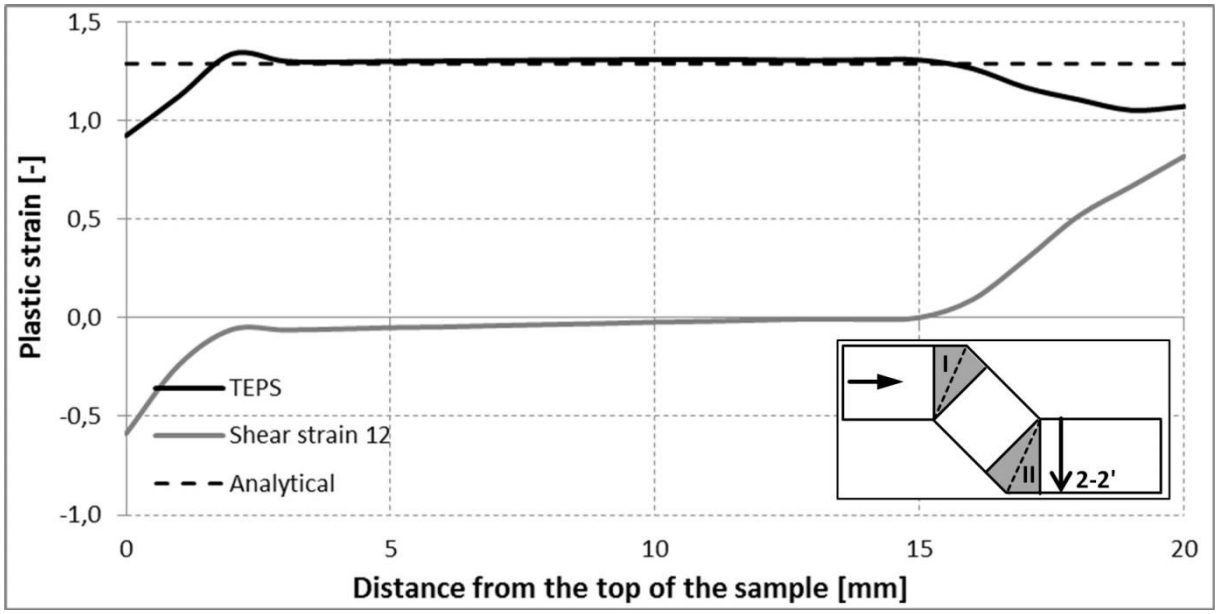

Figure 8-8 Plastic strain distribution in the exit channel

Since the forming pattern follows the route C in ECAS, in the case of a completely homogeneous deformation, it would be expected that the plastic shear strains in the exit channel are equal to zero. This information is true for the majority of the cross section of the deformed samples. However, as indicated by the mesh deformation in Figure 8-7, the shear strains in the upper and lower parts deviate from the ideal value of zero. Moreover, due to the unfilled lower corner, this deviation is higher at the lower part than the upper section. A similar pattern is observed also by the total equivalent strain distribution along the same cross-section. The total strains are fairly homogenous in the middle section and differ from that steady value in upper and lower section. Nevertheless, the deviation in total strain is lower than the ones in shear strain. The underlying reason is that the redundant deformation related to the cyclic forming accumulated in the near-surface section of the workpiece.

Another important feature is that the total plastic strains estimated by the finite element simulations are nearly identical to the analytically calculated ones according to the Iwahashi's formula (Equation 2-9). It proves that the plastic strain characteristics of an ECAS process are majorly defined by the tool geometry rather than process kinematics. In order to predict the strain values, the formulas derived for ECAP can be used.

8.2 Results of Experiments with Steel Roundbars (C4C)

In order to validate the derived formulations and numerical simulations, also low carbon steel samples are formed with the same tool system used in the previous studies with copper. However, the first experiments revealed that the forming of steel samples is more challenging. Due to the severe adhesion, a deformation with the same process parameter as the copper samples was only possible to a limited extent. The coating of the workpiece as well as the tool surface with molybdenum disulfide or zinc-phosphate layer couldn't prevent the adhesion (Figure 8-9.left). This can be attributed to the minor bending of the workpiece on the round corners of the tools. This bending stretches the surface and breaks the coating on the sample. Another approach was to PVD coat the tool surfaces with a TiAlN layer. Through the use of TiAlN coating, the adhesion problem could be completely solved (Figure 8-9.right).

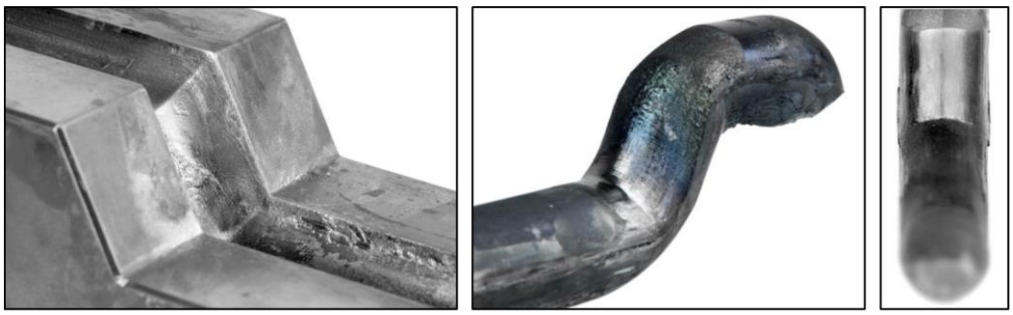

Figure 8-9 Adhesion problem on the forming tool (left), temperature effects on the workpiece (middle) and a sample formed with TiAlN coated tools with active cooling (right)

The finite element simulation in Chapter 7 predicts temperatures above 370°C during the forming of low carbon steel. Such a temperature would cause blue brittleness in the samples and would result in cracks in the workpiece. In order to prove the validity of the simulations, first steel samples are formed without an active cooling/lubrication. The formed workpieces were indeed bluish on the surface and had cracks (Figure 8-9.middle). These first experiments confirm that an active cooling system is inevitable during the forming of steel samples.

Another difference of ECAS forming of low carbon steels compared to copper lies in the yield strength of the deformed material. ECAS processed copper samples experienced a yield strength increase of 17.6 MPa. This value could be predicted

with the Johnson-Cook material model parameters defined in Chapter 5.1. However, the strength increase in steel samples was approximately 132 MPa. This value is higher than the previous material model predictions. Therefore, the parameters of the Johnson-Cook model are adjusted for the low carbon steel. The new parameters are shown in Table 8-1. These parameters are used in the later finite element simulations.

Table 8-1 Parameters of Johnson-Cook material model of low carbon steel

Parameter	**C4C**
A – Yield strength [MPa]	424.88
B – Strain hardening effect [MPa]	111.67
n – Strain hardening exponent	0.198
C – Strain rate sensitivity	0.0124
$\dot{\varepsilon}_0$ – Initial strain rate	1
T_{room} – Room temperature [K]	298
T_{melt} – Melting temperature [K]	1803
m – Thermal softening exponent	0.83

Process Forces

The results of the process force measurements are shown in Figure 8-10. As in the deformation of copper samples, the forming at the first yielding line starts with a sudden increase in the axial forces up to 80 kN. Shortly after, the axial force levels stabilize at about 60 kN. The deformation along the second yielding line starts also with an abrupt increase reaching 130 kN and stabilizes afterwards at 104 kN.

The first deformation in the tool causes radial loads of maximum 108 kN. As the workpiece passes the second forming zone, this value increases to 278 kN. Unlike the deformation of copper samples, the radial forces more than double during forming of low carbon steel. This is due to the high strength increase in the severe plastic deformed steels.

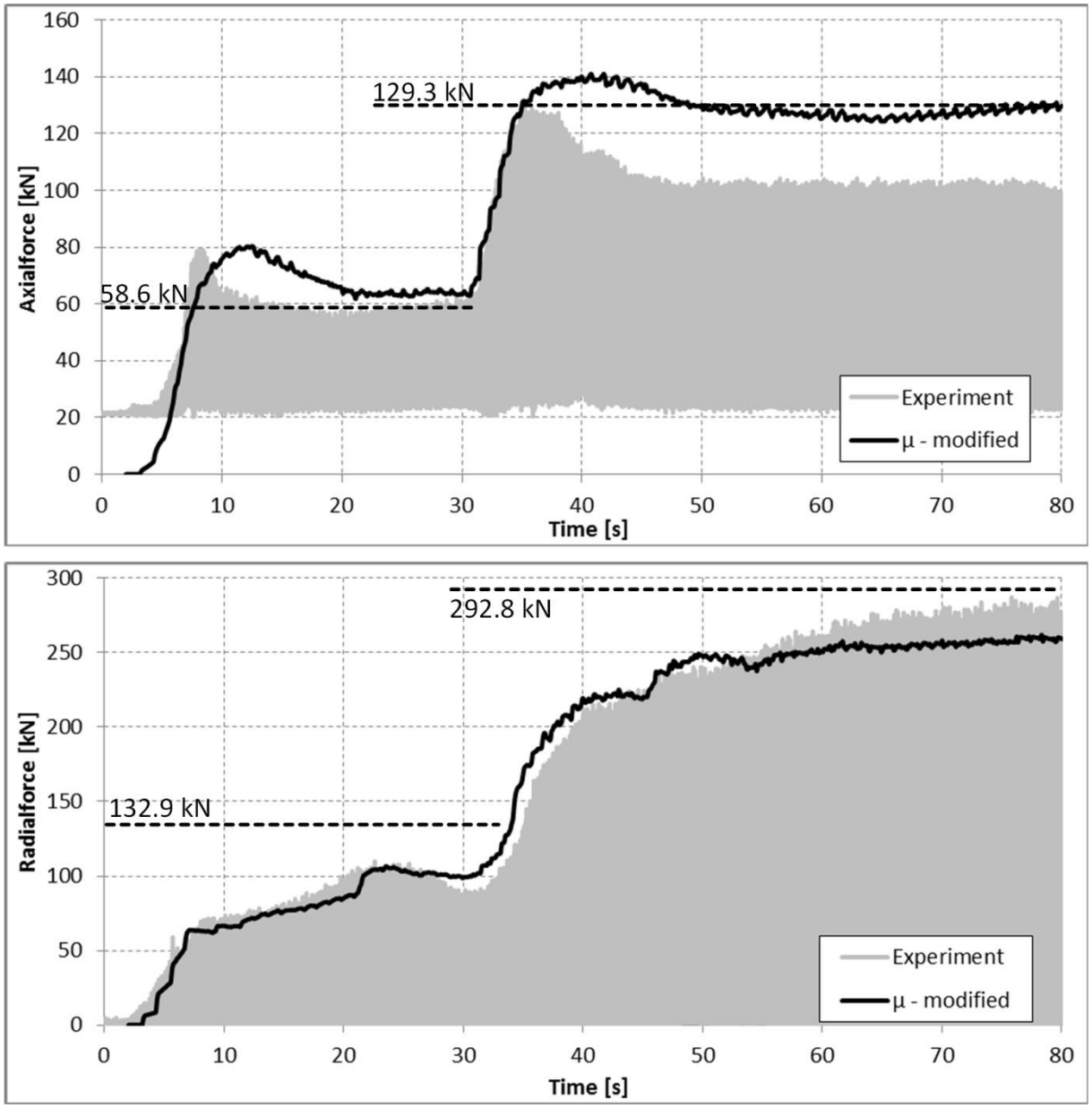

Figure 8-10 Measured, numerically simulated and analytically predicted (dashed lines) process forces required to deform low carbon steel workpieces (Feeding speed 1 mm/s)

The modified friction concept defined in the previous chapter is also used by the finite element simulation of the low carbon steels. Similarly, it is assumed that the friction coefficient on the middle channel wall of the upper tool and on the exit channel of the lower tool changes during the course of the process. Other surfaces are assumed to have a constant friction coefficient of 0.065. Since the tool surfaces are sufficiently lubricated before starting the forming, the friction coefficient on these both channel

walls is assumed 0.03 before the workpiece comes to first contact with these. After this first contact, the friction coefficient is linearly increased up to 0.1 in the next 20 mm of the feeding and kept constant afterwards. The predicted results with this modified friction concept are demonstrated in Figure 8-10 together with the force measurements.

Axial forces predicted with the finite element simulation reach the same level as the measured ones after the workpiece comes into contact with the tools for the first time. Afterwards, a continuous decrease is observed in the simulated values. However, the drop in the forces is slower than in the real process. Unlike the simulations of the copper sample, the steady state section after the first yielding line is slightly overestimated by the finite element analysis of the workpieces made of steel. The maximum axial forces at the second forming zone are also slightly overestimated. Nevertheless, the drop in the loads after the force peak is also observed in the simulations. As in the numerical simulation of copper samples, this decrease deviates from real process and is overestimated by 18%.

The numerically calculated radial forces are nearly identical to the measured ones in the first deformation zone. Moreover, the force trend is predicted accurately. Nevertheless, the radial loads in the steady state after the second yielding line is underestimated by about 8% in the finite element simulations. The higher forces in the real process are caused by the formation of burrs on both sides of the sample. These thin burrs flow in the gap between the tool halves and increase therefore the forces in radial direction.

As in the investigation of copper samples, the measured loads are compared with the ones predicted with the analytical formulas derived in Chapter 6.2 (Equation 6-39, Equation 6-47, Equation 6-51 and Equation 6-52). In the calculations, it is assumed that the temperature of the sample is 175°C and the friction coefficient is constant at 0.1. Analytical estimations are also displayed in Figure 8-10 together with the measurements and finite element simulation results. The analytically predicted forces are shown as dashed lines.

While the axial forces in the first deformation zone are predicted precisely, the radial forces in the same region are overestimated by about 28%. After the second deformation zone, the deviations in axial and radial directions are 24% and 6%, respectively. Especially the overestimation in the radial direction is lower than by

copper samples. This is caused by the increase in the measured process loads corresponding to the burr formation.

In conclusion, as in the deformation of copper samples, the derived analytical formulas are also capable of defining the correlations between the forming loads and the resulting friction forces by ECAS processing of low carbon steel workpieces. Nevertheless, due to the idealization of the deformation by the analytical studies, the predicted loads are overestimated compared to the real process forces.

Workpiece Temperature

The temperature development during the deformation of low carbon steel by ECAS process is also investigated by means of measurements and finite element simulations. Temperature indicating sticks are used for the measurement. The results are displayed in Figure 8-11 together with the temperature distribution obtained from numerical simulations with modified material parameters.

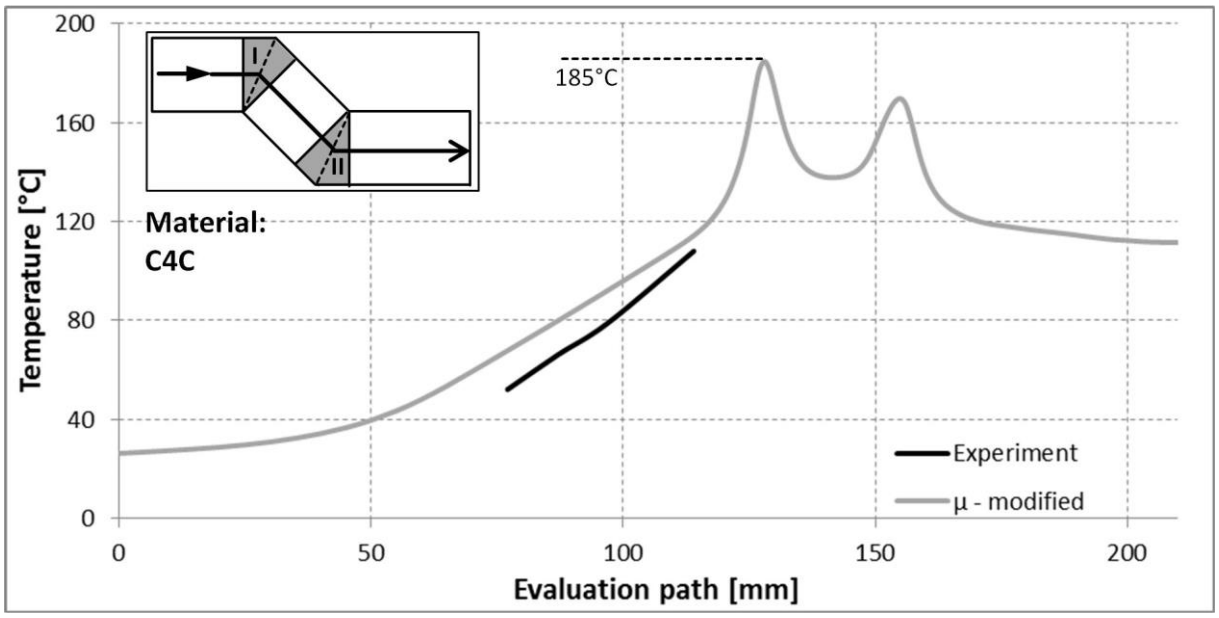

Figure 8-11 Numerically simulated and measured temperatures in low carbon steel samples

Experimentally acquired temperature data slightly deviate from the numerical ones. Temperatures are overestimated in the finite element simulations. However, their distribution correlates well with the measurements. The finite element simulation of the ECAS process predicts the maximum temperature in the first deformation zone.

In this case, the maximum value is 185°C. This temperature is below the blue brittleness limit of the material. The non-bluish color of the experimental parts proves that this prediction is valid. Despite the overestimation, it is concluded that the finite element simulations is accurate enough to predict the temperature distribution in the low carbon steel samples with the defined simulation parameters.

8.3 Effect of ECAS Processing on Material Properties

Severe plastic deformation (SPD) has a significant effect on mechanical and microstructural properties of materials. In order to investigate this effect in ECAS processed samples, round bars are deformed by this process repeatedly. The deformation in one pass which involves two forming sections corresponds to the route A. The samples are rotated around 90° after every pass. Therefore, the processing route E is realized when the whole process is considered.

The mechanical properties of the investigated materials are determined by tensile testing. Tensile specimens with geometry according to the DIN 50125-B4x20 are prepared for each state of the materials, i.e. as received and two passes through ECAS process. All samples are characterized with a ZWICK universal testing machine Z100. The results of the copper samples are displayed in Figure 8-12.

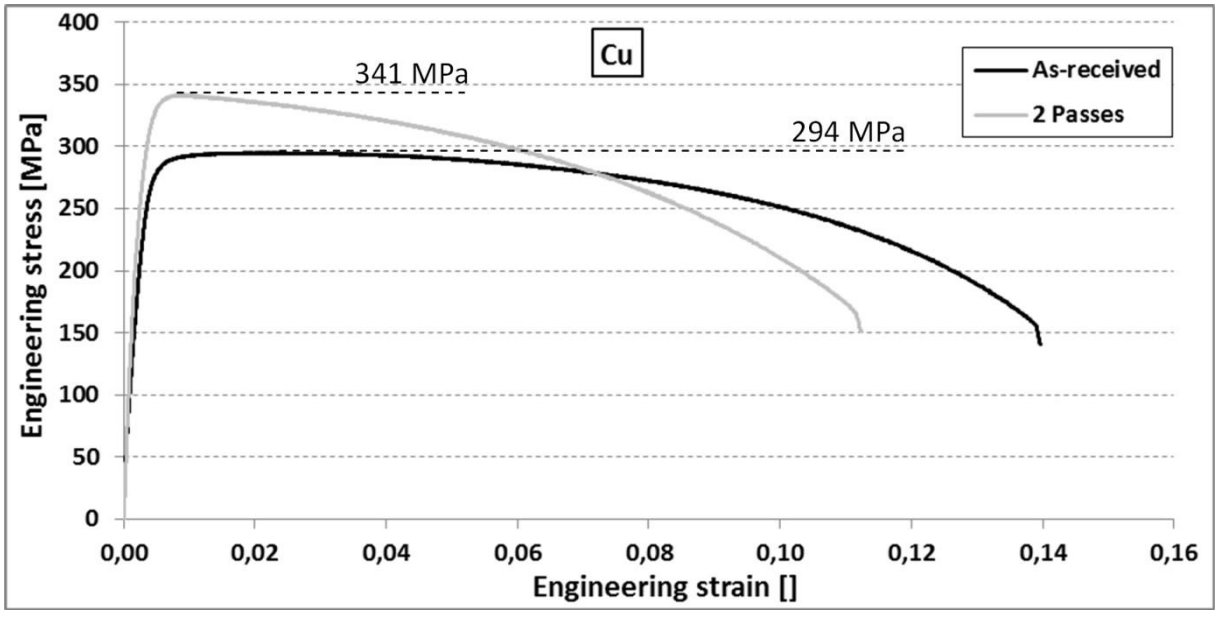

Figure 8-12 Stress strain diagram of copper

The initial state of the copper was a highly strain hardened with a little strain hardening potential. Nevertheless, after processing with ECAS, the ultimate yield strength of the investigated material increased by 16%. Moreover, although there has been a decrease in the strain to failure values in the ECAS processed samples, this strain value is still about 11% after the severe plastic deformation.

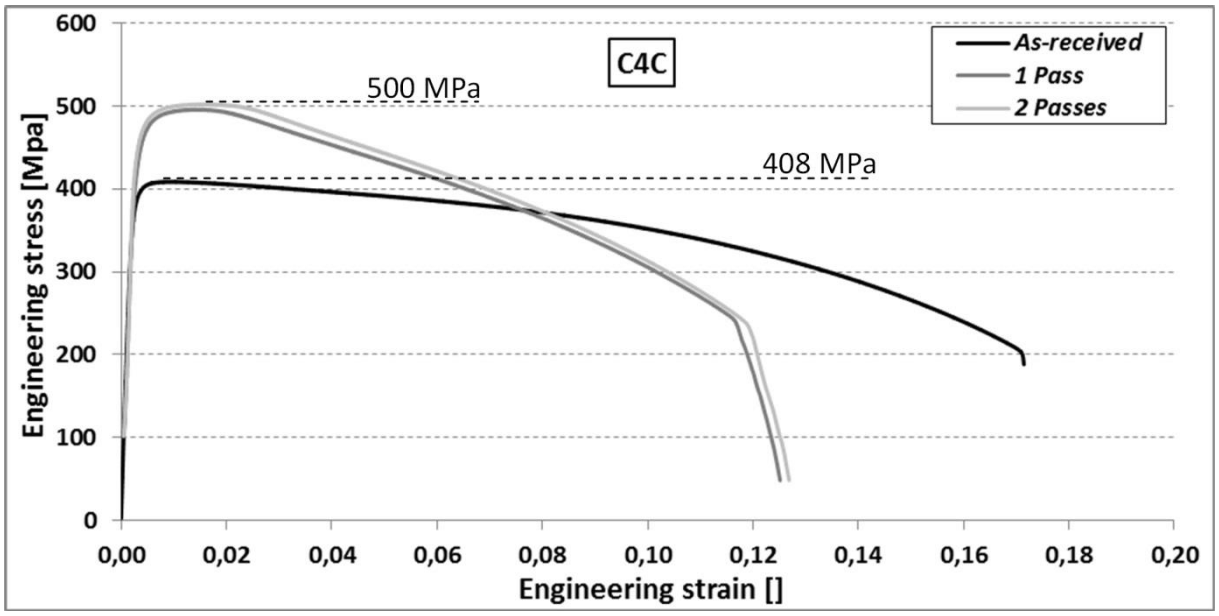

Figure 8-13 Stress strain diagram of low carbon steel

Tensile testing results of the low carbon steel samples are displayed in Figure 8-13. Similar to copper, as-received low carbon steel samples were highly strain hardened with a little strain hardening potential. However, after processing with ECAS, the ultimate yield strength of the low carbon steel increased by 22%. Despite the decrease in the strain to failure values in the ECAS processed samples, this strain value is still about 12% after the severe plastic deformation.

Although as-received samples did only have a slight strain hardening potential, both materials, copper and low carbon steel are distinguished with an increased strength after ECAS processing. Moreover, this ultimate tensile strength is reached at low strain values, which is characteristic for severely plastic deformed materials.

The microstructure of the ECAS processed copper and low carbon steel samples is analyzed using Electro Backscatter Diffraction (EBSD) in a high resolution Scanning Electron Microscope (SEM) in transversal direction. The microstructure of both materials, copper and low carbon steel, after two pass ECAS processing is shown in

Figure 8-14 and Figure 8-15, respectively. The black lines in these figures indicate high angle grain boundaries (HAGBs).

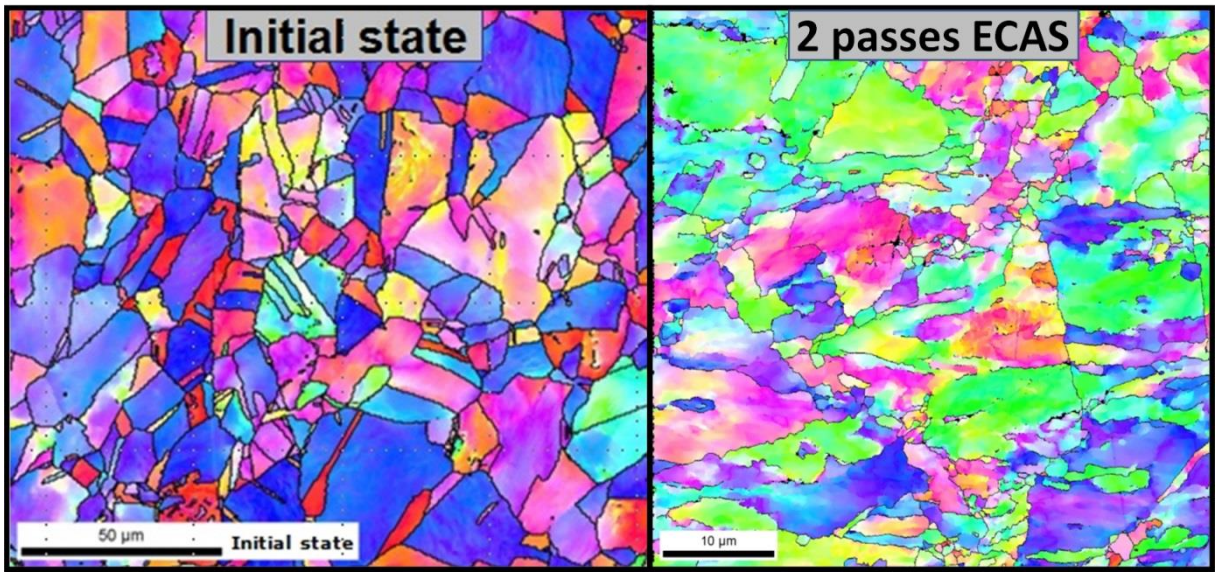

Figure 8-14 Microstructure of copper samples in as-received state and after two passes of ECAS

The average grain size in the as-received copper samples is about 5.3 µm. After two severe plastic deformation (SPD) steps by ECAS process, average grain size decreased to 0.8 µm. Additionally, the grain structure in the as-received material cannot be observed in the deformed state. Although comparatively large grains are still present in the microstructure, areas with significantly small grains start to emerge. Further deformation results in a less significant drop in the grain size of 0.6 and 0.57 µm after three times and four times ECAS processing, respectively. Nevertheless, high angle grain boundaries (HAGB) proportion starts to increase as copper samples are formed four times by ECAS.

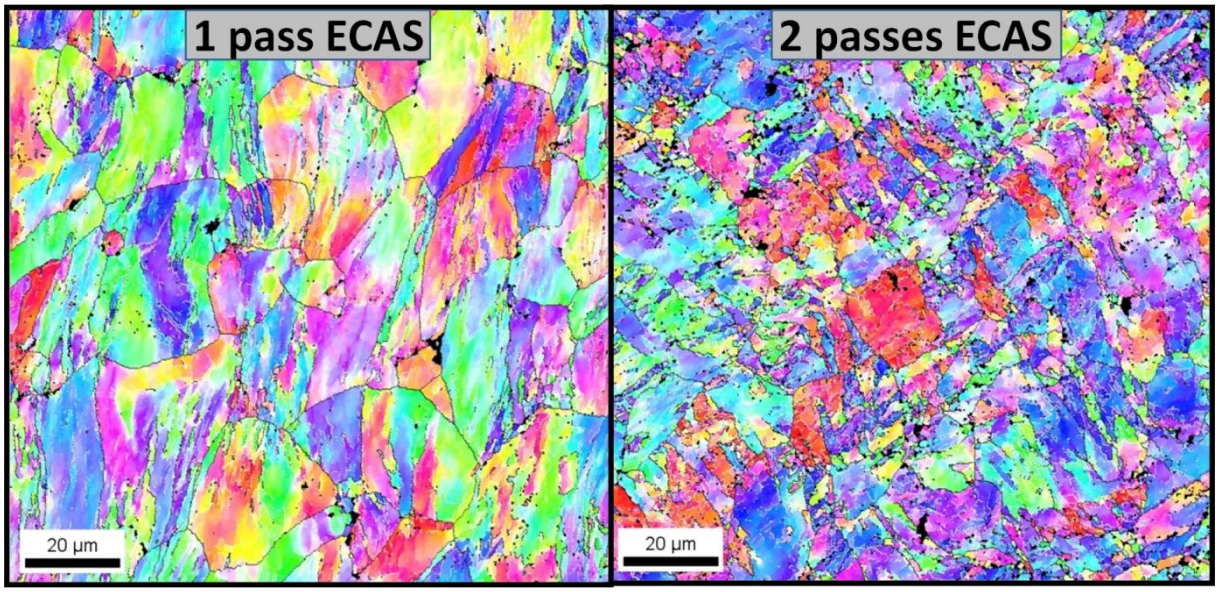

Figure 8-15 Microstructure of low carbon steel samples in one pass and two passes of ECAS

Similar results are obtained from the microstructural investigations of ECAS processed low carbon steel samples. After the first and second deformation by ECAS, the average grain size reduces to 0.79 µm and 0.55 µm, respectively. Moreover, HAGB proportion tends to increase after the second deformation by the developed process [GÖR12]. Investigations on the microstructural properties prove that a significant grain refinement can be achieved after deformation of materials by ECAS process.

8.4 Validity of the Derived Formulas for Higher Channel Angles

In order to investigate the validity of the formulas derived in Chapter 6.2 for channel angles other than 120°, an ECAS tool containing four forming sections each with a channel angle of 150° has been used (Figure 8-16). A plastic strain of 1.24 is induced with this tool system, which is similar to the strain of 1.27 induced with the tool having two deformation zones each with a channel angle of 120°.

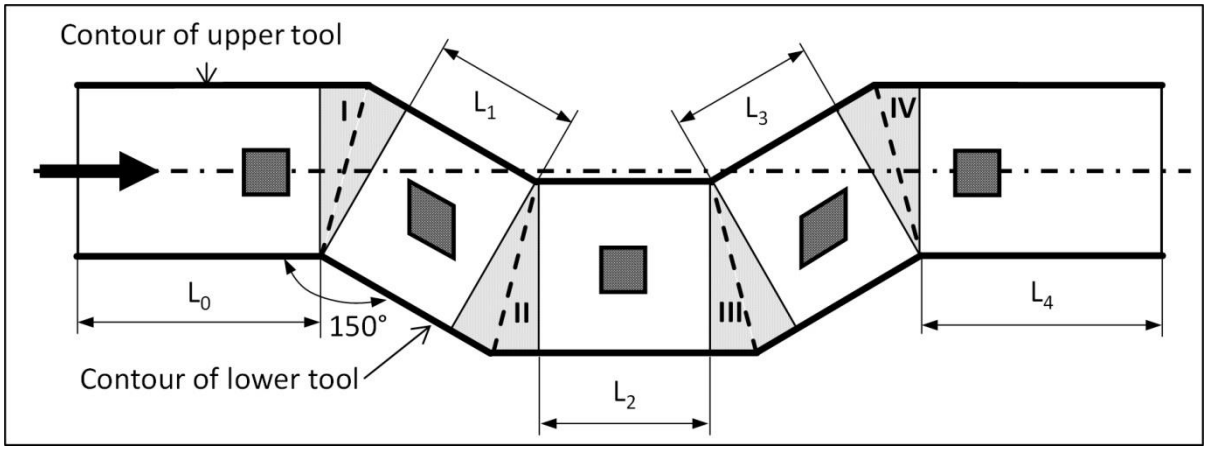

Figure 8-16 Schematic illustration of ECAS tool containing for deformation zones each with a channel angle of 150°

For the validation of the analytically calculated values with Equation 6-51 and Equation 6-52, forces in axial as well as in radial direction are measured during the ECAS process. Only the material copper has been used in these investigations. For the measurements, the geometry of the samples is fitted to the channel geometry by plunge swaging. Afterwards, a copper bar is pushed with a constant speed of 3 mm/s through the oscillating tools while applying a constant counter force of approximately 15 kN (corresponds to a back pressure of 50 MPa) on the sample's end. The measured forces acting on the upper tool in radial direction and acting on the feed equipment in axial direction are shown in Figure 8-17.

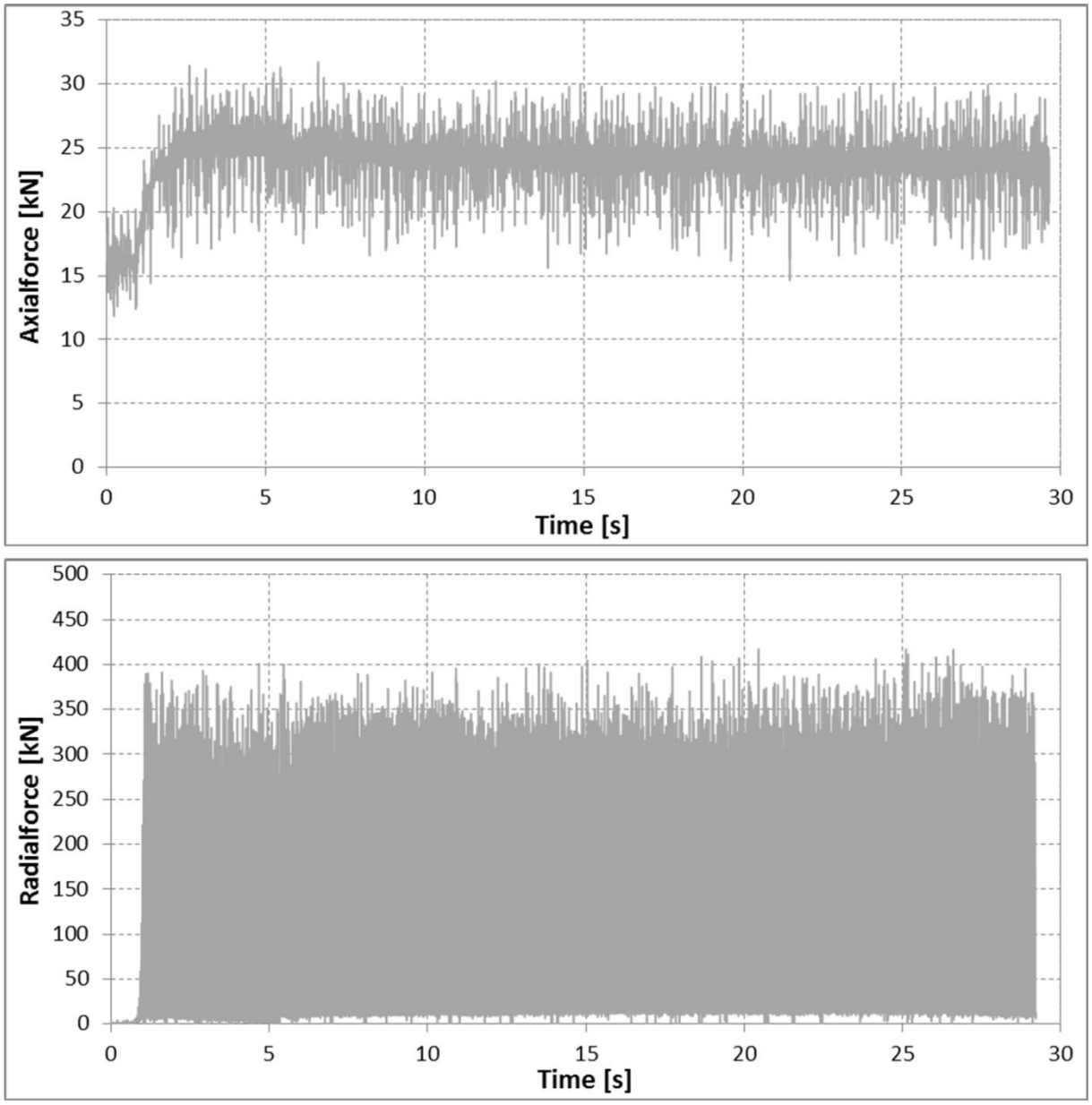

Figure 8-17 Measured process forces required to deform copper samples with the ECAS tool containing for deformation zones each with a channel angle of 150° (Feeding speed 3 mm/s)

The measured radial forces appear to be constant throughout the process and goes up to 400 kN. A slight increase is observed towards the end of the process. The reason that there is only an insignificant increase in the force distribution is that the investigated material has a small strain hardening exponent and therefore exhibits a modest increase in strength after severe plastic deformation. The measured axial forces proceeds also nearly constant and has a maximum value of approximately 30

kN. On the other hand, Equation 6-51 and Equation 6-52 predict axial and radial forces of 75 kN and 227 kN, respectively. These values highly deviate from the measured ones. Moreover, while loads in radial direction are underestimated, axial forces are overestimated. This deviation is a result of the expansion of the samples in radial direction especially in the first and second channels of the tools caused by the applied back pressure. The measured maximum sample radius after deformation by the ECAS process was about 20.12 mm. This expansion of the sample is compensated by the tools during deformation. Therefore, higher forces occur in the radial direction than the analytically predicted ones. However, the rise in the radial forces leads to an increase in the friction forces, which prevent the sample to be pushed back in the feeding direction. As a result, a decrease in the axial forces is expected.

Investigation with the tool system containing four forming zones each with a channel angle of 150° prove that formulas derived in Chapter 6.2 are valid only for the cases where the radial expansion of the sample is insignificant and can therefore be neglected. If samples expand significantly during the deformation, it results in an increase in the radial forces and a decrease in the axial forces.

8.5 Summary of the Experimental Findings

Experimental investigations demonstrate that the ECAS processing of samples made of copper and low carbon steel is possible with the developed tool system. Such a deformation without any buckling of the workpieces proves that the derived analytical hypothesis about the process loads is true. During ECAS deformation, the friction on certain tool walls helps to pull the workpieces into the process rather than generating a resistance to it. Nevertheless, analytically predicted process loads are higher than the measured ones. This overestimation is caused by the highly idealized assumptions during the derivation of the analytical formulas.

On the other hand, finite element simulations estimate the process loads and their trend more accurately. The major deviations from the measured forces are in axial direction and its maximum value account for 18%. Moreover, these simulations are also capable of representing the temperature and plastic strain distribution in the deformed samples.

Additionally, both materials, copper and low carbon steel are distinguished with increased strength after ECAS processing. Furthermore, investigation of microstructural properties reveals that a significant grain refinement can be achieved in the samples processed by ECAS.

Nevertheless, precautions have to be taken for a successful forming by the ECAS process. Especially by the deformation of low carbon steels, the forming machine should be continuously cooled to keep the temperatures low. Moreover, also by steel samples, tool surfaces should be coated in order to prevent any adhesion.

9 Effect of Process Parameters on ECAS

In the previous chapters, the theory of ECAS processing is explained, the tool design guidelines are developed, the feasibility of the process is shown and finite element simulation models, which are capable of representing the process accurately are developed. However, the feeding speed in all investigations was 1 mm/s. Although such a process velocity is comparatively high for severe plastic deformation processes, it is still too slow for an industrial application and would result in a poor outcome. Therefore, the process speed has to be increased for a successful industrial implementation of ECAS process.

In the following chapters, the most important process parameters of friction, temperature, feeding speed and feeding type will be investigated by means of finite element simulations. With this parameter study, it is aimed to show the effect of these on material flow, temperature and process loads. Consequently, suggestions will be made for the speed-up of the ECAS process.

The finite element modelling strategy developed in Chapter 8 will be used. In every finite element model, only a single variable will be changed to better reveal the effect of the investigated parameter. To simplify the analysis, only the material copper will be studied.

9.1 Tribological Parameters

In the first part of the study, the tribological parameters will be investigated. In all finite element simulations, it is assumed that this coefficient follows the modified pattern defined in Chapter 8. The tribological effects are varied by multiplying the modified friction coefficient with a factor. These factors are selected as 0.5, 1.5 and 2.0. Although the frictional stresses cannot exceed the shear yield strength of the material, in order to solely investigate the effect of the friction coefficient, this limit is neglected. The material flow and shear strain distribution after two pass ECAS deformation is shown in Figure 9-1 and Figure 9-2, respectively.

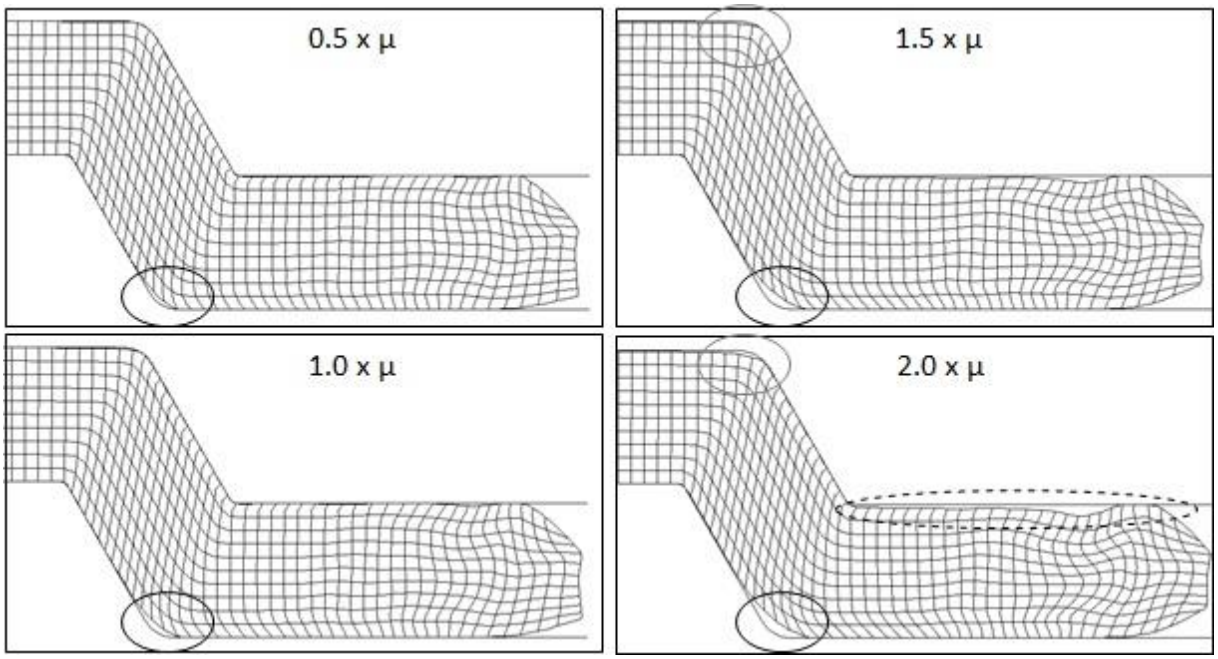

Figure 9-1 Material flow in the finite element simulations with different friction coefficients

The finite element simulations reveal that friction has a significant effect on the material flow during ECAS processing. As the friction coefficient rises, the sample material is drawn into the tools more strongly. This pulling unveils itself as the rise in the gap area around the outer corner of the second yielding line (shown with the black circle). It is basically the result of the friction force acting on the exit wall of the lower tool in the feeding direction. Moreover, for high friction coefficients, even a gap starts to build around the outer corner of the first yielding line (shown with the grey circle). Furthermore, if the friction coefficients are doubled, the sample material doesn't fill the exit channel after deformation (shown with the dashed ellipse).

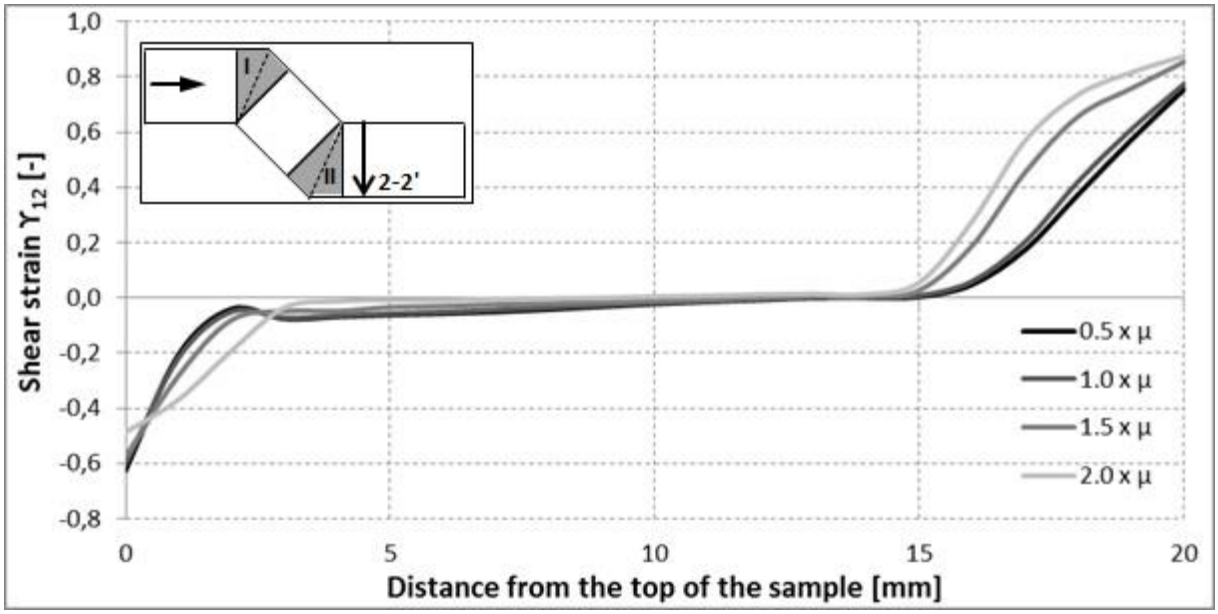

Figure 9-2 Shear strain distribution in the finite element simulations with different friction coefficients

The same effect is also observed in the shear strain distribution. As the friction coefficient increases, the point where the strain values start to deviate from the steady state moves further into the middle of the sample which indicates a more inhomogeneous plastic strain distribution.

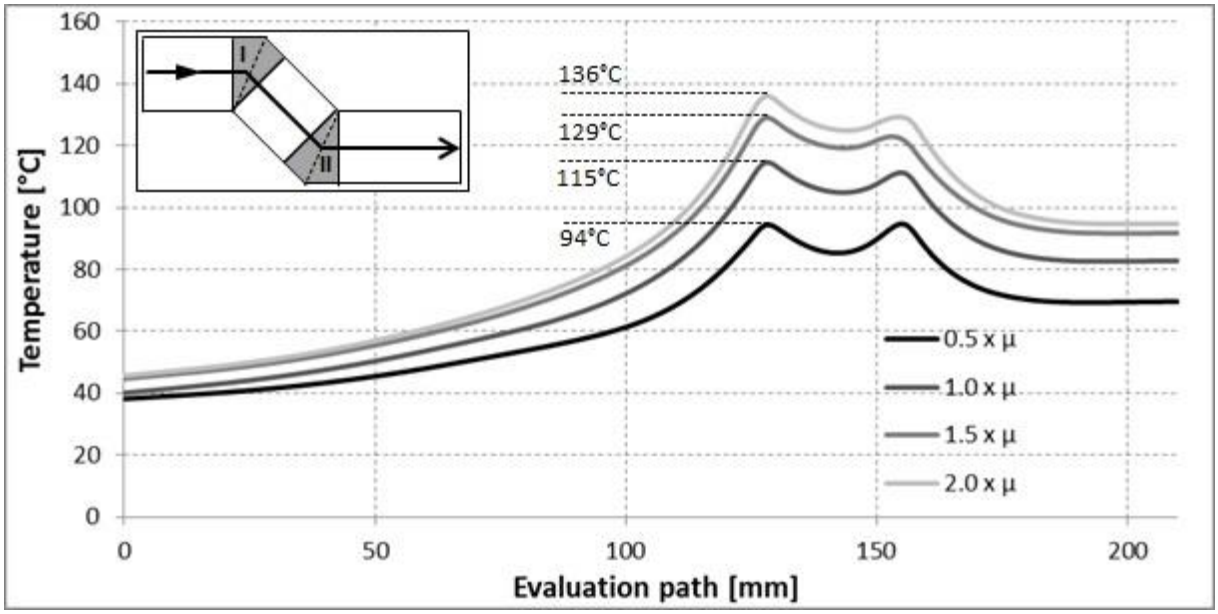

Figure 9-3 Temperature distribution in the finite element simulations with different friction coefficients

The change in the tribological properties has an insignificant effect on the temperature distribution in the deformed sample (Figure 9-3). Although the maximum temperature increases as the friction coefficient rises, doubling this coefficient of the basic model results is an increase in the maximum temperature of just 21°C. Such a small increase is caused on the one hand by the fact that the heat generation is partly a result of friction. On the other hand, as the temperature difference between the workpiece and the forming tools increases, so does also the heat transfer between this contact pair.

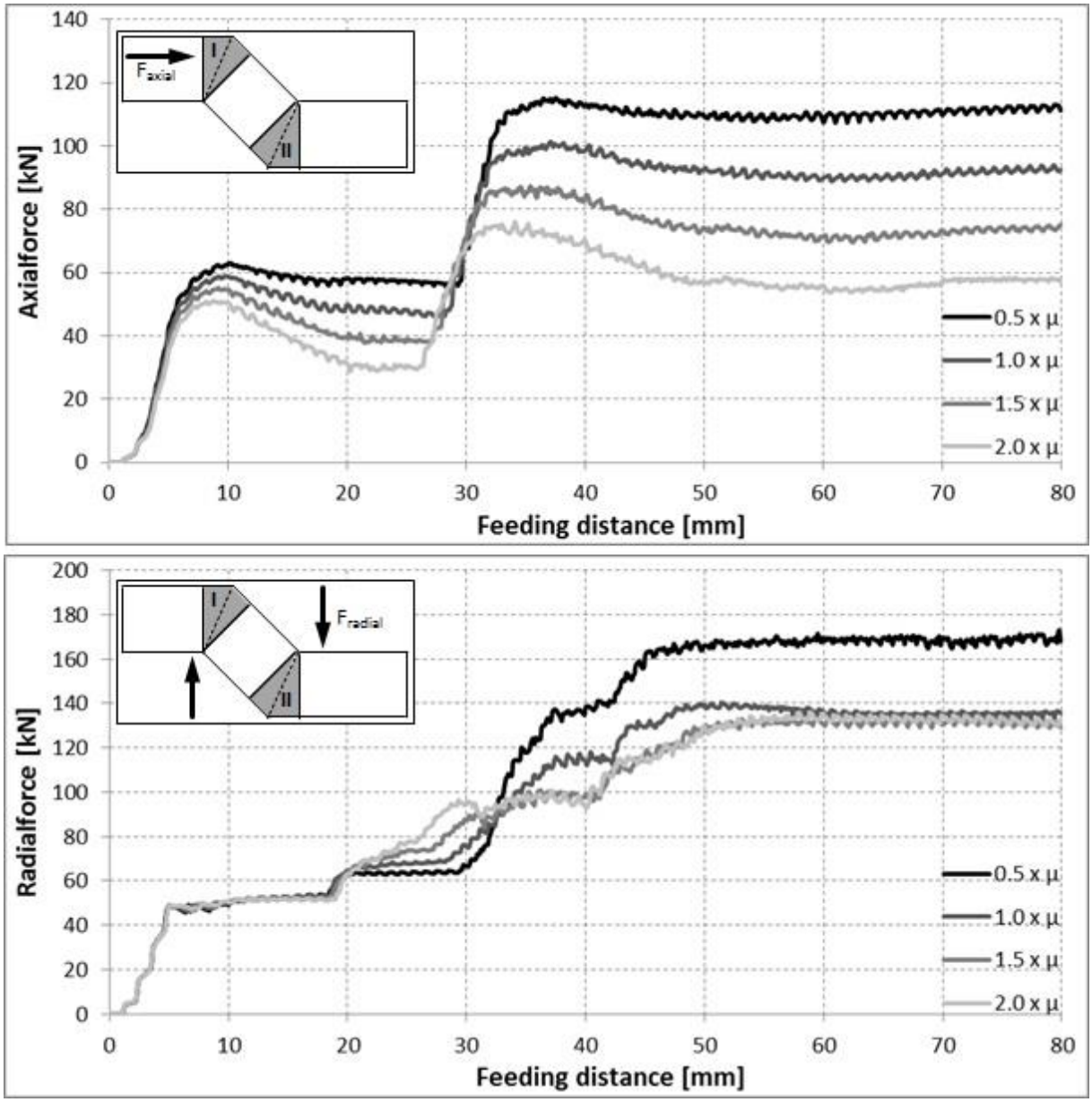

Figure 9-4 Force distribution in the finite element simulations with different friction coefficients

The tribological properties have the most significant effect on the process loads. As the friction coefficient increases, the axial loads decrease continuously. On the other hand, such an increase doesn't have an effect on the radial loads, especially for friction coefficients higher than a certain value. The existence of such a load limit supports the assumption that the deformation is caused majorly by the radial forces during ECAS process. The axial loads serve to compensate the redundant forces in the feeding direction.

9.2 Temperature

Secondly, the effect of temperature is investigated. It is varied by changing the heat dissipation factor in the numerical simulations.

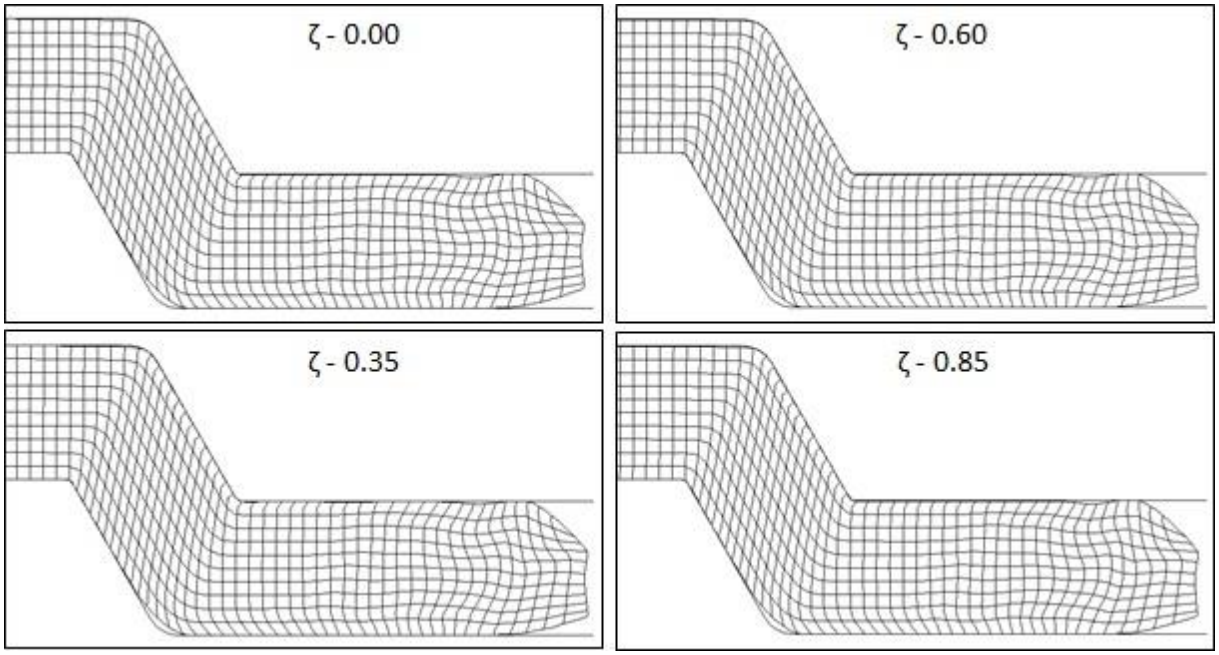

Figure 9-5 Material flow in the finite element simulations with different heat dissipation factors

After inspecting the material flow, it can be concluded that the sample temperature has no effect on the deformation. The numerically calculated mesh doesn't show a sigh of change (Figure 9-5).

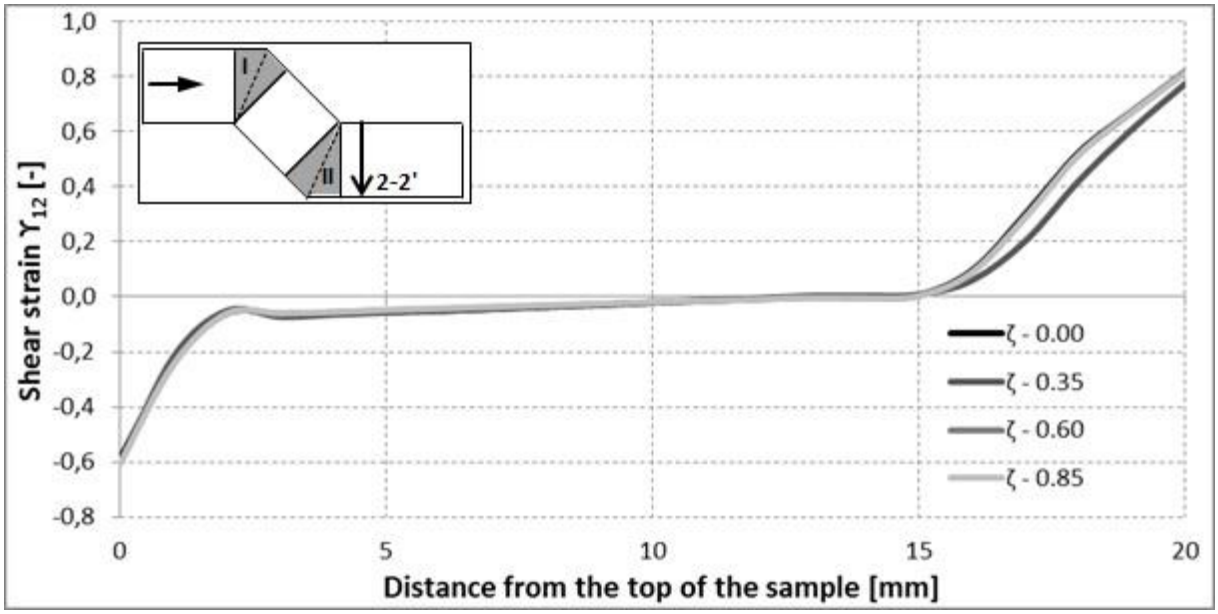

Figure 9-6 Shear strain distribution in the finite element simulations with different heat dissipation factors

The same effect is also observed by the shear strain distribution. As the heat dissipation factor and accordingly the temperature increases, only a minor change is observed in the plastic strain. The change is only on the lower section of the workpiece.

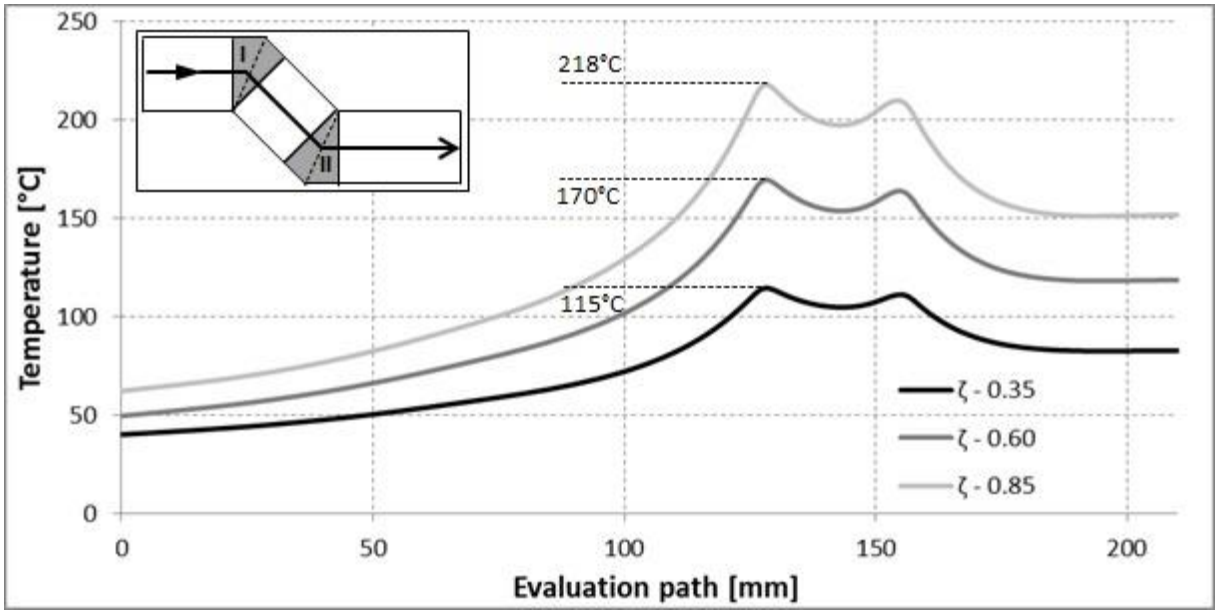

Figure 9-7 Temperature distribution in the finite element simulations with different heat dissipation factors

As expected, changing the heat dissipation factor has a more significant effect on the temperature distribution in the deformed sample than the tribological properties. Nevertheless, as the heat transfer between the workpiece and tool walls increases with higher temperature differences, the rise in the maximum temperature tends to slow down as the dissipation surges.

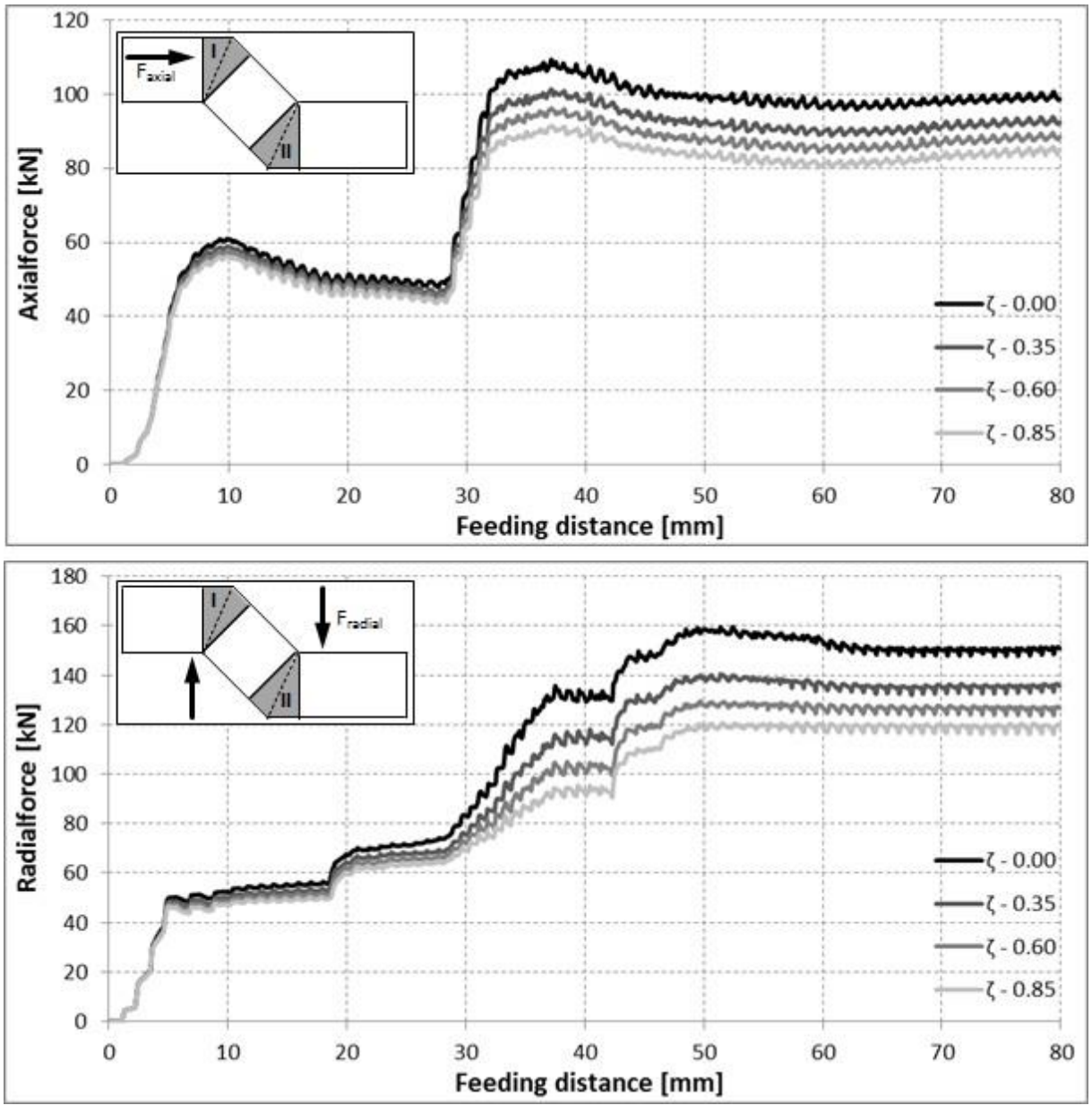

Figure 9-8 Force distribution in the finite element simulations with different friction coefficients

The temperature has a minor effect on the process loads. Since the material softens as the temperature increases, a drop in the axial and radial forces is observed. However, this decrease is associated to the thermal softening.

9.3 Feeding Speed

After the effect of tribological properties and temperature on ECAS process is investigated, the feeding speed is varied. In these variations, it is assumed that the axial velocity of the sample is constant and the workpiece is pushed through the tools even the sample is at the bottom dead center. Four different speeds are investigated; 1 mm/s, 3 mm/s, 5 mm/s and 10 mm/s.

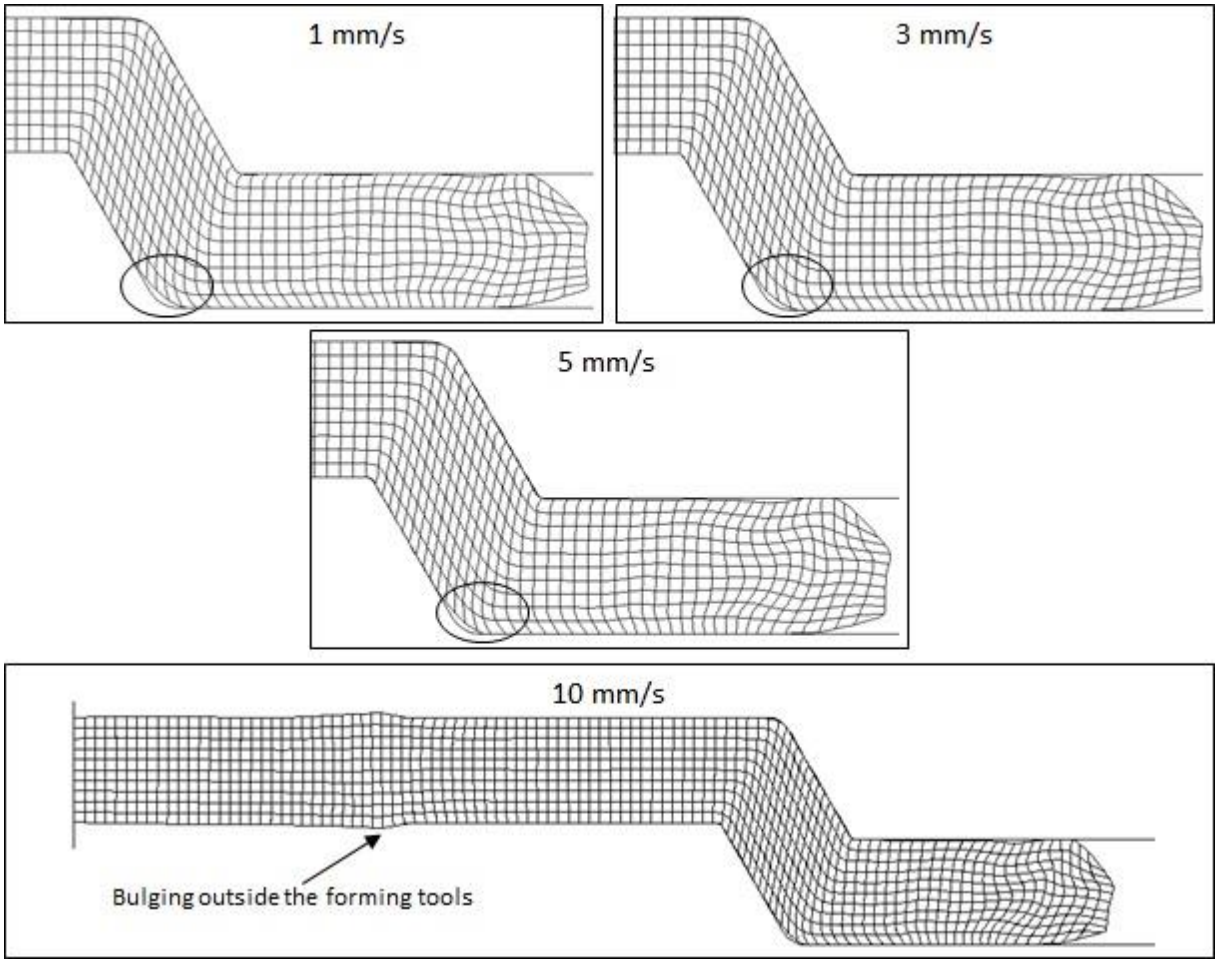

Figure 9-9 Material flow in the finite element simulations with different feeding speeds

As the feeding speed increases, the gap around the outer corner of the second yielding line starts to close (shown with black circles in Figure 9-9). In conventional

ECAP, the friction tends to create a resistance against the feeding and to decrease the corner gap on the workpiece [CER09]. As the feeding speed increases in ECAS process, the portion of the workpiece displacement in axial direction which takes place when the tools are at or near the bottom dead center also increases. Such a displacement eliminates the pulling effect of the tools related to the friction. Moreover, in the investigated case, at an axial velocity of 10 mm/s, this pulling effect is completely canceled and the displacement in the feeding direction generates a resistance against the deformation. Accordingly, ECAS processing with an axial feed rate of 10 mm/s is not possible because of the bulging of the sample outside the tools (Figure 9-9 bottom).

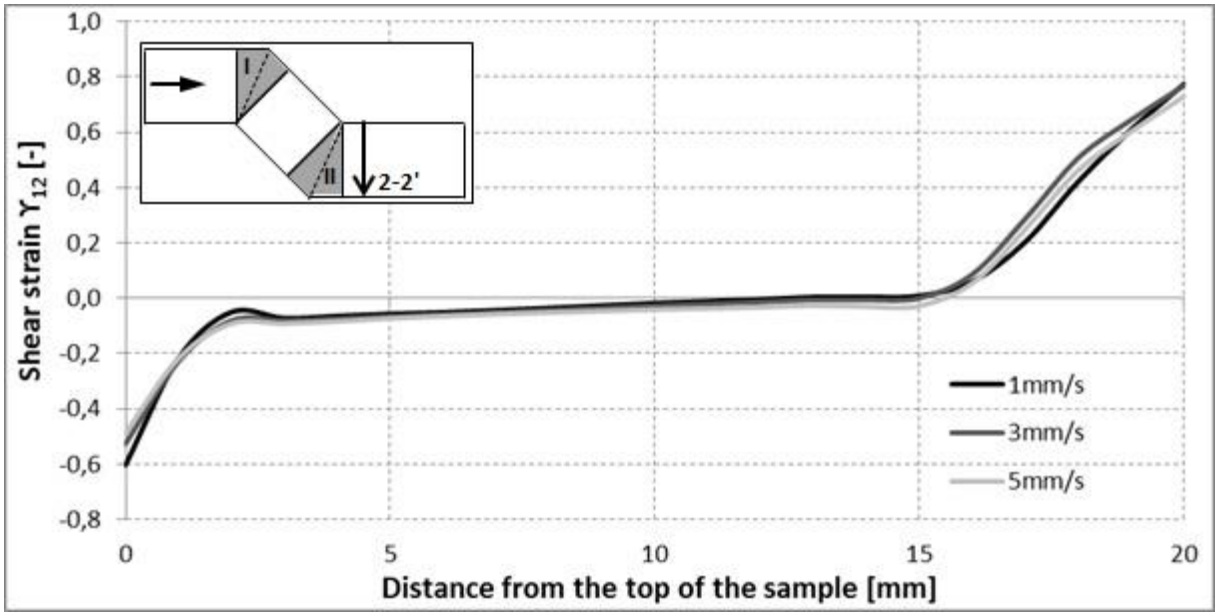

Figure 9-10 Shear strain distribution in the finite element simulations with different feeding speeds

As the corner gap closes with increase feeding speed, the deviations in the plastic strains starts to decrease. Accordingly, the shear strains in the deformed sample tend to homogenize (Figure 9-10).

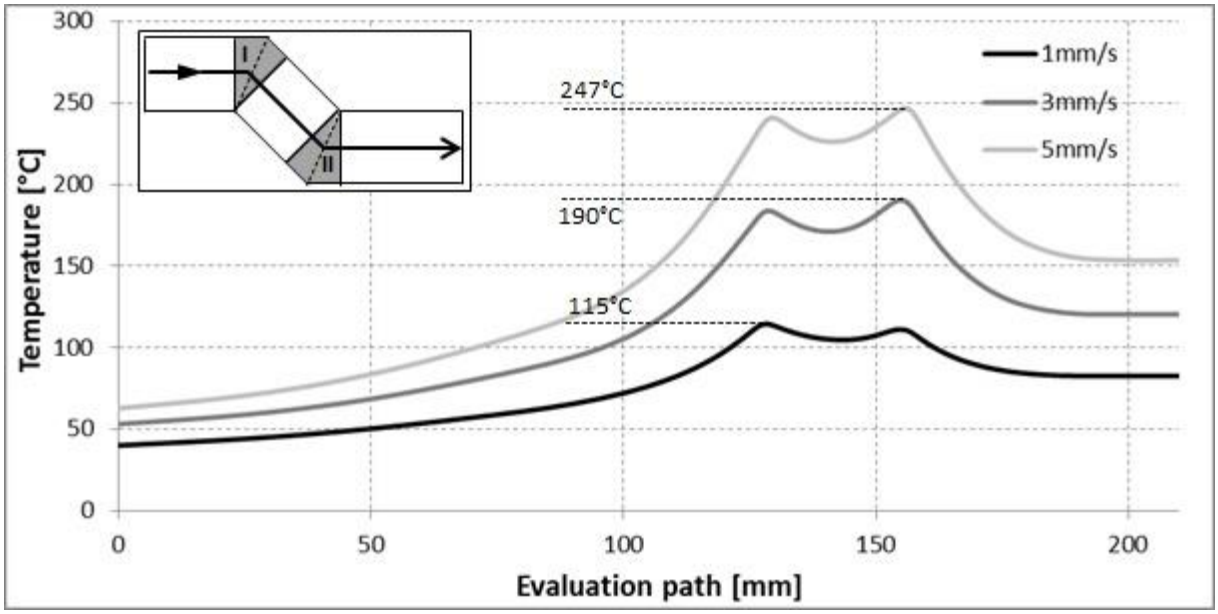

Figure 9-11 Temperature distribution in the finite element simulations with different friction coefficients

The feeding speed has a significant effect on the temperature distribution in the deformed samples (Figure 9-11). As the axial velocity increases, the deformation cycle number to finish the process decreases. Accordingly, the overall contact time between the tools and the workpiece reduces which in turn decreases the heat transfer between this contact pair. Therefore, it is an important process parameter if the feeding rate of ECAS is increased.

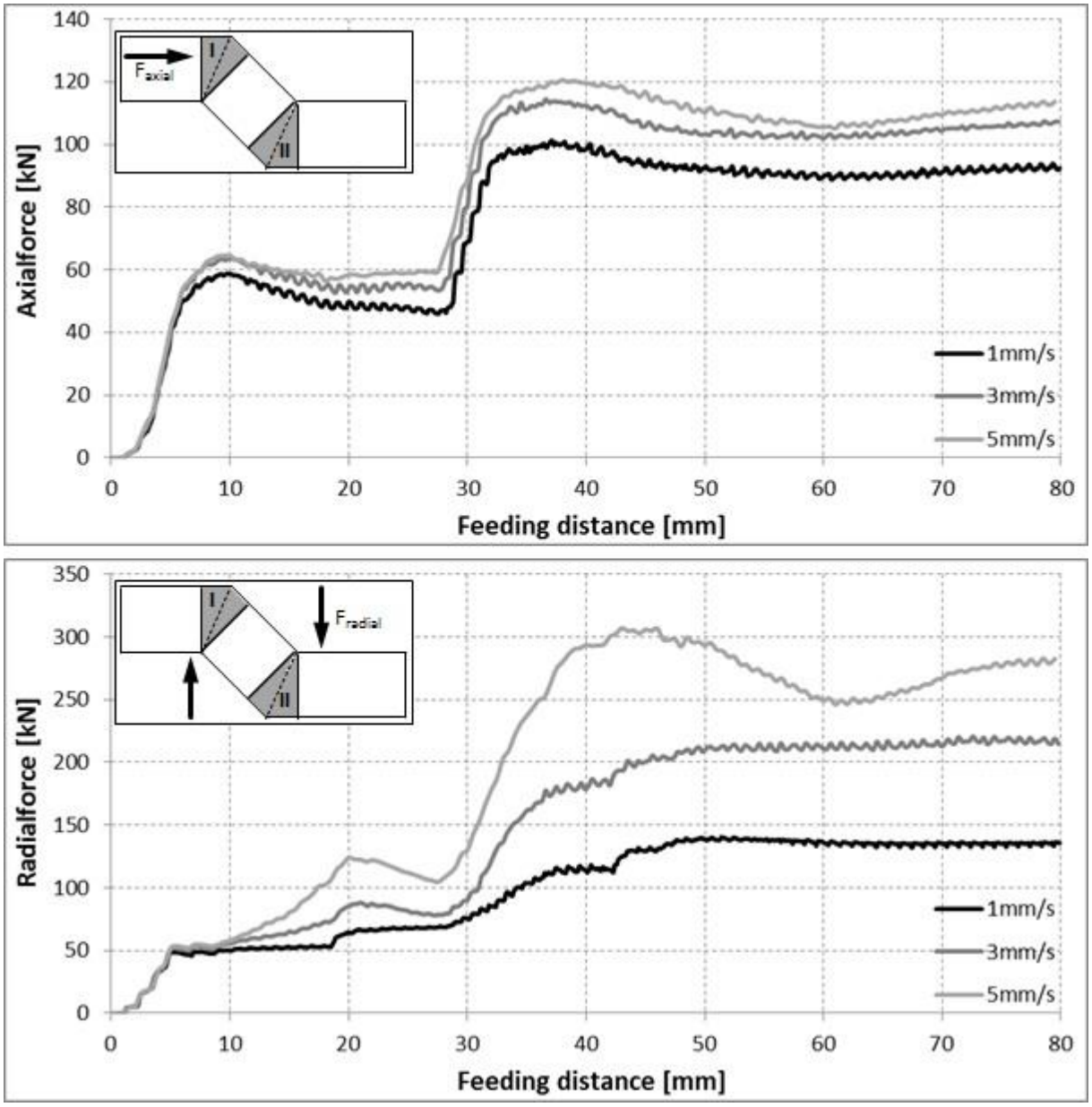

Figure 9-12 Force distribution in the finite element simulations with different feeding speeds

As the tribological parameters, the feeding rate also has a significant effect on the process loads. The forming forces in axial as well as radial direction rise as the axial velocity increases. Moreover, the unusual distribution of the radial forces at a feeding speed of 5 mm/s is caused by the temperature development in the sample. As the sample reaches the second deformation zone, the temperatures start to rise. Therefore, a drop is observed in the radial forces. However, as the process proceeds, a larger sample surface starts to contact the tools and eventually, the

temperatures in the sample balances. Accordingly, a steady load level is attained. Since the contact heat transfer at slower feeding rates already stabilizes the temperatures more easily, such a fluctuation is not observed at lower axial velocities.

9.4 Feeding Type

The continuous feeding of the samples into ECAS process has its limitations. At high axial speeds, the displacement of the sample when the tools are at or near the bottom dead center causes a resistance against feeding and thus increases the process loads. Therefore, it is intended to separate the axial movement of the sample from the radial oscillation of the tools and feed it into the process only when the tools are not in contact with the workpiece. That way, it is planned to omit the redundant friction loads against the feeding direction.

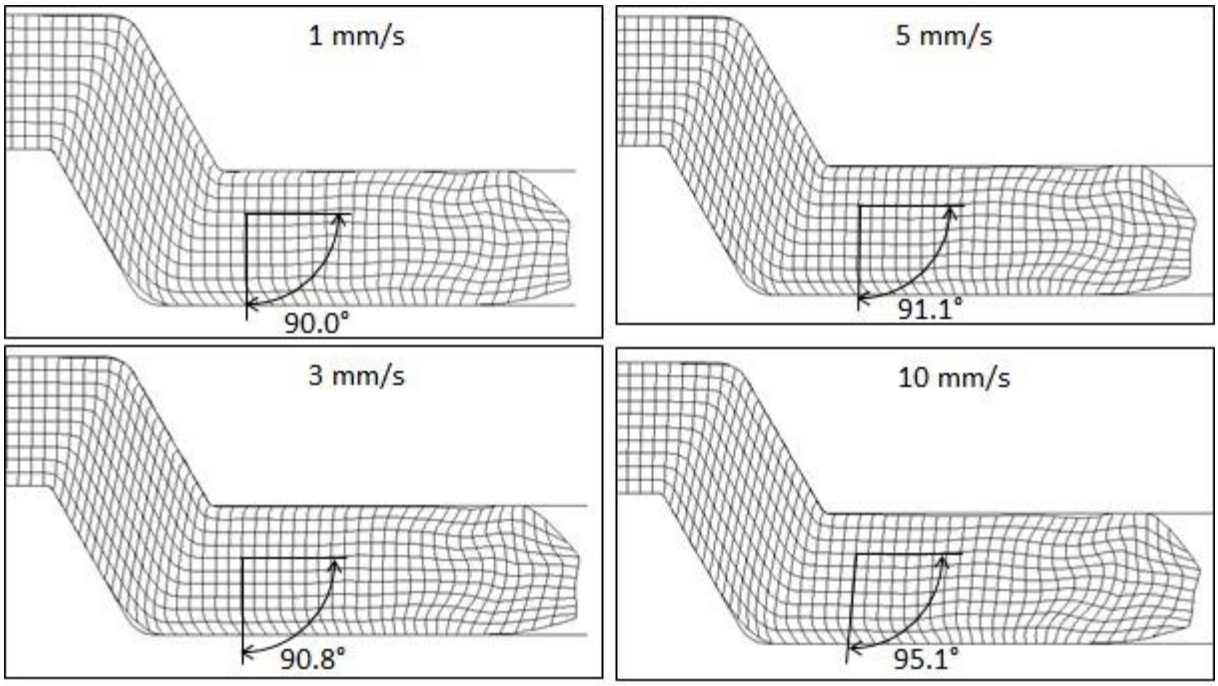

Figure 9-13 Material flow in the finite element simulations with different feeding speeds (oscillating feeding)

The finite element simulation of the oscillating type feeding speed investigations predict that the deformation of the samples by ECAS process is possible without any bulging or buckling in the workpieces. However, as the feeding speed increases, an inhomogeneity in the mesh deformation is observed (Figure 9-13). This effect is

clearer when the axial velocity is 10 mm/s. In this case, the mesh and accordingly the shear strain doesn't fully recover after the second yielding line. Nevertheless, the deformation on the upper side of the sample appears to be more homogeneous. Such a change in the deformation character of the workpiece is majorly caused by friction. Due to the kinematics of the ECAS process, only a small portion of the entire sample is formed in every tool cycle. It also limits the area of the contact where the tools majorly pull the workpiece into the process. However, as the feeding speed increases, the contact time during pulling and the sliding distance of the tool over that contact surface rises. As a result, the drawing effect becomes more significant causing the change in the mechanics of the process.

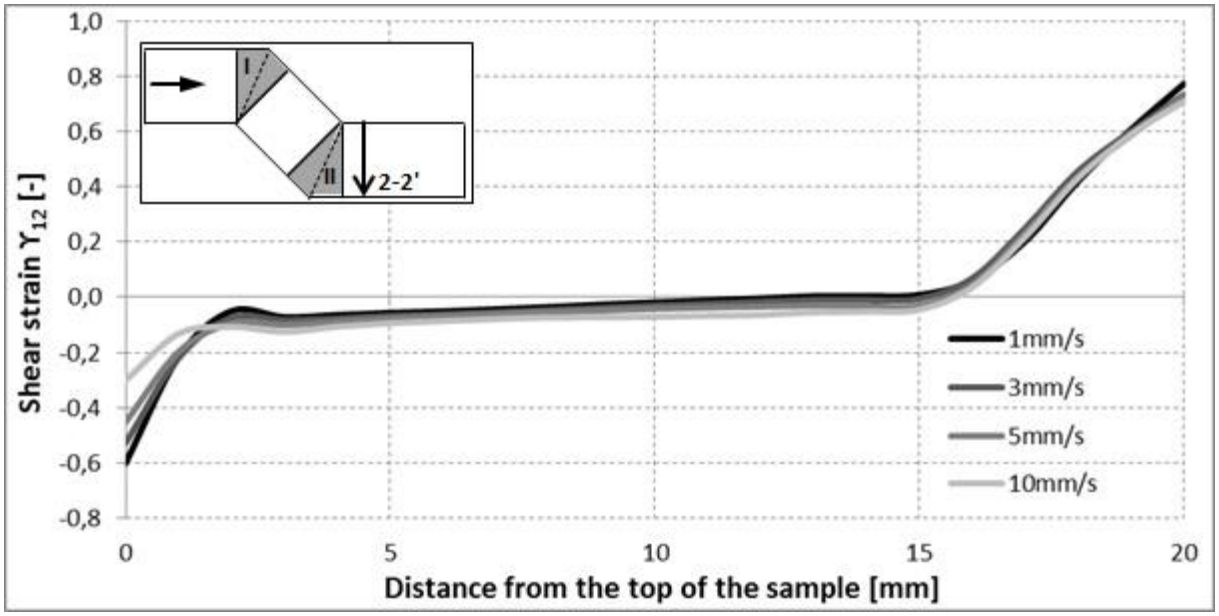

Figure 9-14 Shear strain distribution in the finite element simulations with different feeding speed (oscillating feeding)

A similar effect is also observed by the shear strain distribution. As the feeding speed increases, the shear strain distribution in the middle section of the deformed sample becomes more inhomogeneous while the strains on the upper side tend to near the steady state value of the distribution.

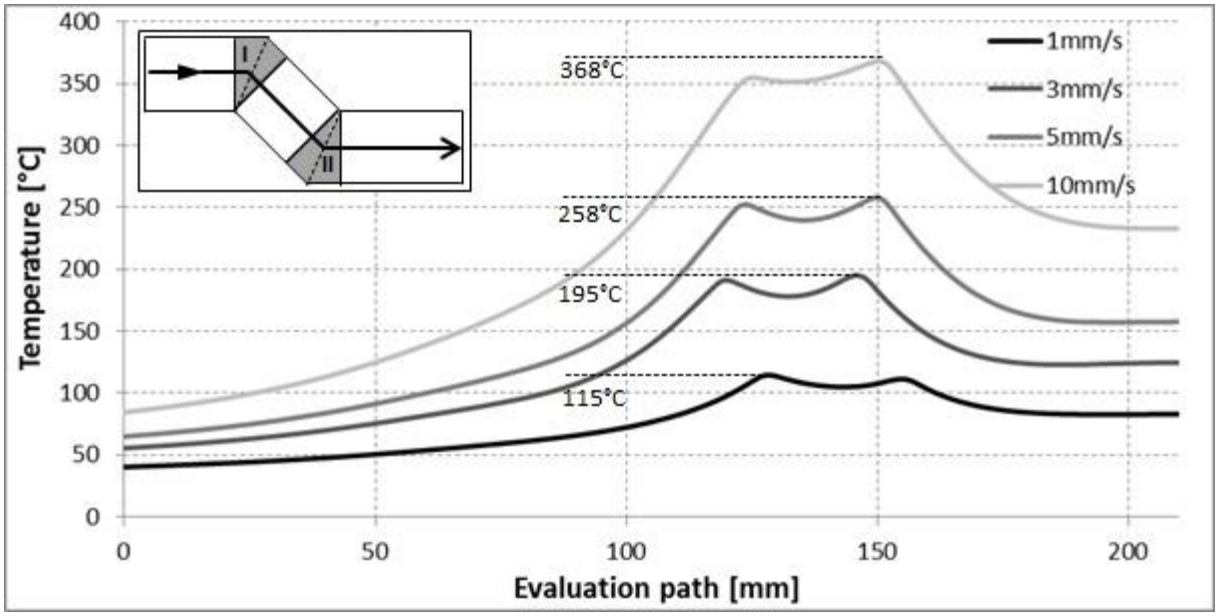

Figure 9-15 Temperature distribution in the finite element simulations with different feeding speeds (oscillating feeding)

As in the case of continuous feeding, the axial velocity has a significant effect on the temperature distribution in the deformed samples (Figure 9-15). Since the contact time declines while the feeding rate increases, less heat transfer is expected between the tools and the workpiece. Accordingly, the maximum temperatures rise significantly. Special precautions have to be taken to avoid temperature effects when it is intended to increase the feeding rate of an ECAS process.

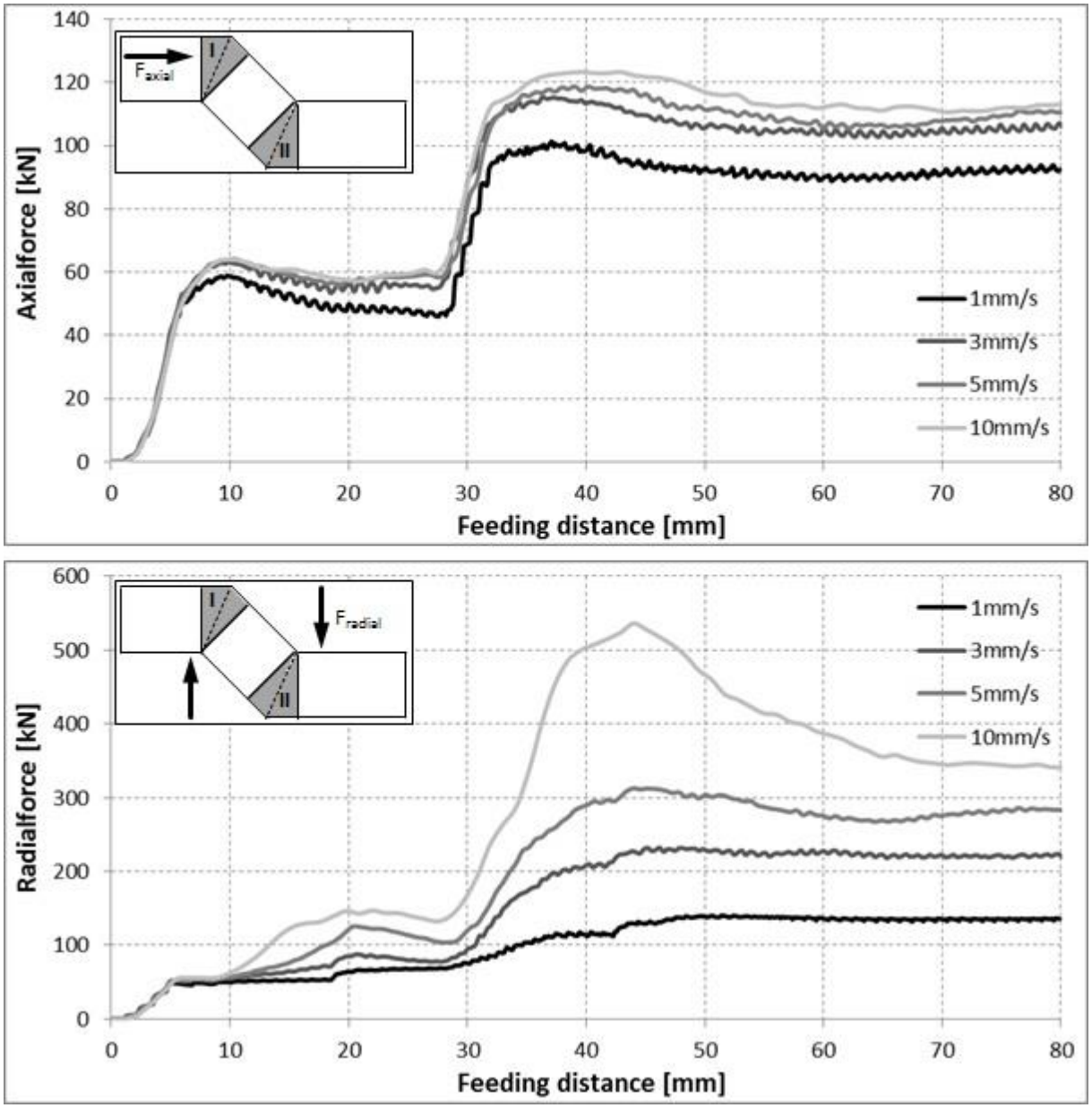

Figure 9-16 Force distribution in the finite element simulations with different feeding speeds (oscillating feeding)

Also in the case of the oscillating feeding, increasing the axial velocity of the samples has a significant effect on the process loads. Nevertheless, although a higher portion of the sample is deformed in every forming cycle of the tools, the rise in the axial loads are insignificant compared to the radial ones. A difference of just about 20% is observed when the feeding speed is increased tenfold. On the other hand, the radial loads nearly quadruples at the same feeding speed increase rate. Such a rise is

basically caused by the amount of material formed in every cycle of the tools. Nevertheless, as the process proceeds, the temperature in the deformed sample starts to increase and results in a drop in the forces as for the case of continuous feeding.

9.5 Process Design Suggestions for Future Applications

The finite element simulations in the previous chapters aim to demonstrate the effect of tribological properties, temperature and feeding rate on the ECAS process and hence to develop strategies for the speed-up. These simulations revealed important facts.

One of the key factors to increase the speed of ECAS process is the separation of the axial feed of the sample from the radial oscillation of the tools. In case of a continuous feeding, the samples are pushed into the process even the forming tools are at or near the bottom dead center which results in redundant friction forces against the advancement of the workpiece in axial direction. Nevertheless, the feeding of the workpiece into the process should proceed only when the tools are not in contact with the sample. Therefore, an oscillating type feeding is inevitable for the increase of the axial velocity. Such an application can be realized by implementing a conventional feeding device used in stamping operations into the ECAS process.

Moreover, for a successful implementation of a feed rate increase, the loads in axial direction should be kept at minimum. It can be achieved by increasing the friction factor between forming tools and sample. Accordingly, an efficient lubrication is not recommended. On the other hand, an increase in the feeding rate as well the friction coefficient causes a substantial rise in the workpiece temperatures during deformation. Although high temperatures ease the deformation by lowering the process loads, it could also jeopardize the successful grain refinement in the ECAS processed materials. Therefore, it is highly recommended to actively cool the forming system without lubricating it. Such a cooling can be achieved by spraying conventional industrial coolants on to the samples during deformation.

10 Summary and Outlook

Due to the recent market-driven requirements to reduce product weights and simultaneously material costs as well as to save energy and environment, the development of high-strength engineering materials has been increasingly gaining importance in the recent decades. Taking into account the limitation of natural resources, the production of such materials, especially for the bulk metal forming, without adding costly alloying elements or an additional secondary process such as heat treatment, is a major challenge for the forming industry.

Ultrafine-grained metals produced by severe plastic deformation processes are distinguished with many outstanding mechanical properties such as a combination of high strength and ductility or improved fatigue behavior and thus can be used to meet the high strength requirements of the metal forming industry. Although several severe plastic deformation processes have been developed over the last three decades, the industrial utilization of such materials is still in an early stage. Production of bulk UFG materials is still expensive. Therefore, the few applications are limited to the sports goods, biomedical parts or sputtering targets where the price of the parts mostly doesn't play a major role in the buying decision. To overcome the efficiency problems of current SPD methods, a new process, called "Equal Channel Angular Swaging" has been proposed which is based upon the combination of the conventional ECAP and the incremental bulk metal forming method of infeed rotary swaging.

In the current study, firstly, mechanics of the process is investigated by using slip line field approach. It is determined that unlike conventional ECAP, due to the kinematics of the process, the friction forces help the deformation by drawing the samples into the forming operation. Accordingly, the loads in the feeding direction are relatively low. Therefore, ECAS has a great potential as a continuous and so economical SPD process.

Secondly, in order to validate the slip line solution, a tool system has been developed. By the development, a thermo-mechanical coupled finite element simulation approach is utilized to investigate the effect of the geometrical parameters

on material flow and temperature formation as well as process loads. It is determined that both, channel length and outer corner radius has a significant effect on the process. Accordingly, a middle channel length of 15 mm and an outer corner radius of 5 mm have been selected for the tool system of the model experiments.

First experiments with the developed tool system prove the feasibility of the ECAS process. The deformation of round bars from two different materials, commercially pure copper and low carbon steel was possible. Moreover, the deformation on the samples follows predominantly a simple shear pattern. Developed thermo-mechanical coupled finite element models are capable of representing the deformation as well as the process loads required to form the materials. However, due to the highly idealized assumptions by the slip line field approach, defined analytical formulas overestimate the real process forces. Nonetheless, the analytical theory is capable of representing the load correlations.

The materials deformed by ECAS process are distinguished by an increased tensile strength compared to their as-received state. Moreover, microstructural investigations reveal that an average grain size under 1 µm can be achieved even after a single pass with the developed SPD process.

Although model experiments prove the feasibility of ECAS and the process loads, especially in the feeding direction are low which demonstrate the potential for a continuous and economical processing, the investigated feed rate of 1 mm/s isn’t appropriate for a wide commercial implementation. Therefore, in the last step of investigations, the effect of the most important process parameters of friction, temperature, feeding speed and feeding type is investigated by means of finite element simulations. These simulations reveal that a discontinuous feeding is inevitable for the speed-up of ECAS process. Moreover, an active cooling is definitely necessary to keep the temperatures at acceptable levels and to ensure an efficient grain refinement.

Further studies about ECAS should focus on three different topics. First of all, the theory about the increasing the feed rate should be proven with model experiments. As mentioned in the previous chapter, an oscillating type feeding is recommended in these experiments. Secondly, the analytical theory to predict the process loads has to be improved. Slip line field approach is appropriate for this purpose. However, unlike the current study, it is highly recommended to use a field consisting of many

slip lines in order to foresee the process loads accurately. Thirdly, tool and tool coating life should be investigated. For an industrial utilization, the forming tools and coatings have to endure the deformation for an acceptable time. Since the forming takes place in many cycles by ECAS, this topic represents a major challenge. In order to improve the tool life, hard metals or powder metallurgical tool steels can be used.

11 References

[AID01] Aida, T., Matsuki, K., Horita, Z., Langdon, T.G.: Estimating the equivalent strain in equal-channel angular pressing, Scripta Materialia 44 (2001), 575-579.

[ALE04] Alexandrov, I.V.: Multiscale studies and modeling of SPD materials, Materials Science and Engineering A 387-389 (2004), 772-776.

[ALK02] Alkorta, J., Rombouts, M., De Messemaeker, J., Froyen, L., Sevillano, J.G.: On the impossibility of multi-pass equal-channel angular grawing, Scripta Materialia 47 (2002), 13-18.

[ALL11] Allwood, J.M.: Steel and Aluminum in a Low Carbon Future, steel research international, Special Edition: 10th International Conference on Technology of Plasticity (2011), 27-42.

[AOK03] Aoki, K., Kimura, Y., Asada, Y., Azushima, A.: Properties of Annealed High Strength Steels Deformed by Repetitive Side Extrusion Process, Materials Science Forum 426-432 (2003), 2705-2710.

[AOK07] Aoki, K. and Azushima, A.: Development and Properties of High Strenghthened Carbon Steels Produced by Repetitive Side Extrusion and Heat Treatment Process, Materials Science Forum 539-543 (2007), 2884-2891.

[ARR13] Arrazola, P.J., Özel, T., Umbrello, D., Davies, M., Jawahir, I.S.: Recent advances in modelling of metal machining processes, CIRP Annals - Manufaturing Technology 62 (2013), 695-718.

[AZU02a] Azushima, A. and Aoki, K.: Properties of ultrafine-grained steel by repeated shear deformation of side extrusion process, Materials Science and Engineering A 337 (2002), 45-49.

[AZU02b] Azushima, A. and Aoki, K.: Mechanical Properties of Ultrafine Grained Steel Produced by Repetitive Cold Side Extrusion, CIRP Annals Manufacturing Technology 51/1 (2002), 227-230.

[AZU07] Azushima, A., Aoki, K., Tsukagoshi, H., Yanagida, A.: Development of ECAE Process for Reducing Friction, in Proceedings of Japanese Spring Conference on Technology of Plasticity (2007), 5-6.

[AZU08] Azushima, A., Kopp, R., Korhonen, A., Yang, D.Y., Micari, F., Lahoti, G.D., Groche, P., Yanagimoto, J., Tsuji, N., Rosochowski, A., Yanagida, A.: Severe plastic deformation (SPD) processes for metals, CIRP Annals-Manufaturing Technology 57 (2008), 716-735.

[BEY04] Beyerlein, I.J. and Tome, C.N.: Analytical modeling of material flow in equal channel angular extrusion (ECAE), Materials Science and Engineering A 380 (2004), 171-190.

[BON13] Bonnot, E., Helbert, A-L., Brisset, F., Baudin, T.: Microstructure and texture evolituon during the ultra grain refinement of the Armco iron deformed by accumulative rol bonding (ARB), Materials Science and Engineering A 561 (2013), 60-66.

[BRI46] Bridgman, P.W.: The Effect of Hydrostatic Pressure on Plastic Flow under Shearing Stress, Journal of Applied Physics 17 (1946), 692-698.

[CAR11] Carruth, M.A., Allwood, J.M., Moynihan, M.C.: The technical potential for reducing metal requirements through lightweight product design, Resources, Conservation and Recycling 57 (2011), 48-60.

[CCC08] Committee on Climate Change: Interim advice by the Committee on Climate Change, (2008) <http://www.theccc.org.uk/wp-content/uploads/2013/03/Interim-report-letter-to-DECC-SofS-071008.pdf> (accessed June 2013)

[CER09] Cerri, E., De Marco, P.P., Leo, P.: FEM and metallurgical analysis of modified 6082 aluminum alloys processed by multipass ECAP: Influence of material properties and different process setting on induced plastic strain, Journal of Materials Processing Technology 209 (2009), 1550-1564.

[CHA98] Chakkingal, U., Suriadi, A.B., Thomson, P.F.: Microstruture development during equal channel angular drawing of Al at room temperature, Scripta Materialia 39/6 (1998), 677-684.

[CHA99] Chakkingal, U., Suriadi, A.B., Thomson, P.F.: The development of microstructure and the influence of processing route during equal channel angular drawing of pure aluminum, Materials Science and Engineering A 266 (1999), 241-249.

[DAV02] Davey, K. and Ward, M.J.: The practicalities of ring rolling simulation for profilied rings, Journal of Materials Processing Technology 125-126 (2002), 619-625.

[DAV03] Davey, K. and Ward, M.J.: An ALE approach for finite element ring-simulation simulation of profiled rings, Journal of Materials Processing Technology 139 (2003), 559-566.

[DE05] De Ryck, I., Adriaens, A., Adams, F.: An overview of Mesopotamian bronze metallurgy during the 3rd millenium BC., Journal of Cultural Heritage 6 (2005), 261–268.

[DIN50125] DIN 50125, Prüfung metallischer Werkstoffe - Zugproben, Beuth Verlag, 2009 (in German)

[DIN8583] DIN 8583, Fertigungsverfahren Druckumformen - Teil 3: Freiformen; Einordnung, Unterteilung, Begriffe, Beuth Verlag, 2003 (in German).

[DIX11] Dixit, U.S., Joshi, S.N., Davim, J.P.: Incorporation of material behavior in modeling of metal forming and machining processes: A review, Materials and Design 32 (201), 3655-3670.

[DJA10] Djavanroodi, F. and Ebrahimi, M.: Effect of die parameters and material properties in ECAP with parallel channels, Materials Science and Engineering A 527 (2010), 7593-7599.

[DKI12] Niedriglegierte Kupferwerkstoffe, Deutsches Kupferinstitut, Berlin (2012).

[ERN41] Ernst, H. and Merchant, M.E.: Chip Formation, Friction and High Quality Machined Surfaces, Transactions of the American Society of Metals 29 (1941), 299-378.

[EST13] Estrin, Y. and Vinogradov, A.: Extreme grain refinement by severe plastic deformation: A wealth of challenging science, Acta Materialia 61 (2013), 782-817.

[FER08] Ferrasse, S., Segal, V.M., Alford, F., Kardokus, J., Strothers, S.: Scale up and application of equal-channel angular extrusion for the electronics and aerospace industries, Materials Science and Engineering A 493 (2008), 130-140.

[FIG06] Figueiredo, R.B., Pinheiro, I.P., Aguilar, M.T.P., Modenesi, P.J., Cetlin, P.R.: The finite element analysis of equal channel angular pressing (ECAP) considering the strain path dependance of the work hardening of metals, Journal of Materials Processing Technology 180 (2006), 30-36.

[FRI11] Frint, P, Hockauf, M., Halle, T., Strehl, G., Lampke, T., Wagner, M.F.-X.: Microstructural Features and Mechanical Properties after Industrial Scale ECAP of an Al-6060 Alloy, Materials Science Forum 667-69 (2011), 1153-1158.

[GAE99] Gärtner, R.R.: Entwicklung einer optimierten Fertigungsstrategie für das Klatrundkneten (1999), Dissertation, Institute for Production Engineering and Forming Machines, Darmstadt University of Technology (in German).

[GLE89] Gleiter, H.: Nanocrystalline Materials, Progress in Materials Science 33 (1989), 223-315.

[GOF00] Goforth, R.E., Hartwig, K.T., Cornwell, L.R.: Severe plastic deformation of materials by equal channel angular extrusion (ECAE), in Investigations and Applications of Severe Plastic Deformation, ed. T.C. Lowe and R.Z. Valiev, Kluwer, Dordrecht, Netherlands (2000).

[GÖR12] Görtan. M.O., Bruder, E., Groche, P., Müller, C.: Equal channel angular swaging (ECAS) – A new process for the production of high strength lightweight materials, In Proceedings of International Symposium on Plasticity and its Current Applications, San Juan/Puerto Rico (2012).

[GRO05a] Groche, P., Fritsche, D.: Inkrementelle Massivumformung – Eine Technologie vor dem Comeback? wt Werkstattstechnik online 95/10 (2005), 798–802 (in German).

[GRO05b] Groche, P. and Fritsche, D.: Efficient Algorithms for the Simulation of Incremental Bulk Metal Forming, Proceedings of 8th ICTP, Verona, Italy (2005).

[GRO07] Groche, P., Fritsche, D., Tekkaya, E.A., Allwood, J.M., Hirt, G., Neugebauer, R.: Incremental Bulk Metal Forming, CIRP Annals - Manufacturing Technology, 56/2 (2007), 635-656.

[GRO13a] Groche, P., Müller, C., Stahlmann, J., Zang, S.: Mechanical conditions in bulk metal forming tribometers - Part one, Tribology International (2013).

[GRO13b] Groche, P., Müller, C., Stahlmann, J.: Mechanical conditions in bulk metal forming tribometers - Part two, Tribology International (2013).

[GUN13] Gundarov, D.V., Polyakov, A.V., Semenova, I.P., Raab, G.I., Churakova, A.A., Gimaltdinova, E.I., Sabirov, I., Segurado, J., Sitdikov, V.D., Alexandrov, I.V., Enikeev, N.A., Valiev, R.Z.: Evolution of microstructure, macrotexture and mechanical properties of commercially pure Ti during ECAP-conform processing and drawing, Materials Science and Engineering A 562 (2013), 128-136.

[HAL51] Hall, E.O.: The Deformation and Ageing of Mild Steel: III Discusiion of Results, Proceedings of Physical Society B 64 (1951), 747-753.

[HAN02] Han, J.H., Seok, H.K., Chung, Y.H., Shin, M.C., Lee, J.C.: Texture evolution of the strip cast 1050 Al alloy processed by continuous confined strip shearing and ist formability evalution, Materials Science and Engineering A 323 (2002), 342-347.

[HAN04] Han, J.H., Oh, K.H., Lee, J.C.: Effect of accumulative strain on texture evolution in 1050 Al alloys processed by continuous confined strip shearing, Materials Science and Engineering A 387-389 (2004), 240-243.

[HEI01] Heislitz, F.: Optimierung des Axial-Radial-Umformens - eine Verfahrenserweiterung des Rundknetens (2001), Dissertation, Institute for Production Engineering and Forming Machines, Darmstadt University of Technology (in German).

[HOF00] Hofer, F., Seeber, A., Wieser, R.: CNC controlled radial swaging machines and applications, Proceedings of the Global Powertrain Conference (2000).

[HOR01] Horita, Z., Fujinami, T., Langdon, T.G.: The potential for scaling ECAP: effect of sample size on grain refinement and mechanical properties, Materials Science and Engineering A 318 (2001), 34-41.

[HOS07] Hosford, W.F. abd Caddell, R.M.: Metal Forming-Mechanics and Metallurgy, Cambridge University Press (2007).

[IEA08] Energy Technology Perspectives, International Energy Agency, Paris, (2008).

[IEA09] Energy Technology Transitions for Industry, International Energy Agency, Paris, (2009)

[INO13] Inoue, T., Yanagida, A., Yanagimoto, J.: Finite element simulation of accumulative roll-bonding process, Materials Letters 106 (2013), 37-40.

[IWA96] Iwahashi, Y., Wang, J., Horita, Z., Nemoto, M.: Principle of equal-channel angular pressing for the procesing of ultra-fine grained materials, Scripta Materialia 35/2 (1996), 143-146.

[JAM10] Jamaati, R. and Toroghinejad, M.R.: Application of ARB process for manufacturing high-strength, finely dispersed and highly uniform Cu/Al2O3 composite, Materials Science and Engineering A 527 (2010), 7430-7435.

[JAM11] Jamaati, R., Amirkhanlou, S., Toroghimejad, M.R., Niroumand, B.: Effect of particle size on microstruture and mechanical properties of composites produced by ARB process, Materials Science and Engineering A 528 (2011), 2143-2148.

[JIA08] Jiang, H., Fan, Z., Xie, C.: 3D finite element simulation of deformation bahvior of CP-Ti and working load during multi-pass equal channel angular extrusion, Materials Science and Engineering A 485 (2008), 409-414.

[JIN11] Jin, Y.G., Baek, H.M., Im, Y.T., Joen, B.C.: Continuous ECAP process design for manufacturing a microstructure-refined bolt, Materials Science and Engineering A 530 (2011), 462-468.

[JIN12] Jin, Y.G., Baek, H.M., Hwang, S.K., Im, Y.T., Jeon, B.C.: Continuous high strength aluminum bolt manufacturing by the spring-loaded ECAP system, Journal of Materials Processing Technology 212 (2012), 848-855.

[KAN08] Kang, H.G., Lee, J.P., Huh, M.Y., Engler, O.: Stability against coarsening in ultra-fine grained aluminum alloy AA 3103 sheet fabricated by continuous confined strip shearing, Materials Science and Engineering A 486 (2008), 470-480.

[KAN10] Kang, D.H., Kim, T.W.: Mechanical behavior and microstructural evolution of commercially pure titanium in enhanced multi-pass equal channel angular pressing and cold extrusion, Materials and Design 31 (2010), 554-560.

[KEN11] Kent, D., Wang, G., Yu, Z., Ma, X., Dargush, M.: Strength enhancement of a biomedical titanium alloy through a modified accumulative roll bonding technique, Journal of the Mechanical Behavior of Biomedical Materials 4 (2011), 405-416.

[KIE03] Kienhöfer, C., Grupp, P.: Rundknettechnik - Verfahren, Vorteile, Möglichkeiten, verlag moderne industrie, Landsberg/Lech (2003) (in German).

[KIM01] Kim, H.S., Seo, M.H., Hong, S.I.: Plastic deformation analysis of metals during equal channel angular pressing, Journal of Materials Processing Technology 113 (2001), 622-626.

[KIM02a] Kim, H.S.: Finite element analysis of deformation behaviour of metals during equal channel multi-angular pressing, Materials Science and Engineering A 328 (2002), 317-323.

[KIM02b] Kim, H.S., Seo, M.H., Hong, S.I.: Finite element analysis of equal channel angular pressing of strain rate sensitive metals, Journal of Materials Processing Technology 130-131 (2002), 497-503.

[KIM03] Kim, J-C., Nishida, Y., Arima, H., Ando, T.: Microstructure of Al-Si-Mg alloy processed by rotary-die equal channel angular pressing, Materials Letters 57 (2003), 1689-1695.

[KRA04] Krallics, G. and Lenard, J.G.: An examination of the accumulative roll-bonding process, Journal of Materials Processing Technology 152 (2004), 154-161.

[KRÜ96] Krüßmann, M.: Rundkneten im Einstechverfahren, Dissertation (1996), Institut für Umformtechnik, University of Stuttgart (in German).

[LAP08] Lapovok, R., Timokhina, I., McKenzie, P.W.J., O'Donnell, R.: Processing and properties of ultrafine-grain aluminum alloy 6111sheet, Journal of Materials Processing Technology 2000 (2008), 441-450.

[LEE01] Lee, J.C., Seok, H.K., Han, J.H., Chung, Y.H.: Controlling the testures of the metal strips via the continuous confined strip shearing (C2S2) process, Materials Research Bulletin 36 (2001), 997-1004.

[LEE02] Lee, S.H., Saito, Y., Tsuji, N., Utsunomiya, H., Sakai, T.: Role of shear strain in ultragrain refinement by accumulative roll-bonding (ARB) process, Scripta Materialia 46 (2002), 281-285.

[LI04] Li, S., Bourke, M.A.M., Beyerlein, I.J., Alexander, D.J., Clausen, B.: Finite element analysis of the plastic deformation zone and working load in equal channel angular extrusion, Materials Science and Engineering A 382 (2004), 217-236.

[LI06] Li, B.L., Tsuji, N., Kamikawa, N.: Microstructure homogeneity in various metallic materials heavily deformed by accumulative roll-bonding, Materials Science and Engineering A 423 (2006), 331-342.

[LIM98] Lim, T., Pillinger, I., Hartley, P.: A finite-element simulation of profile ring rolling using a hybrid mesh model, Journal of Materials Processing Technology 80-81 (1998), 199-205.

[LIU98] Liu, Z.Y., Liang, G.X., Wang, E.D., Wang, Z.R.: The effect of cumulative large plastic strain on the structure and properties of Cu-Zn alloy, Materials Science and Engineering A 242 (1998), 137-140.

[LU09] Lu, C., Tieu, K., Wexler, D.: Significant enhancement of bond strength in the accumulative roll bonding process using nano-sized SiO2 particles, Journal of Materials Processing Technology 209 (2009), 4830-4834.

[MA05] Ma, A., Nishida, Y., Suzuki, K., Shigematsu, I., Saito, N.: Charactersitics of plastic deformation by rotary-die equal-channel angular pressing, Scripta Materialia 52 (2005), 433-437.

[MAH10] Mahallawy, N.E., Shehata, F.A., Hameed, M.A.E., Aal, M.I.A.E., Kim, H.S.: 3D FEM simulations for the homogeneity of plastic deformation in Al-Cu alloys during ECAP, Materials Science and Engineering A 527 (2010), 1404-1410.

[MÄN12] Mänz, T.: Ermittlung von Werkstoffdaten zur Berechnung großer plastischer Verformungen mittels Finite-Elemente-Methoden, IMW-Institutsmitteilung 37 (2012), 57-64.

[MAT06] Mathieu, J.P., Suwas, S., Eberhardt, A., Toth, L.S., Moll, P.: A new design for equal channel angular extrusion, Journal of Materials Processing Technology 173 (2006), 29-33.

[McK10a] McKenzie, P.W.J. and Lapovok, R.: ECAP with back pressure for optimum strength and ductility in aluminum alloy 6010. Part 1: Microstructure, Acta Materialia 58 (2010), 3198-3211.

[McK10b] McKenzie, P.W.J. and Lapovok, R.: ECAP with back pressure for optimum strength and ductility in aluminum alloy 6010. Part 2: Mechanical properties and texture, Acta Materialia 58 (2010), 3212-3222.

[MIN06] Min, W., He, Y., Zhi-chao, S., Liang-gang, G., Xin-zhe, O.: Dynamic explicit FE modelling of hot ring rolling process, Transactions of Nonferrous Metals Society of China 16 (2006), 1274-1280.

[MIR10] Mirzakhani, B., Khoddam, S., Arabi, H., Salehi, M.T., Sietsma, J.: A coupled thermal-mechanical FE model of flow localization during the hot torsion test, Steel reasearch international 80 (2009), 846-854.

[MUE97] Müller, F.: Verfahrensgrundlagen des Rundknetens, (1997), Dissertation, Institute for Production Engineering and Forming Machines, Darmstadt University of Technology (in German).

[NAG04] Nagasekhar, A.V. and Hon, Y.T.: Optimal tool angles for equal channel angular extrusion of strain hardening materials by finite element analysis, Computational Materials Science 30 (2004), 489-495.

[NAK00] Nakashima, K., Horita, Z., Nemoto, M., Langdon, T.G.: Development of a multi-pass facility for equal-channel angular pressing to high total strains, Materials Science and Engineering A 281 (2000), 82-87.

[NAK98] Nakashima, K., Horita, Z., Nemoto, M., Langdon, T.G.: Influence of channel angle on the development of ultrafine grains in equal-channel angular pressing, Acta Materialia 46/5 (1998), 1589-1599.

[NIS01] Nishida, Y., Arima, H., Kim, J-C., Ando, T.: Rotary-die equal-channel angular pressing of an Al-7 mass% Si - 0.35 mass% Mg alloy, Scripta Materialia 45 (2001), 261-266.

[OLE08] Olejnik, L., Rosochowski, A., Richert, M.: Incremental ECAP of plates, Materials Science Forum 584-586 (2008), 108-113.

[OSA08] Osakada, K.: History of Plasticity and Metal Forming Analysis, In: Proceedings of 9th International Conference on Technology of Plasticity, Gyeongju/Korea, (2008).

[PAU06] Pauskar, P.: Finite Element Modelling of Incremental Forming Processes at the Timken Company, Workshop on Modelling of Incremental Bulk Forming Processes, Darmstadt, Germany (2006).

[PER03] Perez, C.J.L., Berlanga, C., Ilzarbe, J.P.: Processing of aluminum alloys by equal channel angular drawing at room temperature, Journal of Materials Processing Technology 143-144 (2003), 105-111.

[PER04] Perez-Prado, M.T., del Valle, J.A., Ruano, O.A.: Grain refinement og Mg-Al-Zn alloys vi accumulative roll bonding, Scripta Materialia 51 (2004), 1093-1097.

[POL11] Polyakov, A.V., Gunderov, D.V., Raab, G.I.: Evolution of microstructure and mechanical properties of titanium Grade 4 with the increase of the ECAP-Conform passes, Materials Science Forum 667-669 (2011), 1165-1170.

[PRA97] Prangnell, P.B., Harris, C., Roberts, S.M.: Finite element modelling of equal channel angular extrusion, Scripta Materialia 37/7 (1997), 983-989.

[RAA04] Raab, G.J., Valiev, R.Z., Lowe, T.C., Zhu, Y.T.: Continuous processing of ultrafine grained Al by ECAP-Confrom, Materials Science and Engineering A 382 (2004), 30-34.

[RAT06] Rathmann, T.: Entwicklung eines Technologieprozessors zur Untersuchung des Kaltrundknetens mit Hilfe der Finite Elemente Analyse, (2006), Dissertation, Institute for Production Engineering and Forming Machines, Darmstadt University of Technology (in German).

[RON07] Rong, L., Nie, Z., Zuo, T.: 3D finite element modeling of cogging-down rotary swaging of pure magnesium billet-Revealing the effect of high-frequency pulse stroking, Materials Science and Engineering A 464 (2007), 28-37.

[ROS02] Rosochowski, A. and Olejnik, L.: Numerical and physical modelling of plastic deformation in 2-turn equal channel angular extrusion, Journal of Materials Processing Technology 125-126 (2002), 309-316.

[ROS07] Rosochowski, A. and Olejnik, L.: FEM Simulation of Incremental Shear, in Proceedings of 10th ESAFORM Conference on Material Forming (2007), 653-658.

[ROS08a] Rosochowski, A., Olejnik, L., Richert, M.: Double-Bilet Incremental ECAP, Materials Science Forum 584-586 (2008), 139-144.

[ROS08b] Rosochowski, A., Olejnik, L.: Finite element analysis of two-turn Incremental ECAP, International Journal of Material Forming (2008), 483-486.

[ROS10] Rosochowski, A., Rosochowska, M., Olejnik, L., Verlinden, B.: Incremental Equal Channel Angular Pressing of Sheet, steel research international 81 (2010), 470-473.

[ROS11] Rosochowski, A., Olejnik, L.: Current Practice and Future Opportunities for Two-Turn ECAP, Materials Science Forum 667-669 (2011), 121-126.

[SAI00] Saito, Y., Utsunomiya, N., Suzuki, H., Sakai, T.: Improvement in the r-value of aluminum strip by a continuous shear deformation process, Scripta Materialia 42 (2000), 1139-114.

[SAI98] Saito, Y., Tsuji, N., Utsunomiya, H., Sakai, T., Hong, R.G.: Ultra-fine grained bulk aluminum produced by accumulative roll-bonding (ARB) process, Scripta Materialia 39/9 (1998), 1221-1227.

[SAI99] Saito, Y., Utsunomiya, N., Suzuki, H.: Proposal of novel continuous high straining process - Development of Conshearing process, in Proceedings of the 6th ICTP September 19-24 (1999), Nuremberg/Germany, 2459-2464.

[SAK05] Sakai, G., Nakamura, K., Horita, Z., Langdon, T.G.: Developing high-pressure torsion for use with bulk samples, Materials Science and Engineering A 406 (2005), 268-273.

[SCH95] Schmoeckel, D. and Speck, F.D.: Axial-Radial Forming of Tubular Components, CIRP Annals - Manufacturing Technology 44-1 (1995), 235-238.

[SEG03] Segal, V.M.: Slip line solutions, deformation mode and loading history during equal channel angular extrusion, Materials Science and Engineering A 345 (2003), 36-46.

[SEG04] Segal, V.M.: Engineering and commercialization of equal channel angular extrusion, Materials Science and Engineering A 386 (2004), 269-276.

[SEG95] Segal, V.M.: Materials processing by simple shear, Materials Science and Engineering A 197 (1995), 157-164.

[SEG99] Segal, V.M.: Equal channel angular extrusion: from macromechanics to structure formation, Materials Science and Engineering A 271 (1999), 322-333.

[SHA08] Shaarbaf, M. and Toroghinejad, M.R.: Nano-grained copper strip produced by accumulative roll bonding process, Materials Science and Engineering A 561 (2013), 145-151.

[SHE01] Sherby, O.D., Wadsworth, J.: Ancient blacksmiths, the Iron Age, Damascus steels and modern metallurgy, Journal of Materials Processing Technology 117 (2001), 347–353.

[SON06] Son, I.H., Lee, J.H., Im, Y.T.: Finite element investigation of equal channel angular extrusion with back pressure, Journal of Materials Processing Technology 171 (2006), 480-487.

[SRI06] Srinisavan, R., Cherukuri, B., Chaudury, P.K.: Scaling up of Equal Channel Angular Pressing (ECAP) for the Production of Forging Stock, Materials Science Forum 503-504 (2006), 371-378.

[STE07] Steinke, P.: Finite Elemente Methode - Rechnergestützte Einführung, 2. edition, Springer Verlag, Berlin (2007) (in German).

[STO01] Stoica, G.M. and Liaw, P.K.: Progress in Equal-Channel Angular Processing, Journal of the Minerals, Metals and Materials Society 53-3 (2001), 36-40.

[STO07] Stoica, G.M.: Equal-Channel-Angular Processing (ECAP) of Materials: Experiment and Theory, (2007), Dissertation, The University of Tennessee, Knoxville.

[SUH01] Suh, J.Y., Kim, H.S., Park, J.W., Chang, J.Y.: Finite element analysis of material flow in equal channel angular pressing, Scripta Materialia 44 (2001), 677-681.

[SUO06] Suo, T., Li, Y., Guo, Y., Liu, Y.: The simulation of deformation distribution during ECAP using 3D finite element method, Materials Science and Engineering A 432 (2006), 269-274.

[SUO07] Suo, T., Li, Y., Deng, Q., Liu, Y.: Optimal pressing route for confined equal channel angular pressing by finite element analysis, Materials Science and Engineering A 466 (2007), 166-171.

[TER07] Terada, D., Inoue, S., Tsuji, N.: Microstructure and mechanical properties of commercial purity titanium severely deformed by ARB process, Journal of Materials Science 42 (2007), 1673-1681.

[TOR13] Toroghinejad, M.R., Ashrafizadeh, F., Jamaati, R.: On the use of accumulative roll bonding process to develop nanostrutured aluminum alloy 5083, Materials Science and Engineering A 561 (2013), 145-151.

[TSU99] Tsuji, N., Saito, Y., Utsunomiya, H., Tanigawa, S.: Ultra-fine grained bulk steel produced by accumulative roll-bonding (ARB) process, Scripta Materialia 40/7 (1999), 795-800.

[TUR11] Türk, M.: Integration von Funktionswerkstoffen in metallische Tragstrukturen mittels inkrementeller Umformverfahren, (2011), Dissertation, Institute for Production Engineering and Forming Machines, Darmstadt University of Technology (in German).

[UTS01] Utsunomiya, H., Saito, Y., Suzuki, H., Sakai, T.: Development of the continuous shear deformation process, Proceedings of the Institution of Mechanical Engineers, Part B: Journal of Engineering Manufacture 215 (2001), 947-957.

[UTS04] Utsunomiya, H., Hatsuda, K., Sakai, T., Saito, Y.: Continuous grain refinement of aluminum strip by conshearing, Materials Science and Engineering A 372 (2004), 199-206.

[VAL02] Valiev, R.Z. and Alexandrov, I.V.: Paradox of strength and ductility in metals processed by severe plastic deformation, Journal of Materials Research 17/1 (2002), 5-8.

[VAL05] del Valle, J.A., Perez-Prado, M.T., Ruano, O.A.: Accumulative roll bonding of a Mg-based AZ61 alloy, Materials Science and Engineering A 410-411 (2005), 353-357.

[VAL06] Valiev, R.Z. and Langdon, T.G.: Principles of equal-channel angular pressing as a processing tool for grain refinement, Progress in Materials Science 51 (2006), 881-981.

[VAL90] Valiev, R.Z., Mulyukov, R.R., Ovchinnikov, V.V.: Direction of a grain-boundary phase in submirometre-grained iron, Philosophical Magazine Letters 62/4 (1990), 253-256.

[VAL91] Valiev, R.Z., Krasilnikov, N.A., Tsenev, N.K.: Plastic deformation of alloys with submicron-grained structure, Materials Science and Engineering A 137 (1991), 35-40.

[VDI93] VDI Richtlinie 3633, Blatt 1, Simulation von Logistik-, Materialfluß- und Produktionssytemen - Grundlangen, Düsseldorf (1993) (in German).

[VOR04] Vorhauer, A. and Pippan, R.: On the homogeneity of deformation by high pressure torsion, Scripta Materialia 51 (2004), 921-925.

[WEI06] Wie, W., Nagasekhar, A.V., Chen, G., Hon, Y.T., Wie, K.X.: Origin of inhomogenous behavior during equal channel angular pressing, Scripta Materialia 54 (2006), 1865-1869.

[WEI09] Wie, W., Zhang, W., Wie, K.X., Zhong, Y., Cheng, G., Hu, J.: Finite element analysis of deformation behavior in continuous ECAP process, Materials Science and Engineering A 516 (2009), 111-118.

[WET04] Wetscher, F., Vorhauer, A., Stock, R., Pippan, R.: Structural refinement of low alloyed steels during severe plastic deformation, Materials Science and Engineering A 387-389 (2004), 809-816.

[WUN05] Wunderlich, J.: Präziser planen mit Simulation, angewandte Arbeitswissenschaft 186 (2005), 16-30 (in German).

[XIE00] Xie, C., Dong, X., Li, S., Huang, S.: Rigid-viscoplastic dynamic explicit FEA for the ring rolling process, International Journal for the Machine Tool and Manufacture 40 (2000), 81-93.

[XU06] Xu, S., Zhao, G., Luan, Y., Guan, Y.: Numerical studies on processing routes and deformation mechanism of multi-pass equal channel angular pressing process, Journal of Materials Processing Technology 176 (2006), 251-259.

[XU07] Xu, C., Horita, Z., Langdon, T.G.: The evolution of homogeneity in processing by high-pressure torsion, Acta Materialia 55 (2007), 203-212.

[XU08] Xu, S., Zhao, G., Ren, X., Guan, Y.: Numerical investigation of aluminum deformation behavior in three-dimensional continuous confined strip shearing proecss, Materials Science and Engineering A 476 (2008), 281-289.

[XU10] Xu, C., Schroeder, S., Berbon, P.B., Langdon, T.G.: Principles of ECAP-Conform as a continuous process for achieving grain refinement: Application to an aluminum alloy, Acta Materialia 58 (2010), 1379-1386.

[YAN10] Yang, D., Cizek, P., Hodgson, P., Wen, C.: Ultrafine equiaxed-grain Ti(Al composite produced by accumulative roll bonding, Scripta Materialia 62 (2010), 321-324.

[YEA03] Yea, Y., Ko, Y., Kim, N., Lee, J.: Prediction of spread, pressure distribution and roll force in ring rolling process using rigid-plastic finite element method, Journal of Materials Processing Technology 140 (2003), 478-486.

[ZAN14] Zang, S., Müller, C., Bodenmüller, D., Groche, P.: Influence of temperature on environmentally benign tribological systems in cold forging operations, Proceedings of NAMRI/SME 42 (2014).

[ZHA05] Zhao, W.J., Ding, H., Ren, Y.P., Hao, S.M., Wang, J., Wang, J.T.: Finite element simulaton of deformation behavior of pure aluminum during equal channel angular pressing, Materials Science and Engineering A 410-411 (2005), 348-352.

[ZHI08] Zhilyaev, A.P., Langdon, T.G.: Using high-pressure torsion for metal processing: Fundamentels and applications, Progress in Materials Science 53 (2008), 893-979.

[ZHU04] Zhu, Y.T., Lowe, T.C., Langdon, T.G.: Performance and applications of nanostructured materials produced by severe plastic deformation, Scripta Materialia 51 (2004), 825-830.

[ZIS06] Zisman, A.A., Rybin, V.V., Van Boxel, S., Seefeldt, M., Verlinden, B.: Equal channel angular drawing of aluminum sheet, Materials Science and Engineering A 427 (2006), 123-129.

[ZUY99] Zuyan, L. and Zhongjin, W.: Finite-element analysis of the load of equal-cross-section lateral extrusion, Journal of Materials Processing Technology 94 (1999), 193-196.

Figure List

Table List

Appendix

Appendix A – Effect of Channel Length on Low Carbon Steel (C4C)

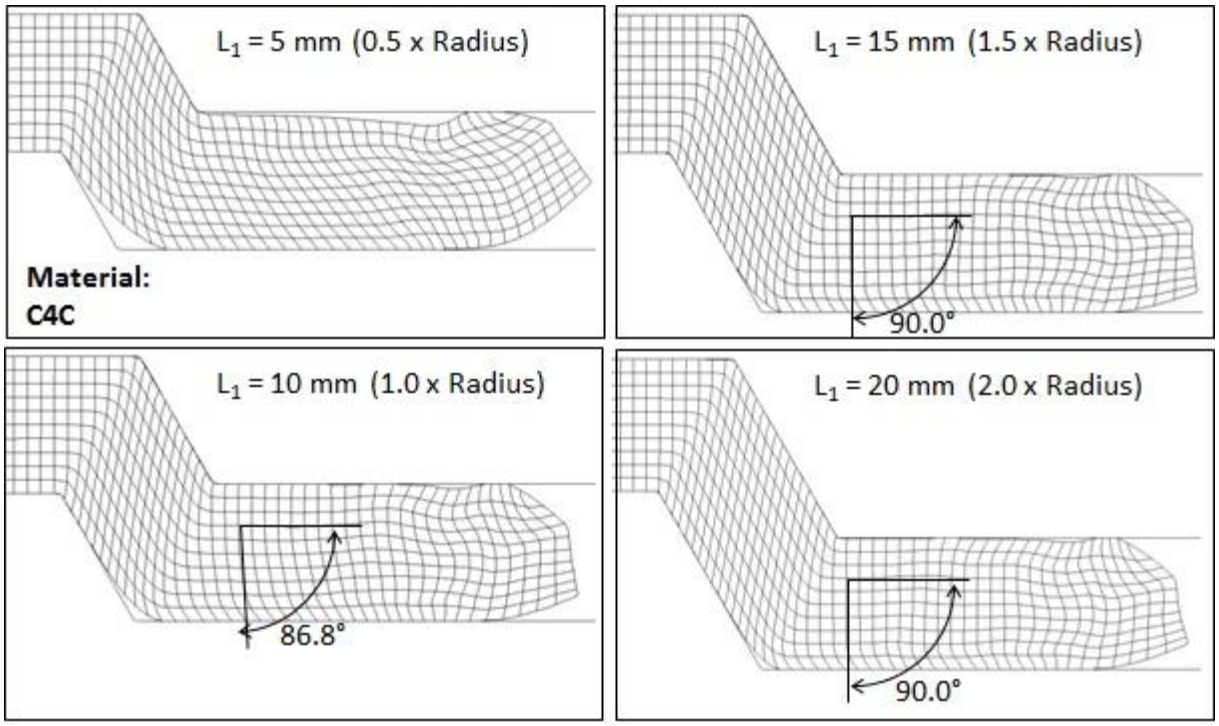

Figure A-1 Comparison of mesh deformation in low carbon steel

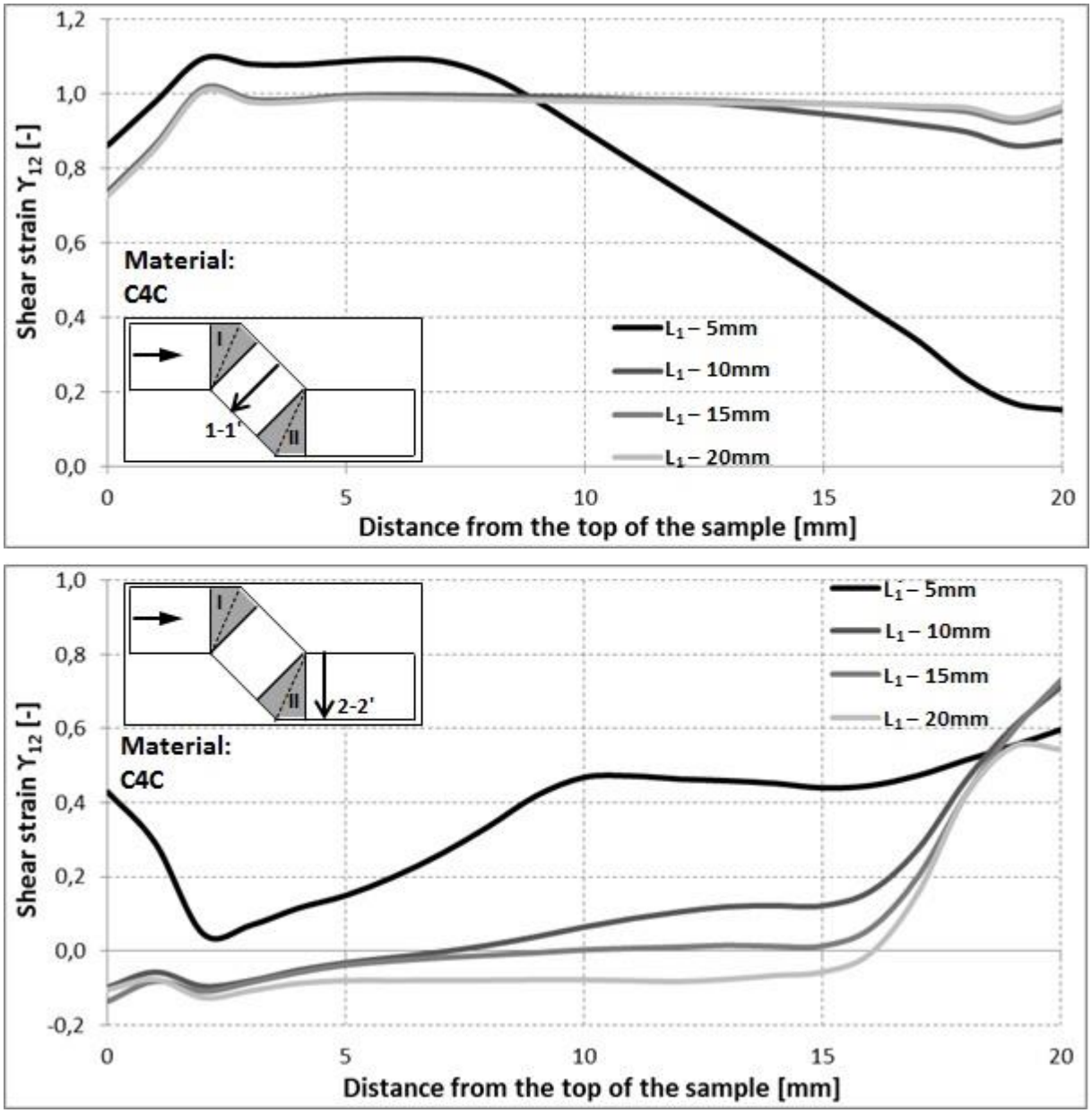

Figure A-2 Comparison of plastic strain distribution in low carbon steel

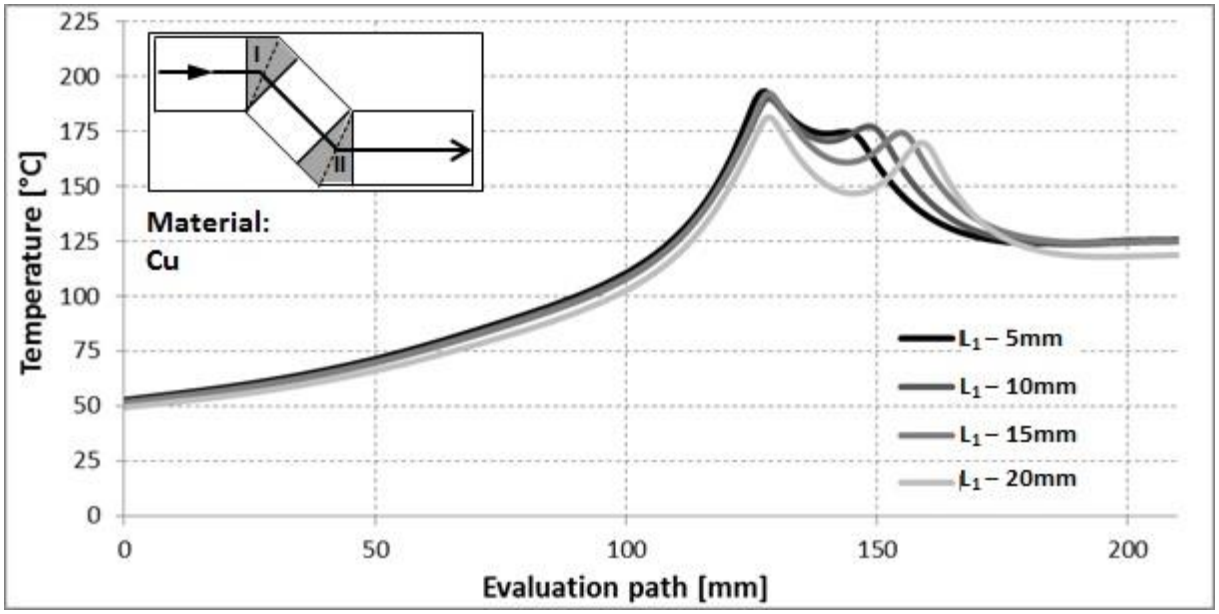

Figure A-3 Comparison of temperature distribution in copper

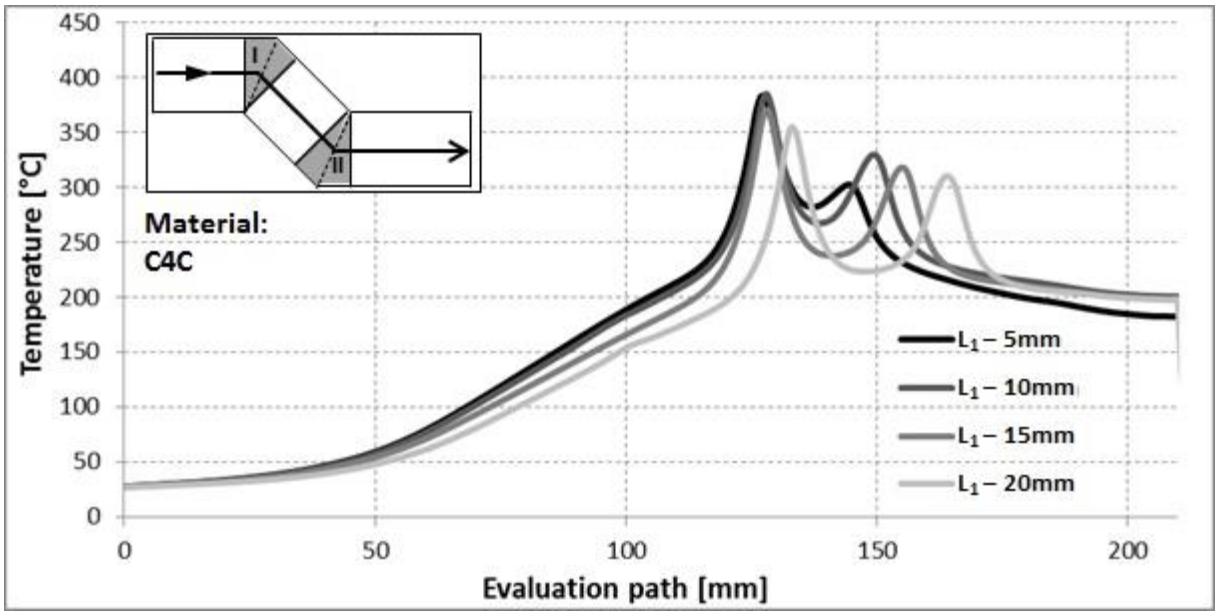

Figure A-4 Comparison of temperature distribution in low carbon steel

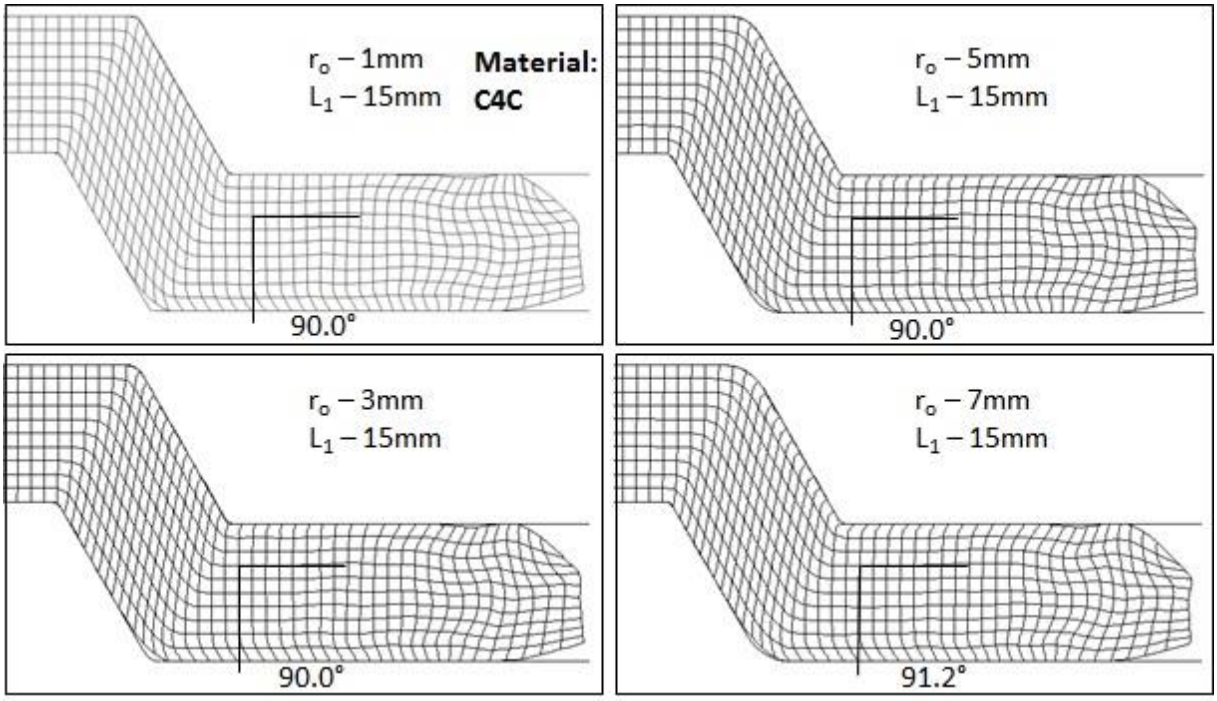

Figure A-5 Comparison of mesh deformation in low carbon steel

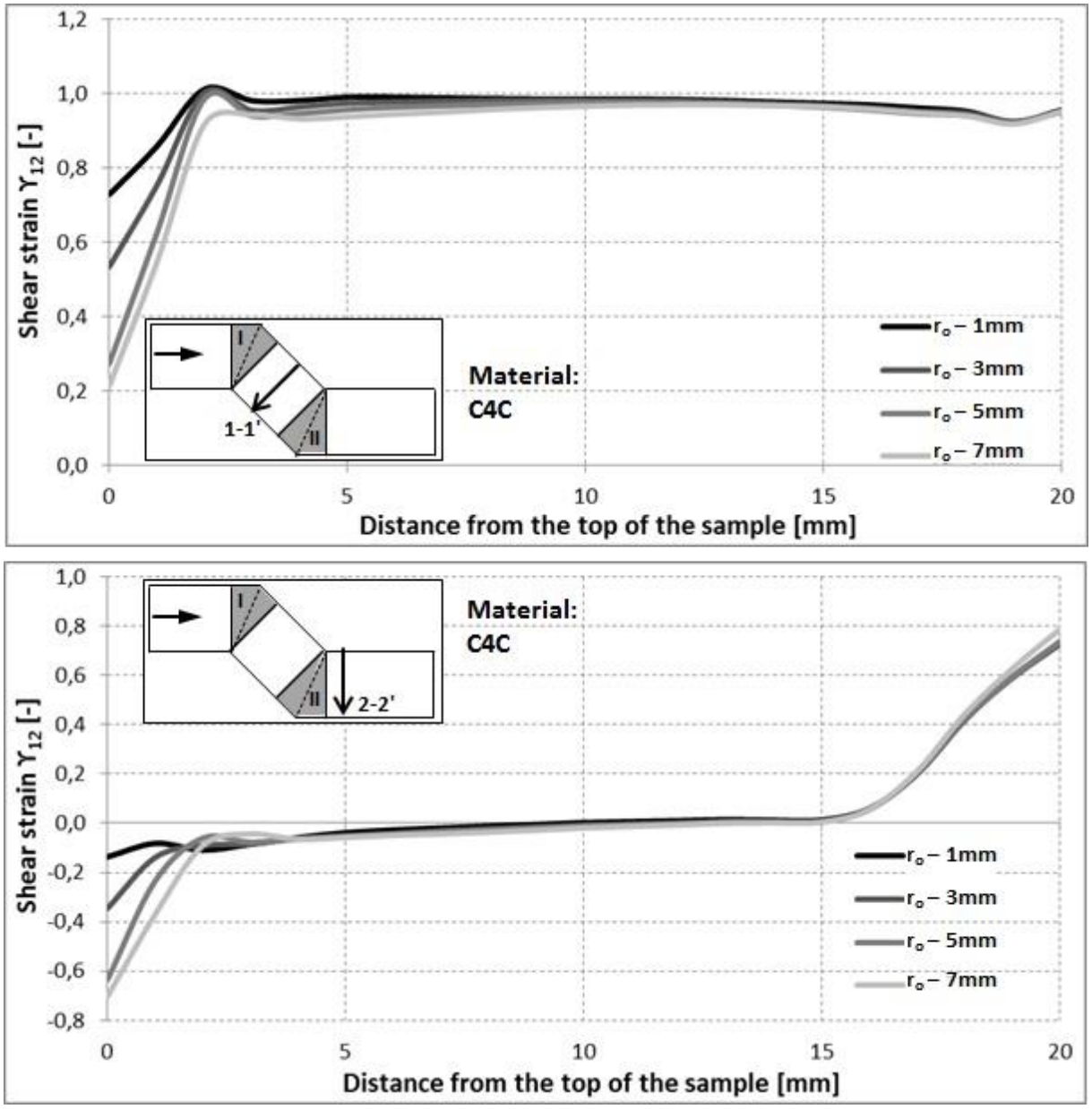

Figure A-6 Comparison of plastic strain distribution in low carbon steel

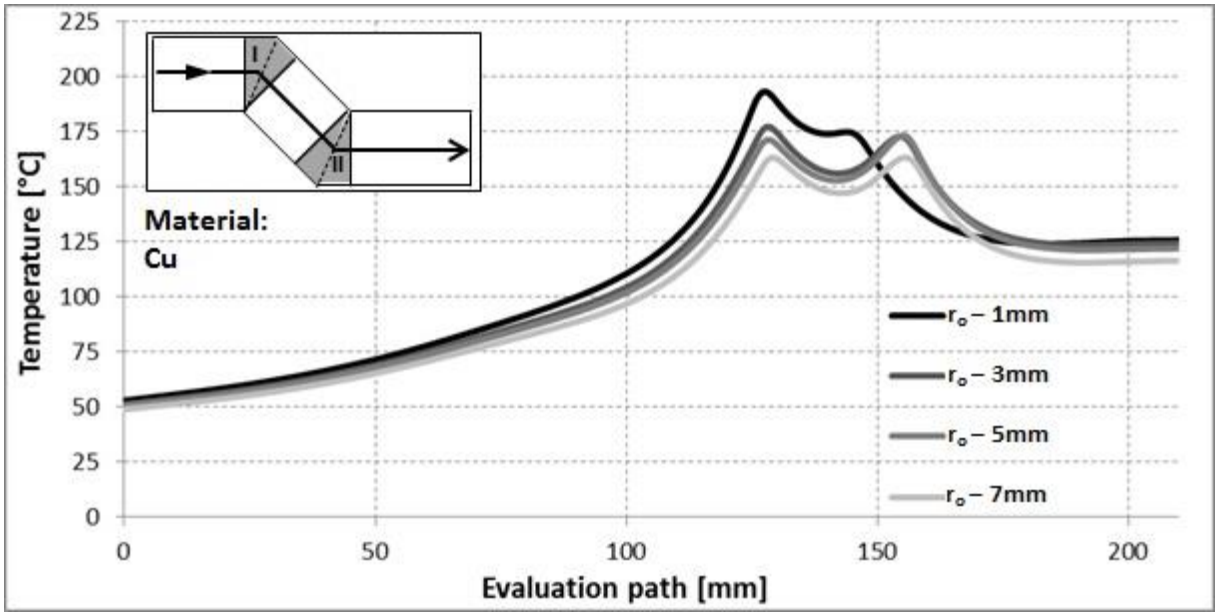

Figure A-7 Comparison of temperature distribution in copper

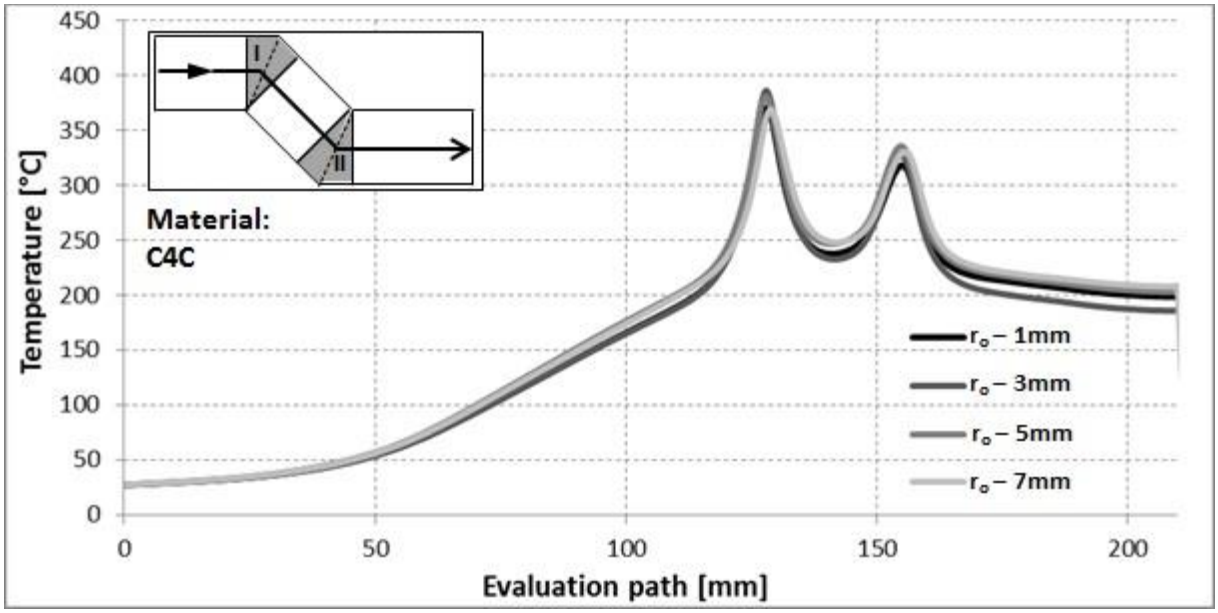

Figure A-8 Comparison of temperature distribution in low carbon steel

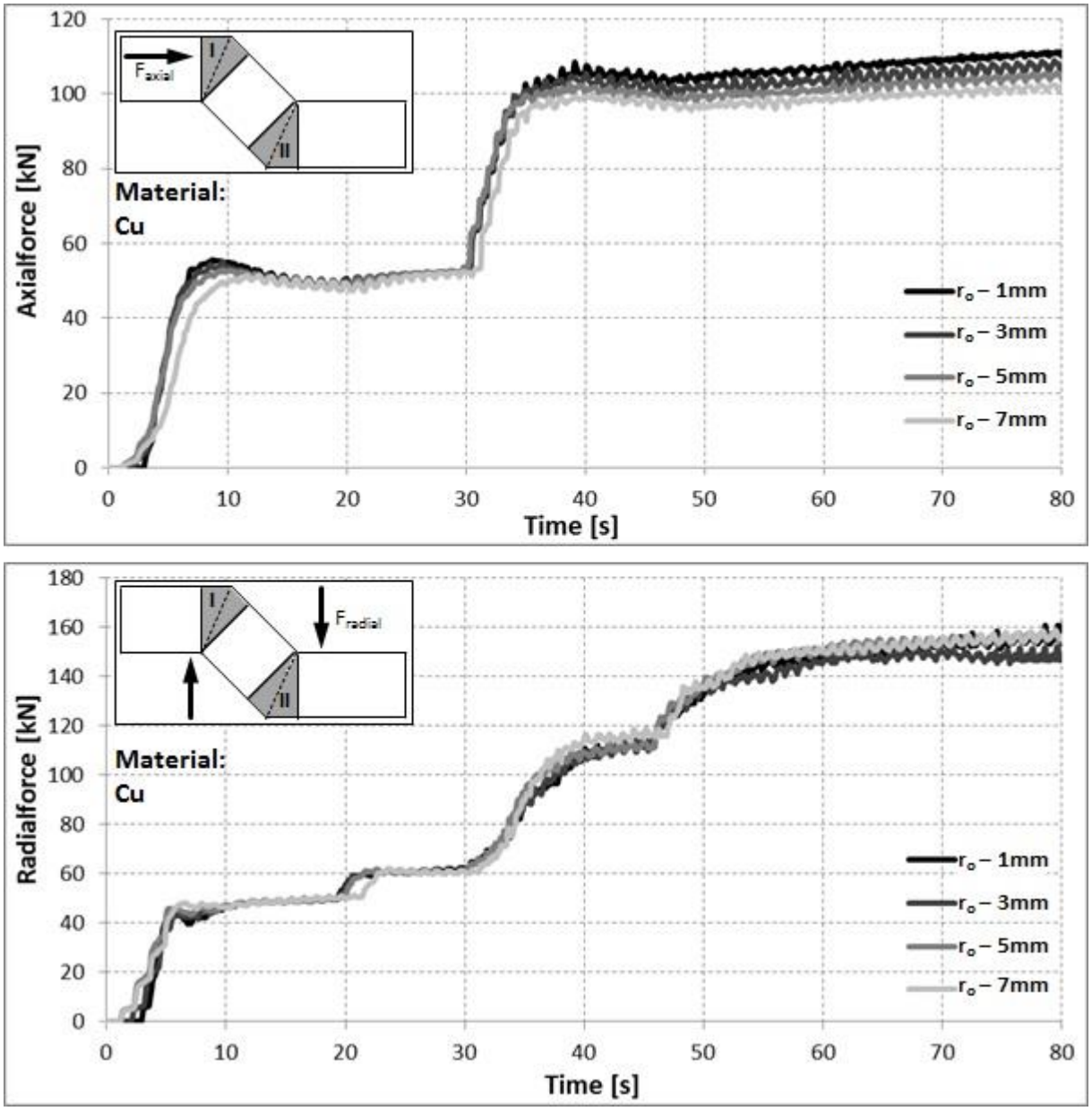

Figure A-9 Comparison of axial and radial forces during ECAS processing of copper

Résumé

Personal Information

Name	Mehmet Okan Görtan
Date of Birth	January 21st , 1981
Birthplace	Kocaeli, Turkey
Marital Status	Married
Nationality	Turkish

Education

09/1987 – 06/1992	Elementary school, Petkim Ilkokulu, Kocaeli
09/1992 – 06/2000	High school, Istanbul Lisesi, Istanbul
09/2000 – 06/2005	B.Sc. in Mechanical Engineering Istanbul Technical University, Istanbul
09/2005 – 07/2008	M.Sc. in Mechanical Engineering Istanbul Technical University, Istanbul
09/2008 – 12/2013	Doctorate, Institute for Production Engineering and Forming Machines Prof. Dr.-Ing. Dipl.-Wirtsch.-Ing. Peter Groche Technische Universität Darmstadt